A NEW ACCOUNT OF ROSS SEA WATERS: CHARACTERISTICS, VOLUMETRICS, AND VARIABILITY

A Thesis

by

CHRISTINA LEE STOVER

Submitted to the Office of Graduate Studies of
Texas A&M University
in partial fulfillment of the requirements for the degree of

MASTER OF SCIENCE

May 2006

Major Subject: Oceanography

A NEW ACCOUNT OF ROSS SEA WATERS: CHARACTERISTICS, VOLUMETRICS, AND VARIABILITY

A Thesis

by

CHRISTINA LEE STOVER

Submitted to the Office of Graduate Studies of
Texas A&M University
in partial fulfillment of the requirements for the degree of

MASTER OF SCIENCE

Approved by:

Co-Chairs of Committee,	Alejandro H. Orsi
	Achim Stoessel
Committee Members,	Thomas Whitworth III
	Gerald R. North
Interim Head of Department,	John Morse

May 2006

Major Subject: Oceanography

ABSTRACT

A New Account of Ross Sea Waters: Characteristics,
Volumetrics, and Variability. (May 2006)
Christina Lee Stover, B.S., Coastal Carolina University
Co-Chairs of Advisory Committee: Dr. Alejandro H. Orsi
Dr. Achim Stoessel

A new high-resolution climatology and volumetric θ-S census ($\Delta\theta = 0.1°C$, $\Delta S = 0.01$) is constructed for the Ross Sea. Property maps (potential temperature, salinity, and dissolved oxygen) along 40 depth levels and 21 neutral density (γ^n) surfaces are analyzed.

A major inflow of Antarctic Surface Water (AASW) is observed branching off the westward-flowing coastal current near Cape Colbeck. One portion continues poleward hugging the coast while the other follows the shelf break to the west. The characteristic "V" shape of the Antarctic Slope Front over the western Ross Sea is indicated by a narrow stream of thickened AASW. The entire AASW layer shoals from east to west.

Two major shoreward inflows of Lower Circumpolar Deep Water (LCDW) are inferred. A warm and salty tongue from the Balleny Gyre enters the Drygalski and Joides troughs. A similar tongue is exported from the Ross Gyre and enters the Glomar Challenger Trough. No significant LCDW inflow is observed over the eastern slope of the Ross Sea.

The thickest outflows of Shelf Water (SW: $\theta \leq -1.85°C$, $S > 34.5$) and new Antarctic Bottom Water (AABW: $\theta > -1.85°C$, $\gamma^n > 28.27$ kg m^{-3}) are found along the Drygalski and Joides troughs. Their saltiest ($S > 34.7$) components are concentrated in the western Ross Sea, whereas the low-salinity varieties are found throughout the Ross Sea shelf.

The most voluminous water mass in the Ross Sea is LCDW. The least abundant is AABW found primarily over the western slope. Modified CDW (MCDW) in the western Ross is inferred to be a mixture of 30% AASW and 70% LCDW; whereas central (eastern) MCDW is 40% (60%) AASW and 60% (40%) LCDW. The same water

mass composition is inferred for new AABW in the western and central Ross Sea: 25% SW and 75% MCDW.

A 40-year freshening trend is detected at different sites along the coastal transit of AASW from Cape Colbeck to Ross Island. In addition to a freshening, the MCDW and high-salinity SW also reveal a cooling trend. Conversely, a warming and salinification is indicated at the main inflows of LCDW.

DEDICATION

To my “fabulous five” who have supported every crazy decision I have ever made, loved me unconditionally, and believed in me even when I didn’t. To them I owe everything for they have allowed me to see the world in the most beautiful ways.

ACKNOWLEDGEMENTS

First, thank you to my committee co-chairs, Dr. Alejandro Orsi and Dr. Achim Stoessel for giving me the opportunity to pursue a master's degree and for always having an open door. Their tremendous encouragement, guidance, and financial support are greatly appreciated. I thank my other committee members, Dr. Thomas Whitworth III and Dr. Gerald North for their advice and expertise throughout the course of this research. An additional thanks is extended to the National Science Foundation whose funding made this project possible.

A very big thank you goes out to my friends, fellow Oceanographers at Texas A&M University, and the ladies of 716B. I am indebted to them for the great adventures and opportunities I have experienced while being here.

An infinite amount of gratitude goes to Brian Wiederwohl who offered endless hours of support, encouragement, and love.

Finally, to my parents and brothers I owe many thanks for their moral support and wisdom; and to Grannie for just loving me "bushels."

NOMENCLATURE

AABW	Antarctic Bottom Water
ACC	Antarctic Circumpolar Current
AASW	Antarctic Surface Water
ASF	Antarctic Slope Front
CDW	Circumpolar Deep Water
HSMSW	High-Salinity Modified Shelf Water
HSSW	High-Salinity Shelf Water
ISW	Ice Shelf Water
LCDW	Lower Circumpolar Deep Water
LSMSW	Low-Salinity Modified Shelf Water
LSSW	Low-Salinity Shelf Water
MCDW	Modified Circumpolar Deep Water
MSW	Modified Shelf Water
SODB	Southern Ocean Database
SW	Shelf Water
θ-max	Temperature Maximum
θ-min	Temperature Minimum

TABLE OF CONTENTS

LIST OF FIGURES

FIGURE Page

LIST OF TABLES

INTRODUCTION

The Southern Ocean has long been recognized for hosting important water mass transformations and unique exchanges of heat and freshwater with the rest of the World Ocean (Wüst, 1935; Deacon, 1937, 1984). Surface waters of the Antarctic Zone undergo intense cooling from the polar atmosphere and brine injection during sea-ice formation in the austral winter. Over certain continental margins around Antarctica, cooling and sea-ice formation can further convert this near-freezing Antarctic Surface Water (AASW) into the densest water mass found around Antarctica, known as Shelf Water (SW; Carmack, 1977). In turn the meridional circulation of the Southern Ocean brings relatively warm and saline Circumpolar Deep Water (CDW) exported from the Antarctic Circumpolar Current (ACC) to subsurface levels near the Antarctic shelf break (Figure 1).

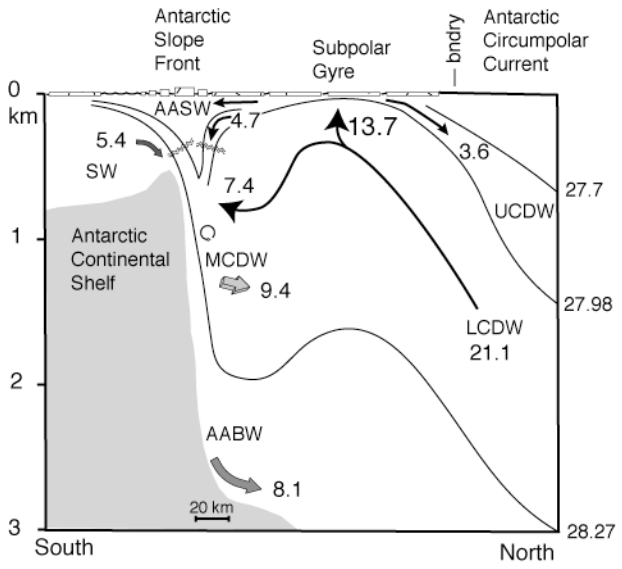

Figure 1. Schematic cross-slope section of the overturning of Southern Ocean water masses. Solid lines represent neutral density surfaces (kg m^{-3}). Numbered arrows correspond to water mass transport and production rate estimates derived from indirect CFC budgets (Orsi *et al.*, 2002).

This thesis follows the style of Deep-Sea Research: Part I.

Sharp subsurface property gradients are found across much of the narrow transition between the Antarctic shelf and oceanic regimes. These gradients indicate the presence of the Antarctic Slope Front (ASF), where intense diapycnal mixing is inferred between the temperature maximum of the Lower CDW (LCDW) and the AASW lying at the base of the winter mixed layer. As a result, Modified Circumpolar Deep Water (MCDW) is formed having properties intermediate to those of its parent water masses. Its circulation further inshore is commonly deduced from temperature patterns along a subsurface core layer (temperature maximum and oxygen minimum).

Dense SW flows cyclonically within the major depressions of the Antarctic shelves, often reaching the sills located along the shelf break. At a few of these sites bottom waters even denser than the CDW continuing eastward through Drake Passage can be produced, namely AABW (Orsi *et al.,* 1999). This AABW results from the intense vertical mixing of SW and MCDW, and it is dense enough to sink down the continental slope and fill the abyssal layer of the World Ocean.

The Ross Sea

The Ross Sea was once thought to be a minor contributor in the global production of AABW. Foldvik and Gammelsrod (1988) accredited 80% of AABW production to the Weddell Sea, leaving a mere 20% to other productive regions. Contrary to this belief, the Pacific (Ross Sea) and Indian sectors of the Southern Ocean can contribute as much as 40% (3.2 Sv) of the AABW total (Orsi *et al.*, 1999). Independent estimates based on regional numerical models also suggest that 3 to 4 Sv of new AABW must outflow from the Ross Sea shelves (Dinniman *et al.,* 2003).

This study attempts to improve the understanding of the regional circulation and stratification in the southwestern corner of the Pacific Ocean (Figure 2), including the Ross Sea: the triangular-shaped region south of the 2000-m isobath between Cape Adare and Cape Colbeck (5.66×10^5 km^2). The Ross Sea occupies about 23% of the Antarctic continental margins (Carmack, 1977). To the south the Ross Sea is bound by the 200 - 250 m thick floating Ross Ice Shelf (Jacobs, 1989), so only deeper subsurface waters can circulate farther inshore (Budillon, *et al.*, 2002).

A conspicuous characteristic of the Ross sea continental shelves is the rugged seafloor topography, which on average is about 685 m deep. There are several deep troughs that connect the continental slope with the grounding line of the Ross Ice Shelf. Their sills' average depth is about 550 m, but 4% of its area inshore of the sills is shallower than 400 m and 46% is deeper than 550 m.

Relatively favorable navigational conditions and a strategic location have played a role in the Ross Sea currently being one of the best sampled coastal regions around Antarctica. This study takes advantage of a new Southern Ocean Database (SODB) derived during the construction of the WOCE Southern Ocean Atlas (http://woceatlas.tamu.edu). Its availability provides incomparable opportunities to analyze a high-quality hydrographic data set first hand. In addition to the SODB, the recent U.S. AnSlope (2003-2004) and Italian CLIMA (1995-2004) programs have provided extensive CTD data: 1464 stations whose data has not yet been released to the public. These two programs have improved considerably the spatial distribution of the available historical data and also have provided the first direct current measurements at the main outflow regions of AABW in the Ross Sea.

The location of the 4364 bottle and CTD stations available for this study are shown as blue dots in Figure 3; but additional outside stations (red dots) were used to reduce errors during the objective mapping of properties near the edges of a high-resolution grid of the study area. All hydrographic stations were collected between 1928 and 2004. Due to the vast sea-ice coverage in the Ross Sea, this database is mainly representative of austral summer conditions (October – April). The expected seasonal differences due to winter surface cooling and sea-ice formation would only affect the properties of the upper 200 m (Gordon, 2000), thus rendering a somewhat cooler and saltier AASW than depicted in this study.

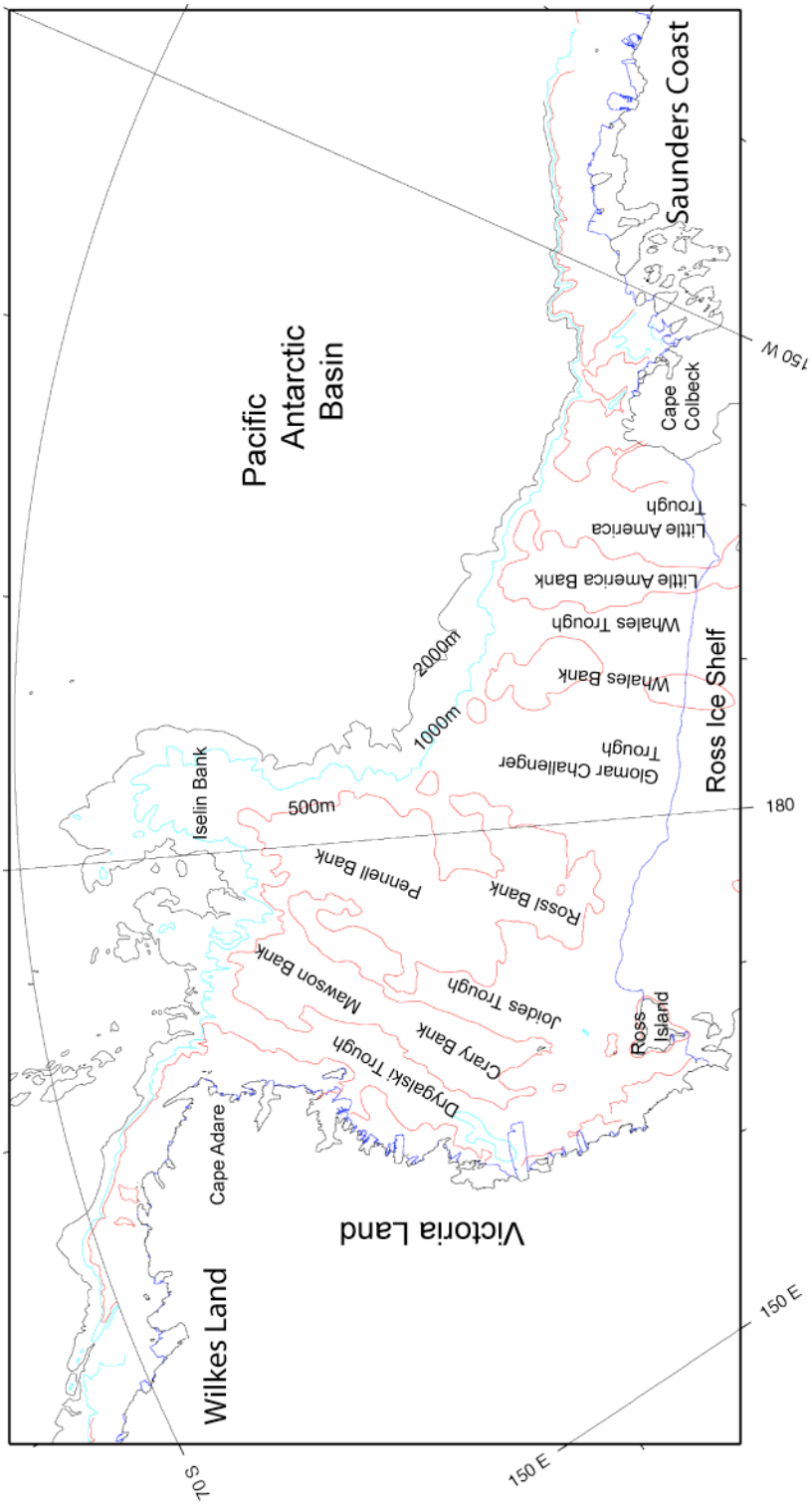

Figure 2. Study area shown in equal-area stereographic projection. The major depressions and banks of the Ross Sea are labeled. The three isobaths shown are 2000-m (solid black line), 1000-m (solid cyan line), and 500-m (solid red line); the ice shelf edge is shown as a solid blue line.

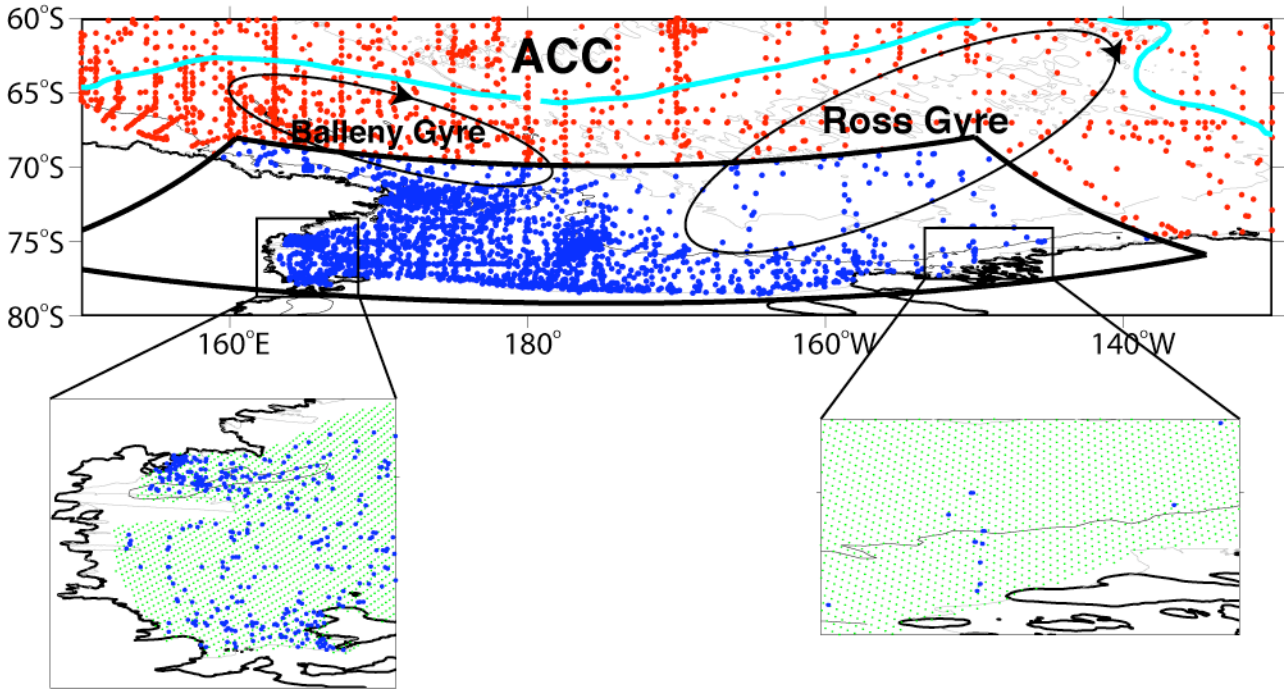

Figure 3. Distribution of all hydrographic stations available during the construction of the Ross Sea climatology. There are 4364 stations (blue dots) within the Ross Sea grid whose boundary is indicated by the thick black line. Additional stations outside of the grid (red dots) were also used to reduce mapping errors near the boundaries. The eastward flow of the Antarctic Circumpolar Current extends north of the cyan line. The two bottom subsets show the contrast between the spatial resolution of the Ross Sea grid (green dots) and the actual station locations (blue dots). Unlabeled gray contours north and south of 75°S are the 4000-m isobath and the Ross Ice Shelf edge.

Water Masses

CDW carried eastward by the ACC is one of the most voluminous water masses in a World Ocean census (Worthington, 1981). Only its Lower portion (LCDW) is able to circulate to the south of the ACC in the subpolar regime (Orsi, *et al.*, 1995), where it is identified as a thick intermediate layer of relatively high temperatures and salinities and low oxygen concentrations (Gordon, 1982). LCDW enters the Ross Gyre (Figure 3) near its eastern limb and continues southwestward to become the major source of heat and salt for the study region (Locarnini, 1994). Ross Sea LCDW (Figure 4) is found within the 28.00 - 28.27 kg m^{-3} neutral density layer (Orsi, *et al.*, 2002). Onshore transport of LCDW is thought to be sporadic and occur only at specific locations, likely dictated by the shelf topography (Dinniman *et al.*, 2003). Shoaling of LCDW to near sea surface levels has also been observed near the shelf break in the past (Jacobs, 1991).

AASW is the relatively light surface water lying above the local subsurface temperature maximum induced by LCDW (Whitworth *et al.,* 1998). Because it lies at the air/sea-ice interface, AASW in the Ross Sea shows a large range of potential temperatures (θ = -2.3 °C to 2°C) and salinities (S $\approx$ 33 to 34.4 along the freezing point). AASW of the oceanic regime extends from the sea surface to the base of the winter mixed layer, which is indicated by the summer subsurface temperature minimum found between 50 m and 200 m (Whitworth, *et al.*, 1998). Relatively warmer AASW in the Ross Sea is found typically along the southern continental shelves, where the pack ice opens up first in early summer (Jacobs *et al.*, 1970).

MCDW is formed near the shelf break from the mixture of the relatively fresh (S < 34.4) and near-freezing AASW with the oxygen-poor LCDW below (Newsom, *et al.*, 1965). Even though there is no apparent void of θ-S points in Figure 4 within the LCDW/MCDW density layer, the spatial distribution of properties on isopycnal maps indicate the relative cold and low salinity signal of MCDW over the continental margin. (Whitworth, *et al.*, 1998).

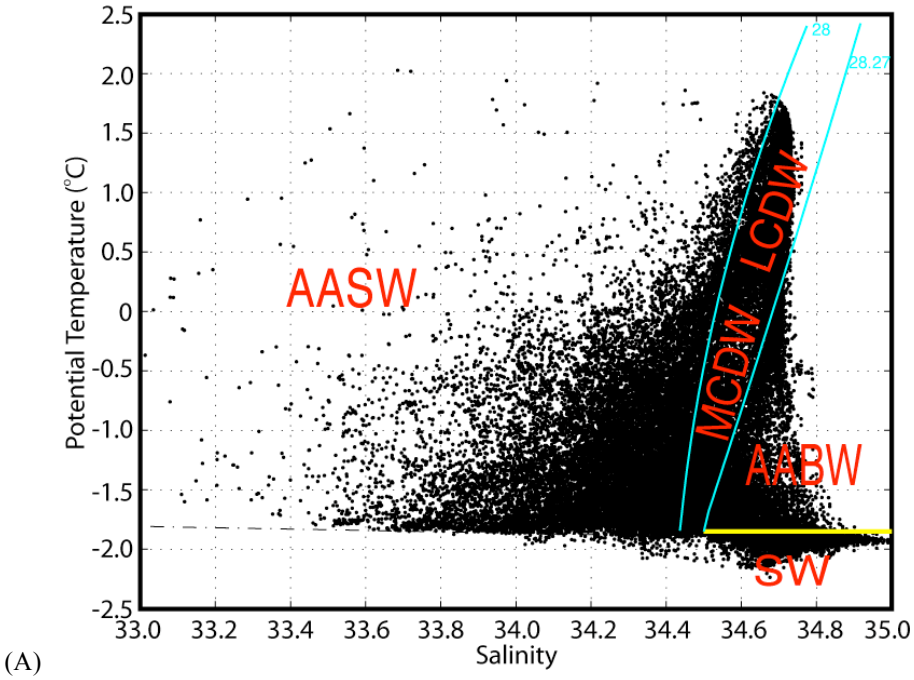

(A)

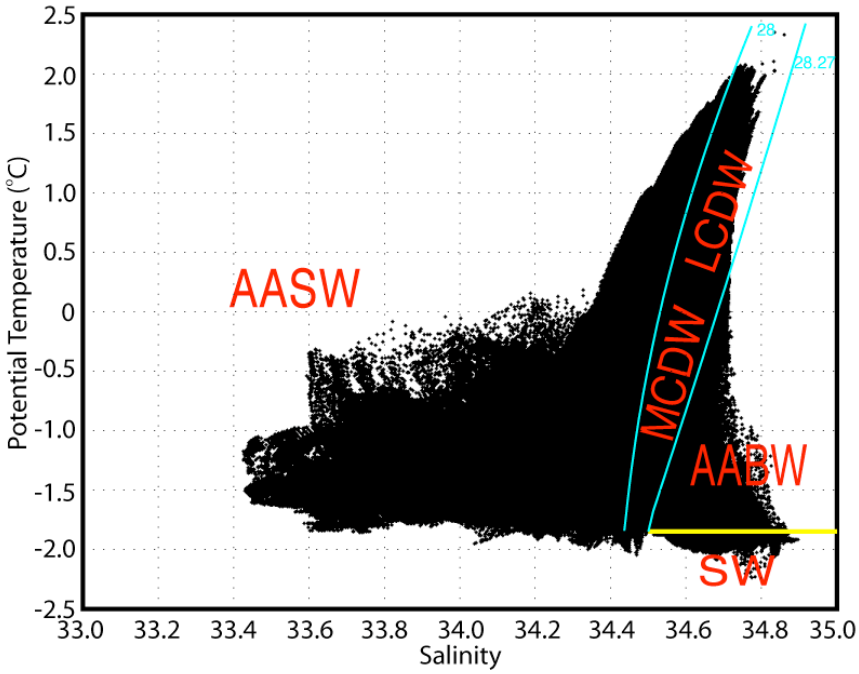

(B)

Figure 4. θ-S scatter plots for data from (A) hydrographic stations within Ross Sea grid and the (B) new climatology. LCDW/MCDW neutral density boundaries (γ^n = 28.00 kg m^{-3} and 28.27 kg m^{-3}) are indicated by the thin cyan curves. SW domain is defined by $\theta \leq$ -1.85°C (thick yellow line) and $\gamma^n >$ 28.27 kg m^{-3}.

SW of the Ross Sea is the saltiest (up to 35) and densest water in the Southern Ocean (Carmack, 1977). It is found in all troughs greater than the average sill depth. SW is produced during the austral winter as the result of intense surface cooling and sustained sea-ice formation, releasing enough brine to increase the density of the surface water to values higher than those found in the oceanic AASW (Locarnini, 1994; Smethie and Jacobs, 2005). Consequently, SW shows a relatively narrow range of potential temperatures near the surface freezing point (Figure 4), but a broad range of salinities, from about S = 34.55 to near 35. SW, as defined here, has neutral densities greater than 28.27 kg m^{-3} (Orsi *et al.*, 1999; Whitworth *et al.,* 1998).

A sharp horizontal salinity gradient within the Ross Sea SW layer is inferred near 175°W (Locarnini, 1994; Orsi *et al.*, 1999), which perhaps leads to its original regional classification into western (high salinity: HSSW) and eastern (low salinity: LSSW) SW types (Jacobs, 1970). Smethie and Jacobs (2005) still refer to HSSW only when considering waters with near-freezing temperatures (-1.91°C to -1.85°C) and west of 180°. It is important to note, however, that these are all arbitrary definitions (Locarnini, 1994), since there is no well-defined demarcation in θ-S space between HSSW and LSSW. For example, Budillon *et al.* (2002) classified Ross Sea HSSW as water with potential temperatures between -1.95°C and -1.75°C and salinities between 34.75 and 35; whereas for Carmack (1977) the HSSW and LSSW found over the entire Southern Ocean domain are divided at the 34.6 isohaline.

The bulk of salty SW moves cyclonically within the Ross Sea (Budillon, *et al.*, 2002) and away from the production sites, which are thought to be restricted to the narrow coastal open water areas off the coast of Victoria Land (Terra Nova Bay Polynya) and along the Ross Ice Shelf (Ross Ice Shelf Polynya). As HSSW flows under the 200-250 m deep underside of the Ross Ice Shelf it is cooled even further. Potential temperatures below the freezing point at the sea surface are commonly identified as Ice Shelf Water (ISW; Carmack, 1977; Budillon, *et al.*, 2002; Dinniman *et al.*, 2003; Smethie and Jacobs, 2005), with an average salinity of 34.62. The characteristic deep temperature minimum of ISW is most commonly found around 180°, surrounded by

HSSW to the west and LSSW to the east (Dinniman, *et al.* 2003; Smethie and Jacobs, 2005). The exact ISW formation mechanism is not fully understood, but Smethie and Jacobs (2005) speculate that a mixture of either HSSW or LSSW and glacial melt water can produce it. Even though the largest volume of relatively fresh SW occupies the eastern Ross Sea, some LSSW is still found west of 180° within a relatively thin layer lying just above HSSW (Whitworth, *et al.*, 1998).

Intense tidal vertical mixing of SW with the local MCDW found near the shelf break of the Ross Sea is known to produce new bottom water (Locarnini, 1994). Consequently, AABW could not be formed without a SW ingredient (Orsi, *et al.*, 1999). This water is always more dense than its lighter MCDW parent ($\gamma^n > 28.27$ kg m^{-3}: Orsi, *et al.,* 1999). When found over the continental shelf it is considered Modified Shelf Water (MSW) until it clears the sills, sinking to become AABW. Documented outflows of AABW are located near 173°E, 177°E, 175°W (Jacobs *et al.*, 1970), and 168°W (Locarnini, 1994). AABW leaving the northwest Ross Sea is the warmest (-0.6°C to -0.3°C) and saltiest ($S > 34.75$) of all outflows around Antarctica. Its high salinity ($S > 34.70$) signal extends off the shelf at 173°E and fills the northwest sector of the Pacific Antarctic Basin (Locarnini, 1994). A relatively fresh ($S \leq 34.70$) AABW outflow colder than 0°C appears to sink across the shelf break at 168°W and to continue northward along the eastern slope of the Iselin Bank (Locarnini, 1994; Orsi, *et al.*, 1999). Relatively fresh AABW also reaches down to as deep as 3000 m at 175°W.

Export of Ross Sea Bottom Water contributes to the net cooling and ventilation of the deep ocean, making the Ross Sea a key player in the Global Thermohaline Circulation (Orsi, *et al.*, 1999). At the northwestern end of the Balleny Gyre (Figure 3), low-salinity AABW ($S < 34.7$) with origins in the Ross Sea continues westward along the continental slope and into the deep Australian-Antarctic Basin (Orsi *et al.*, 1999). This AABW outflow from the Pacific effectively freshens and ventilates the Indian abyssal layer. In contrast, AABW within the interior of the Ross Gyre circulates within two dome-like cells at levels shallower than 2400 m.

AABW circulation patterns and modes of production have long been an area of interest to modelers (e.g. Fichefet and Goosse, 1999; Goosse *et al.*, 2001; Dinniman *et al.*, 2003). Ocean general circulation models tend to produce AABW mostly through open-ocean convection rather than near-boundary convection as observed (Gordon, 1998). Recent studies have improved the match of model results to actual hydrographic measurements. For example, Kim and Stössel (2001) achieved more realistic deep-ocean properties when conventional convection adjustment was replaced by a plume convection parameterization. Model results are generally compared with climatologies, e.g. that from Levitus (1982). With higher resolution and more sophisticated parameterizations, such comparisons will become insufficient. Instead, products of this kind intended here will have to be referred to for model validation.

Quantitative Analysis

Even with all the extensive recent research in the Ross Sea, many uncertainties remain about the major local water mass transformations. There are standing questions with regard to which water masses, and in what proportions, are transformed into other waters, e.g. the amounts of MCDW and SW involved in the formation of AABW. The exact locations where these transformations take place are still unknown. An updated high-resolution volumetric θ-S census will shed new light on these questions at hand.

A volumetric θ-S census, generically, is the computation of water volumes within specific intervals on a θ-S plot. This quantitative approach to water mass analysis is useful because it allows for a concise summary of hydrographic conditions in specific regions. These volumes become practical starting points for more advanced water mass, property budget, and circulation studies (Carmack, 1977). For example, in conjunction with property variance studies derived from station data, the volumetric θ-S census becomes particularly convenient for identifying anomalous regions. An improved spatial sampling and quality of data available to us also warrants better estimates of SW residence times and AABW outflows. Unbiased methods (optimal mapping) used to construct the new climatology in the Ross Sea will improve the overall patterns of property distributions. New estimates of the Ross Sea meridional overturning

circulation will also benefit from the combined examination of temperature-salinity-dissolved oxygen relationships, the volumetric θ-S census, and recent long-term direct current measurements.

A new θ-S census of Ross Sea waters using the SODB is warranted to improve our understanding of its quantitative stratification. The only previous values available are those reported in Carmack (1977), which were based on data from 900 hydrographic stations located south of the Polar Front with just 53 within the Ross Sea. Thus, Carmack's estimates of specific water mass volumes relied heavily on the subjective weighting of sparse data points. Recently, progressively larger data sets with better spatial distributions have naturally prompted the production of climatologies with increased spatial resolution, e.g. the World Ocean Atlas climatology series produced by the National Oceanographic Data Center went from 1-degree horizontal grid in 1994 to a ¼-degree in 2003.

A full water column volumetric θ-S census for the study area will be computed from all new optimally mapped property fields. Additionally, these mapped property fields will aid in the description of regional water mass characteristics and circulation, as well as provide insight to areas of high temporal variability. Analysis of these mapped fields will further pin-point the most suitable local boundaries to regionally study the Ross Sea, e.g. it will assist in separating distinct water mass regions like western, central, and eastern regions, as well as slope, outer shelf and inner shelf areas. More specific mixing recipes will be deduced based on regionally averaged potential temperature and salinity relationships. A new finer-grid climatology and volumetric θ-S census will also foster more accurate comparisons with global ocean models, specifically those indicating a more important role of the Ross Sea's contribution of AABW in the Southern Ocean.

ROSS SEA CLIMATOLOGY

Construction

Fields of potential temperature (°C), salinity, and dissolved oxygen (ml l^{-1}) for the study area were constructed by combining all quality-controlled data from the SODB, as well as AnSlope and CLIMA data. The scarcity of reliable nutrient data (phosphate, nitrate, and silicate) did not justify their inclusion. Profile data were interpolated at 10-m intervals before being optimally mapped onto a high-resolution spatial grid specifically designed for the study area. This Ross Sea grid has nodes 5-km apart distributed uniformly on an equal-area polar projection. Along its edges (thick black lines in Figure 3) there are 207 zonal and 436 meridional nodes, and 65109 grid-points span the oceanic domain of the study area.

Five types of isotropic areas of influence (Figure 5A) were utilized in the objective mapping of properties. All five areas of influence are circles for linear, equal axes. Their radii varied gradually as dictated by the underlying bottom topography, both to resemble the expected change of length-scales in the local oceanographic features and to compensate for the general thinning of station coverage offshore. Property fields estimated at grid points located over the shelves, i.e. at water depths less than or equal to 500 m, were calculated using data from stations at most 55 km away; whereas grid nodes at water depths greater than 3500 m were influenced by data from stations as far as 250 km. Intermediate ranges of influence were used for grid points over the other three depth regimes: 104 km between 501 m and 1500 m deep, 153 km between 1501 m and 2500 m deep, and 201 km between 2501 m and 3500 m deep. Property fields were always computed using data from the nearest 41 stations to each grid point, or if fewer than 41 were available using all of the stations within the area of influence.

Because the majority of the stations occupy the shelf regime, grid points located over shallow waters are most likely influenced by the maximum number (41) of stations nearby, rather than from those located farther along the edge of the local circle of influence. For example, Figure 5B shows a grid point near the Drygalski Ice Tongue that used all 41 nearby stations, distributed at a mean distance of only 7.54 km, thus

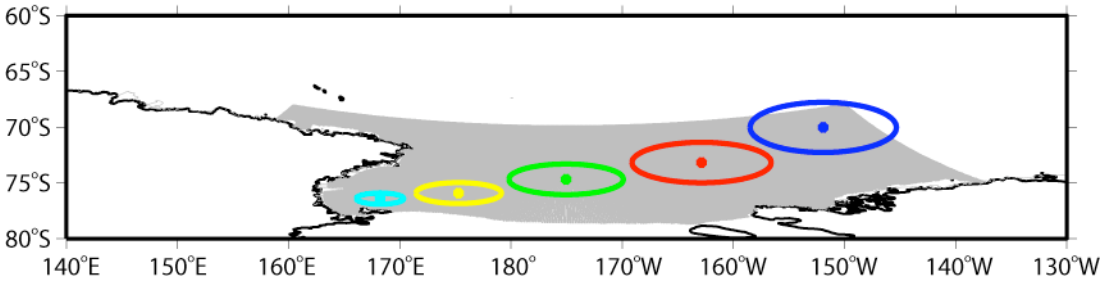

(A)

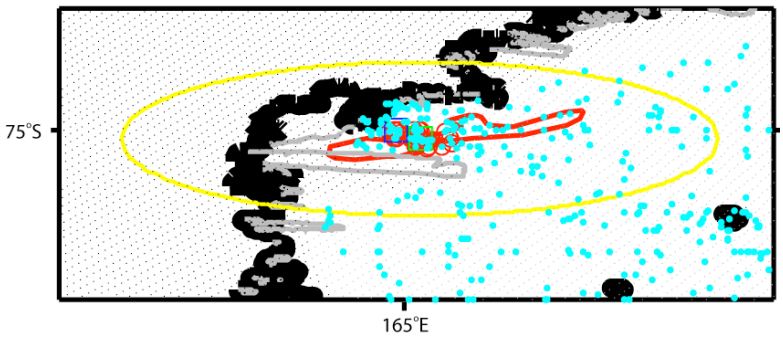

(B)

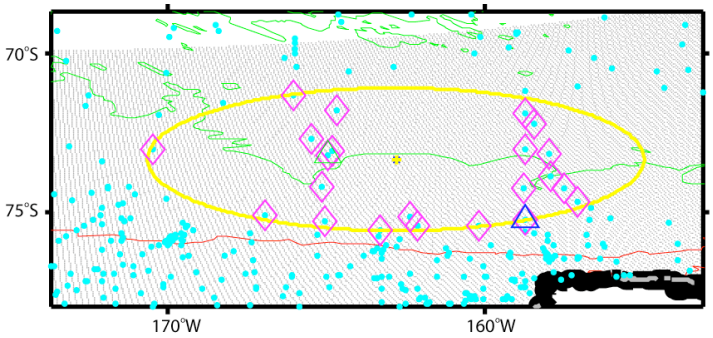

(C)

Figure 5. Isotropic areas of influence utilized for objective mapping with examples. Five sizes of isotropic areas of influence for the Ross Sea grid (gray shaded area). Examples are of (B) very localized influence within the area of influence (yellow circle), (C) poor station coverage, bathymetrically restricted by the (D) slope and (E) a trough, and (F) regions where grid points are near the grid boundary and incorporate stations outside of the grid domain still within the area of influence. These examples show all surrounding stations (cyan dots), stations used in mapping (red circles/magenta diamonds), nearest station to the grid point (green square), furthest station from the grid point (blue square), the coastline (thick black line), 1000-m isobath (red line), and 4000-m isobath (green line). Small black dots indicate grid points of either coastal, ice, or shallower regions, and small gray dots indicate the grid domain that is over oceanic regions.

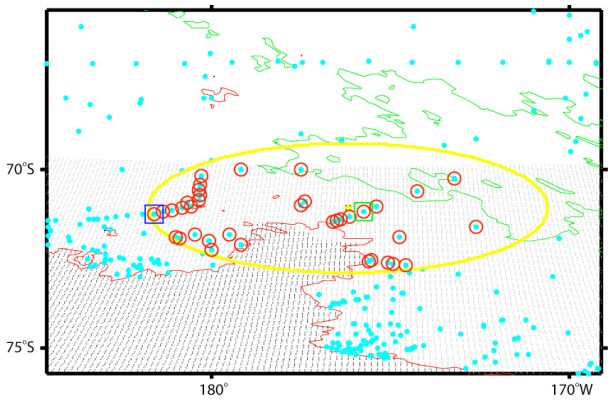

(D)

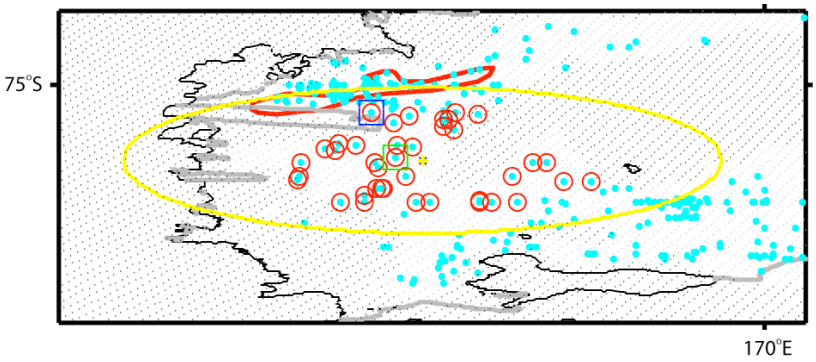

(E)

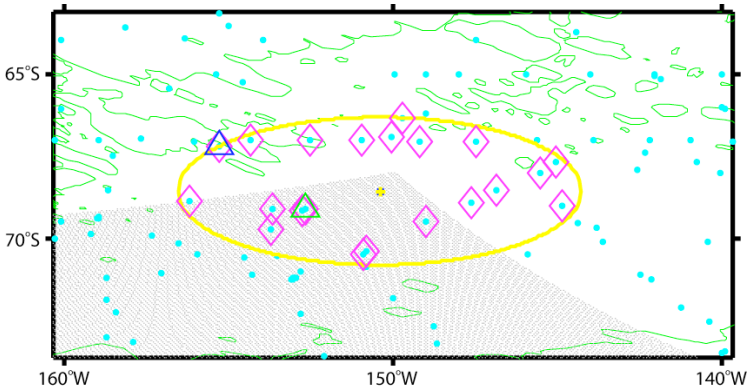

(F)

Figure 5. Continued.

providing a very localized influence. In contrast, some regions of the grid domain offered less than desirable sampling control, i.e. they have poor station coverage. This is the case for the grid point shown in Figure 5C, where only 23 stations are within the local influence circle. The closest is about 70 km away, and the average station distance is 190 km from the grid point. In some instances, obstructing topography can create irregular distributions of stations within the area of influence. This often precludes some grid points from sensing influence from particular directions or grid points being influenced by two hydrologically different regimes. Some of these bathymetrically restricted grid points are located at the slope, like the one shown in Figure 5D, with a non-isotropic influence mainly from stations located on each side of the Iselin Bank. Some grid points are located within inshore depressions of the Ross Sea (Figure 5E), whose orientation and irregular surroundings heavily bias the spatial distribution of the influencing stations. Nodes located near the edge of the offshore grid domain are actually influenced by the nearby stations outside the grid (Figure 5F). This is not only to guarantee a more isotropic influence, but also to minimize the overall mapping error, which tends to decrease when utilizing a larger number of stations. Even though these regions utilize the largest circle of influence, e.g. 250 km in Figure 5F, it is not uncommon to have fewer than 41 stations available to compute property variances. Figure 5F encircles only 23 stations at a mean distance of 192 km with about half of them located outside of the grid domain.

All property fields were mapped onto the grid at 40 standard depths (Table 1), and stacked to construct the new climatology of the Ross Sea.

Quality Control

To ensure static stability throughout the water column, the buoyancy frequency (N^2) was calculated at each grid-point location. Visual inspection of the climatology's N^2 profiles identified critical levels of instabilities (N_c^2) on three separate vertical layers: $N_c^2 = 25 \times 10^{-6}$ between 0 m and 800 m, $N_c^2 = 5 \times 10^{-6}$ between 900 m and 1600 m, and $N_c^2 = 1 \times 10^{-6}$ between 1800 m and 4250 m.

Table 1
Depth and neutral density levels used for the construction of the climatology.

Depth Levels (m)								Neutral Density Levels (γ^n)				
0	100	250	500	900	1400	2200	3250	27.60	27.90	28.10	28.27	28.45
10	125	300	550	1000	1500	2400	3500	27.70	27.95	28.15	28.30	28.50
25	150	350	600	1100	1600	2600	3750	27.75	28.00	28.20	28.35	28.60
50	175	400	700	1200	1800	2800	4000	27.80	28.05	28.25	28.40	28.70
75	200	450	800	1300	2000	3000	4250	27.85				

Grid level points with $N^2 < N_c^2$ were identified (flagged), then visually inspected, and finally minimally corrected to force stability above criticality throughout the water column. Values of potential temperature and salinity corresponding to grid samples flagged unstable were removed. The majority of the flagged properties were replaced with vertically interpolated values derived from an Akima spline interpolation to the stable (unflagged) profile data. A smaller number of corrections involved the replacement of flagged surface and bottom property values with values immediately below or above. In areas where the bathymetry is unreliable, e.g. near the ice shelf edges, entire profiles were flagged and removed. Any remaining flagged property values were visually compared against nearby station data, and corrected to match the local characteristics.

Although labor intensive, we believe this sequence of steps to substitute unstable samples is accurate and reliable. It is favored over other relatively fast automated protocols (Jackett and McDougall, 1995) that may preserve the basic original θ-S relationships, but do not preclude the systematic shifting of entire profiles that can result in the artificial creation of volumes of un-sampled water masses. The risk of having the same problem is much reduced when each unstable grid-point of the climatology is corrected based on the observed θ-S relationship in nearby stations.

Finally, the quality controlled climatological data were used to construct property maps on all of the original 40 depth levels (Table 1). These horizontal property fields were all visually inspected and corrected for potential problems in their spatial

distributions, in particular the likely aliasing from the station locations. A three-dimensional high-resolution field of neutral density (γ^n) was also calculated based on the corrected (stability validated) climatology. Potential temperature, salinity, and oxygen were interpolated along twenty-one neutral density surfaces (Table 1). Maps associated with these isopycnals were analyzed in combination with depth maps to infer lateral distributions of water masses and circulation patterns on and off the continental shelf.

Water Mass Boundaries

Station data is normally collected at sites where the most interesting stratification of water masses is observed and where important modifications take place; thus, the spatial distribution of stations within the Ross Sea is not even. Consequently, certain waters are better sampled than others. To some extent, the spatial uniformity of most existing climatologies, as well as this one, resolve this biased sampling while providing a more subjective estimation of water mass volumes.

Boundaries separating Ross Sea water masses quantified in this volumetric θ-S census are based upon existing criteria. The 28.00 kg m^{-3} neutral density surface serves as the bound between AASW and LCDW since it lies at the temperature maximum of LCDW in hydrographic stations found slightly offshore of the Ross Sea grid (Whitworth *et al.,* 1998). The 28.27 kg m^{-3} neutral density surface was used to separate LCDW and AABW (Orsi *et al.*, 1999). Thus the top, middle, and bottom density layers analyzed in this study span, by definition, the AASW, LCDW/MCDW, and AABW/SW, respectively.

For this study, water within the MCDW/LCDW density layer found inshore (offshore) of the shelf break, the700-m isobath, is MCDW (LCDW). Near-freezing volumes of SW fill the deepest troughs of the Ross Sea. To define the upper limit to this SW, plots of the distribution of potential temperatures versus the change in potential temperature with increasing depth ($\Delta\theta/\Delta z$) for all hydrographic stations found south of 76°S were inspected. Figure 6A shows that the scatter of the vertical thermal gradient versus narrows at a temperature colder than -1.85°C, suggesting this temperature to be a reasonable upper limit to a more thermally homogeneous benthic layer of Shelf Water.

In contrast, SW with potential temperatures above -1.85°C, but still with neutral density greater than 28.27 kg m^{-3}, has likely undergone some modification, e.g. by mixing with the MCDW above, and has not yet exited northward across the shelf break. Water with these characteristics found over the continental shelf (inshore of the 700-m isobath) will be referred to as Modified SW (MSW) or new AABW. This water found offshore of the 700-m isobath is AABW. Water with $\theta \leq$ -1.85°C will retain the SW classification.

SW bottom salinities in the Ross Sea show a dramatic shift at about 173°W (Figure 6B). Salinity at the bottom of the troughs ($z >$ 500 m) found east of this longitude are all lower than 34.70. Furthermore, at 173°W bottom salinities progressively increase from about 34.70 to 35 toward Victoria Land, indicating the western source region of HSSW over the Terra Nova Bay polynya. In this study a salinity of 34.70 is used to distinguish between the relatively saline and fresh SW types of the Ross Sea. Thus, we have divided the volumes of the bottom density layer into four classes: relatively saline ($S >$ 34.70) and fresh ($S \leq$ 34.70) types of both MSW ($\theta >$ -1.85°C) and SW ($\theta \leq$ -1.85°C; Figure 7). This will aid in determining more exactly the location and types of AABW formation.

Waters colder than the seawater freezing point at the sea surface have been generally referred to as ISW. However, the θ-S scatter plot for data from all the Ross Sea stations show that those characteristics are found throughout the continental shelf (Figure 6C). In contrast, SW with potential temperatures below the freezing point at 50 db (roughly -1.95°C) are not likely to originate from the near surface water during winter. Therefore, as a working definition for this study, we consider the -1.95°C isotherm as the upper limit to ISW. SW with potential temperatures colder than -1.95°C also coincides with the ISW definition of Jacobs and Giulivi (1998).

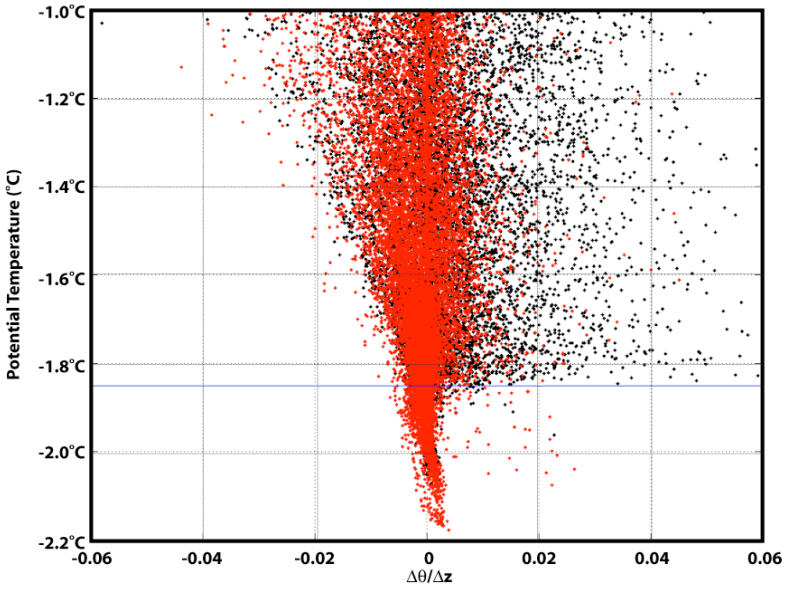

(A)

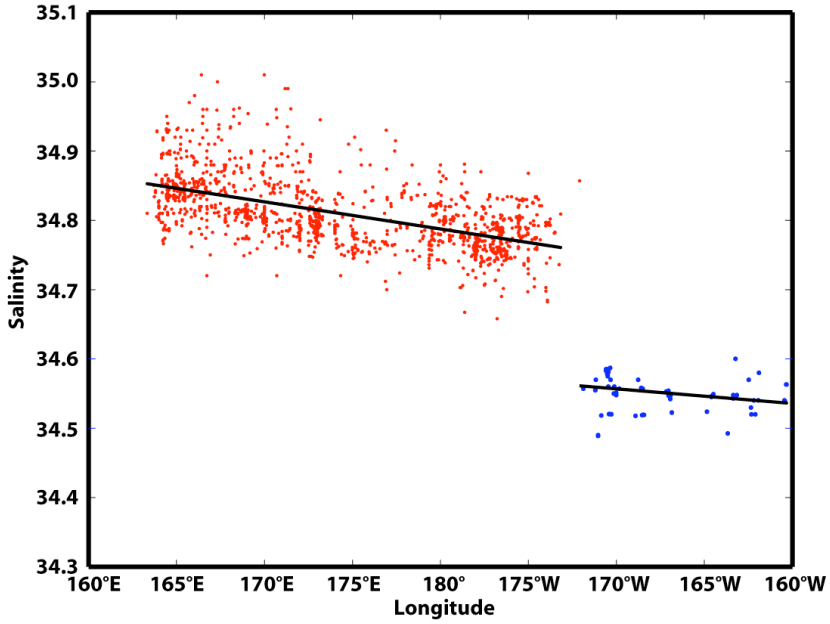

(B)

Figure 6. Water mass boundaries used for the Ross Sea. (A) Potential temperature versus Δθ/Δz of all Ross Sea stations south of 76°S (red dots) and north of 76°S (black dots) demonstrating the scatter of the vertical thermal gradient narrowing near -1.85°C (blue line). (B) Bottom SW salinity versus longitude from all Ross Sea stations (west of 173°W: red dots; east of 173°W blue dots) with best linear fit (black lines) for the two regional groups. (C) θ-S scatter plot of SW domain for all Ross Sea stations (black dots). θ-S values for bottom salinities in (B) are also shown (red and blue dots). The temperature freezing points at the surface (green dashed line) and 50db (cyan dashed line) are shown.

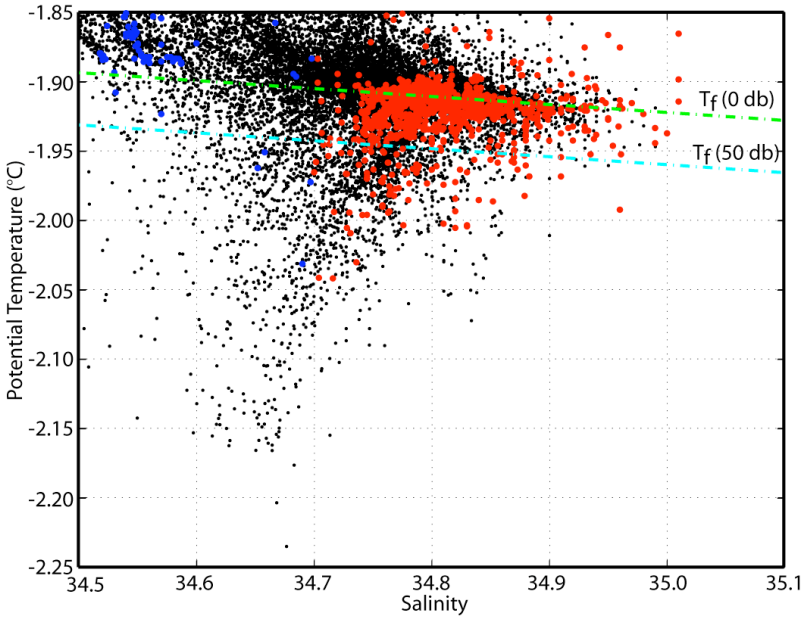

(C)

Figure 6. Continued.

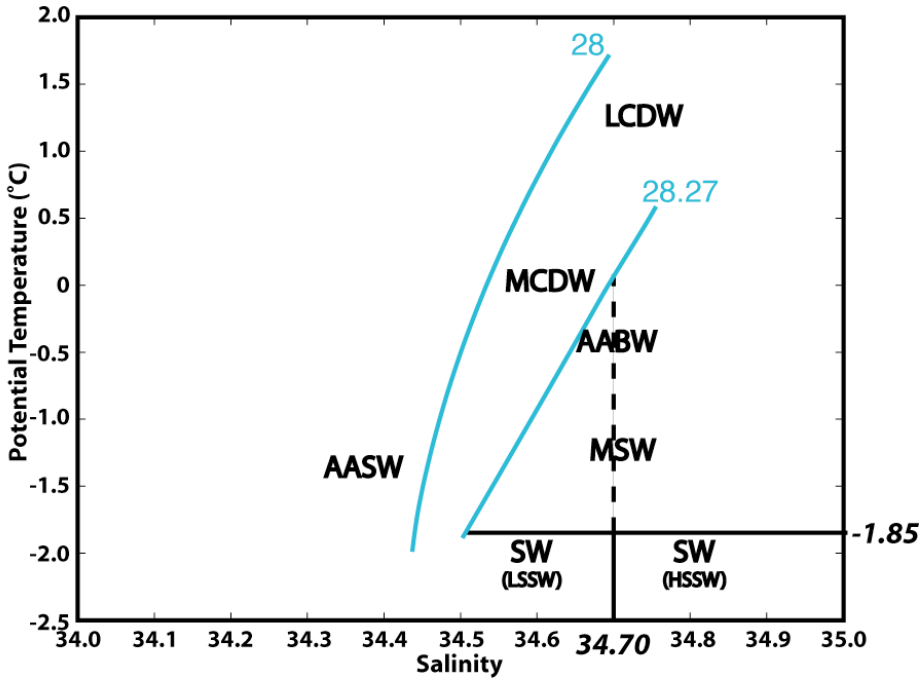

Figure 7. θ-S schematic of water masses present in the Ross Sea. Cyan lines represent the two neutral density surfaces, which encircle LCDW and MCDW. Black horizontal line serves as separations between SW from AABW and MSW, while the vertical black line/dashed line represents the boundary between high and low salinity SW and MSW (new AABW).

CLIMATOLOGICAL CIRCULATION AND STRATIFICATION

Coastal and Slope Currents

To depict the southwestward flow of AASW along the southern limb of the Ross Gyre, its further circulation within the Ross Sea, and the resulting subsurface frontal features, the characteristics and patterns of the top density layer and property maps at a few shallow levels were analyzed.

The topography at the base of the AASW layer, the 28.00 kg m^{-3} neutral density surface, is shown in Figure 8. It intersects the upper continental slope east of 160°W, thus this entire shelf regime (water depths < 500 m) is occupied by a single water mass – AASW. In contrast no AASW can be found within the western sector (west of 170°E) of the Ross Sea, where this isopycnal outcrops at the sea surface. Elsewhere in the Ross Sea the whole AASW layer is shallow enough to allow for the unobstructed flow of AASW, remaining well above the shelf break and the many shoals in the bottom topography. The γ^n = 28.00 kg m^{-3} isopycnal rises all the way from the bottom of the eastern Ross Sea continental shelf to the sea surface near 170°E.

Over the deep oceanic domain of the study area, the southwestward geostrophic flow, relative to a deeper reference level, of AASW along the southern limb of the Ross Gyre is indicated by the broad deepening of the 28.00 kg m^{-3} isopycnal south of about 72°S (Figure 8), from about 250 m to about 500 m at the continental slope east of 165°W. A less pronounced eastward downward tilt of this isopycnal appears across a narrow band oriented roughly along the date line, from the dome-like center shallower than 100 m to the rim depths > 200 m. This indicates a southward flow of AASW near the eastern end of the Balleny cyclone (Figure 3), which reaches towards the western flank of the Iselin Bank before continuing westward along the western slope of the Ross Sea towards Wilkes Land (Figure 2).

Over the continental margins, at water depths less than 2000 m, the relatively thick (H > 275 m), cold (θ < -1.3°C), and fresh (S < 34.25) surface layer (Figure 9A-C) found off of Saunders Coast (Figure 2) reveals a southwestward-flowing transport of AASW within the Antarctic Coastal Current. This southwestward flow splits around

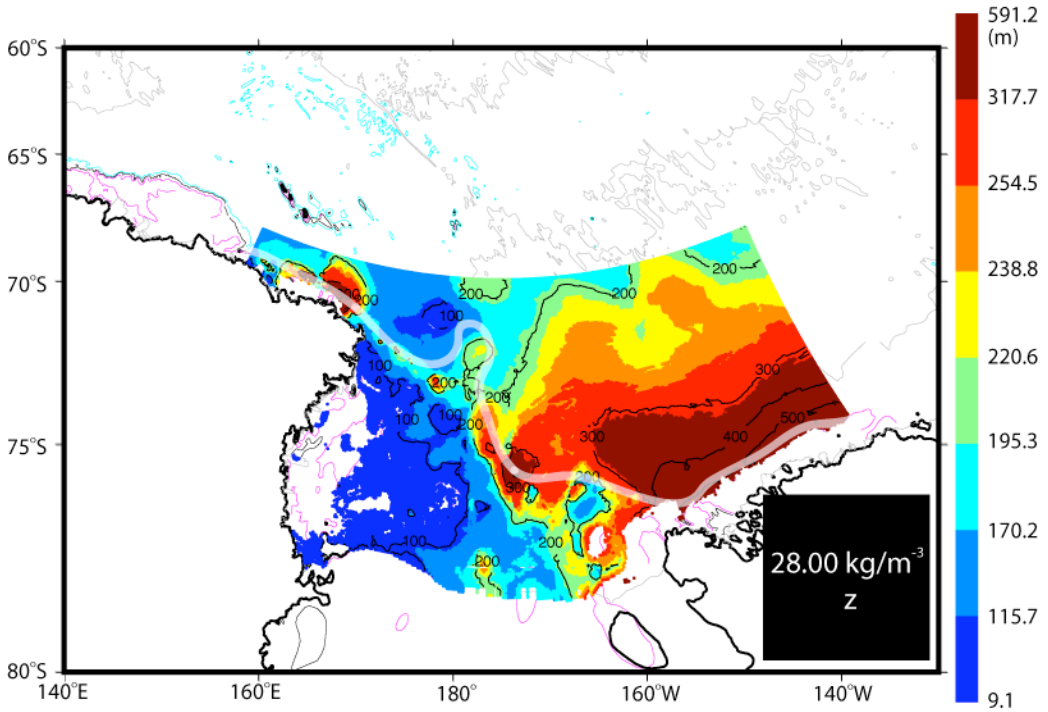

Figure 8. Depth of the 28.00 kg m^{-3} neutral density surface (base of the AASW layer). The four isobaths shown are the 500-m (magenta line), 1000-m (black line), 2000-m (cyan line), and the 4000-m (gray line). A trace of the 1000-m isobath over the grid area is shown by the white line. Color scale divisions are each 1/8 of the total mapped area.

162°W, 76°S (Figures 10A-C). A southward branch continues closer to the coast hugging the western side of the Little America trough (Figure 2) and approaches the eastern edge of the Ross Ice Shelf. At this location the base of the AASW layer is deep enough (~250 m) for some AASW to continue under the floating ice sheet, likely melting the basal ice and further reducing its potential temperature to below the surface freezing point.

The northern limb continues westward hovering near the shelf break in a snake-like fashion, distinguishable to as far west as Cape Adare (Figure 8). The volume carried by this slope current seems to be replenished by a fresher and cooler source (Figure 9B-C) near the northwestern tip of Iselin Bank by an input of AASW derived from the eastern limb of the Balleny Gyre (180°). A relatively thick layer (H > 160 m in

Figure 9A) of AASW is clearly observed roughly along the 800-m isobath between Iselin Bank and Cape Adare, where the 28.00 kg m^{-3} neutral density surface of the adjacent oceanic and shelf regimes surrounding this thick region lies shallower than 100 m (Figure 8).

A fresh river-like pattern on the westward transit of the Antarctic Slope Current along the slope of the western Ross Sea west of the dateline is in agreement with the expected "V" shaped configuration of the Antarctic Slope Front in that region. The low salinity signal of the waters filling this channeled flow is remarkably clear on maps at 175 m, 300 m, 400 m, and 500 m (Figures 10B-13B).

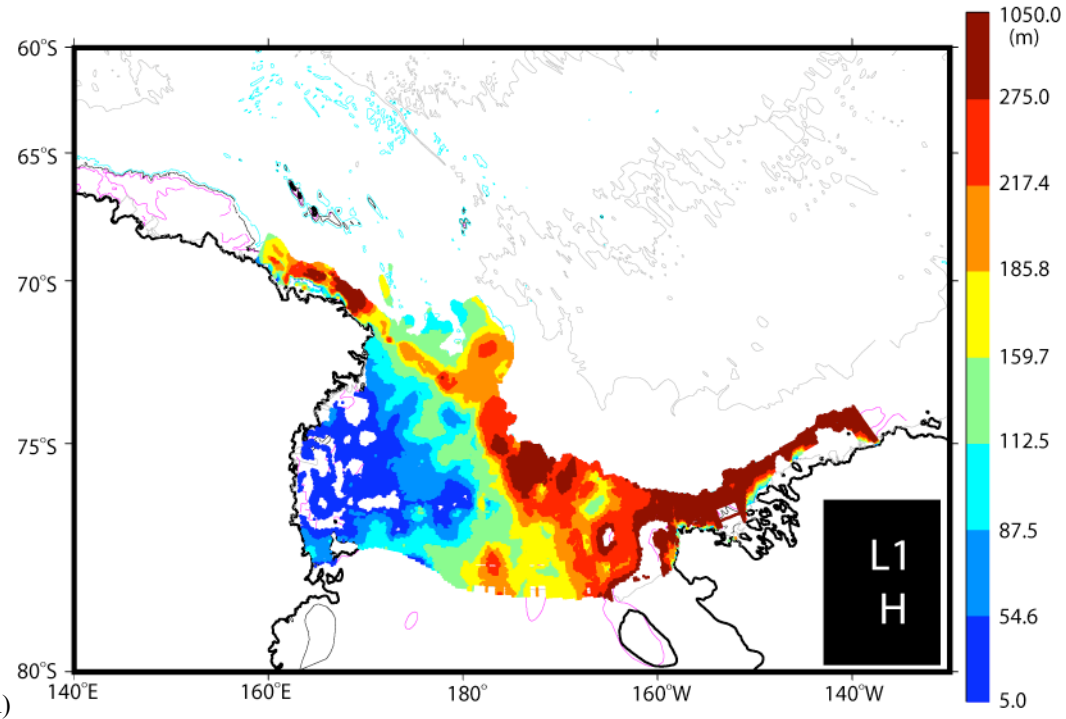

(A)

Figure 9. (A) Thickness, volume weighted (B) potential temperature, and (C) salinity of the top layer (L1: $\gamma^n < 28.00$ kg m^{-3}) representing AASW. Bathymetry and color distribution as in Figure 8.

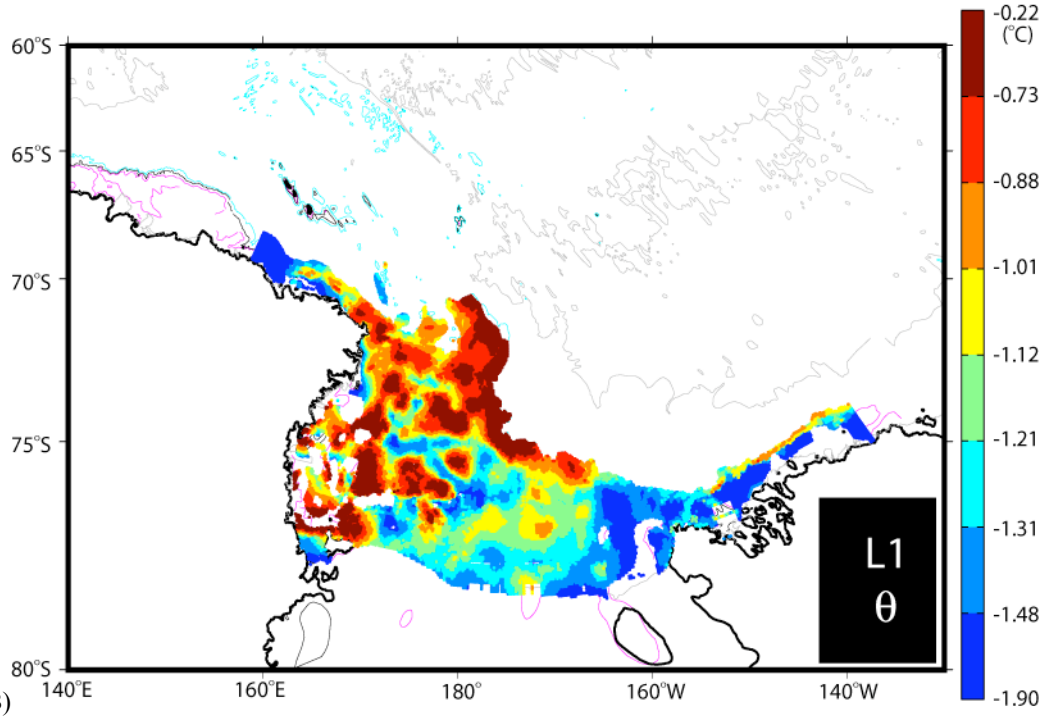

(B)

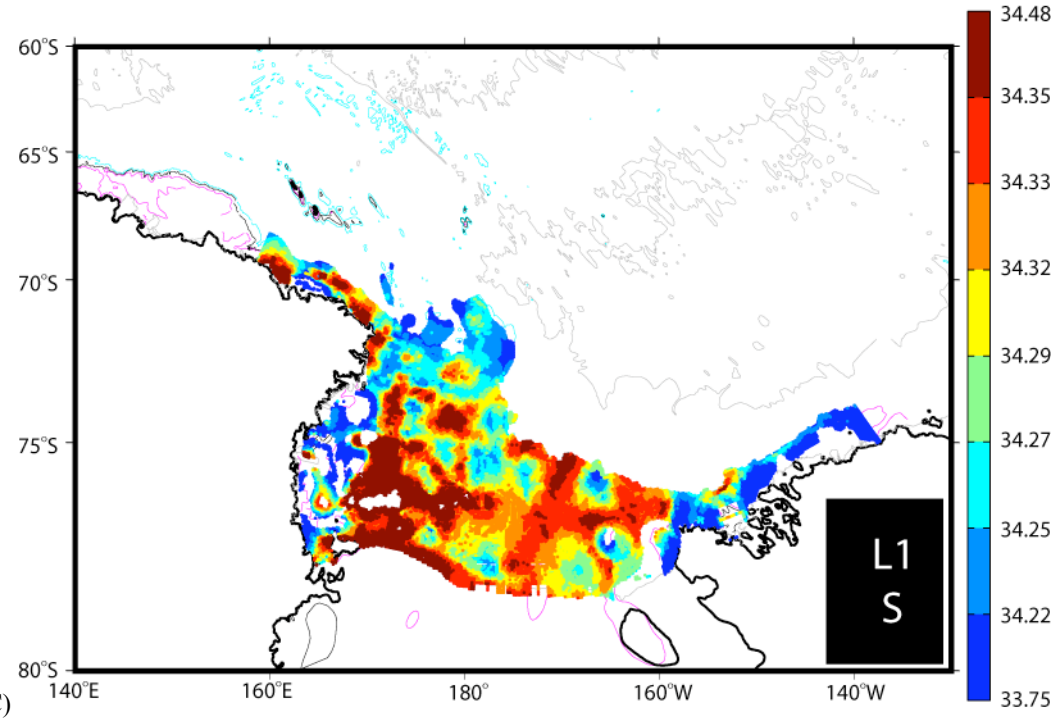

(C)

Figure 9. Continued.

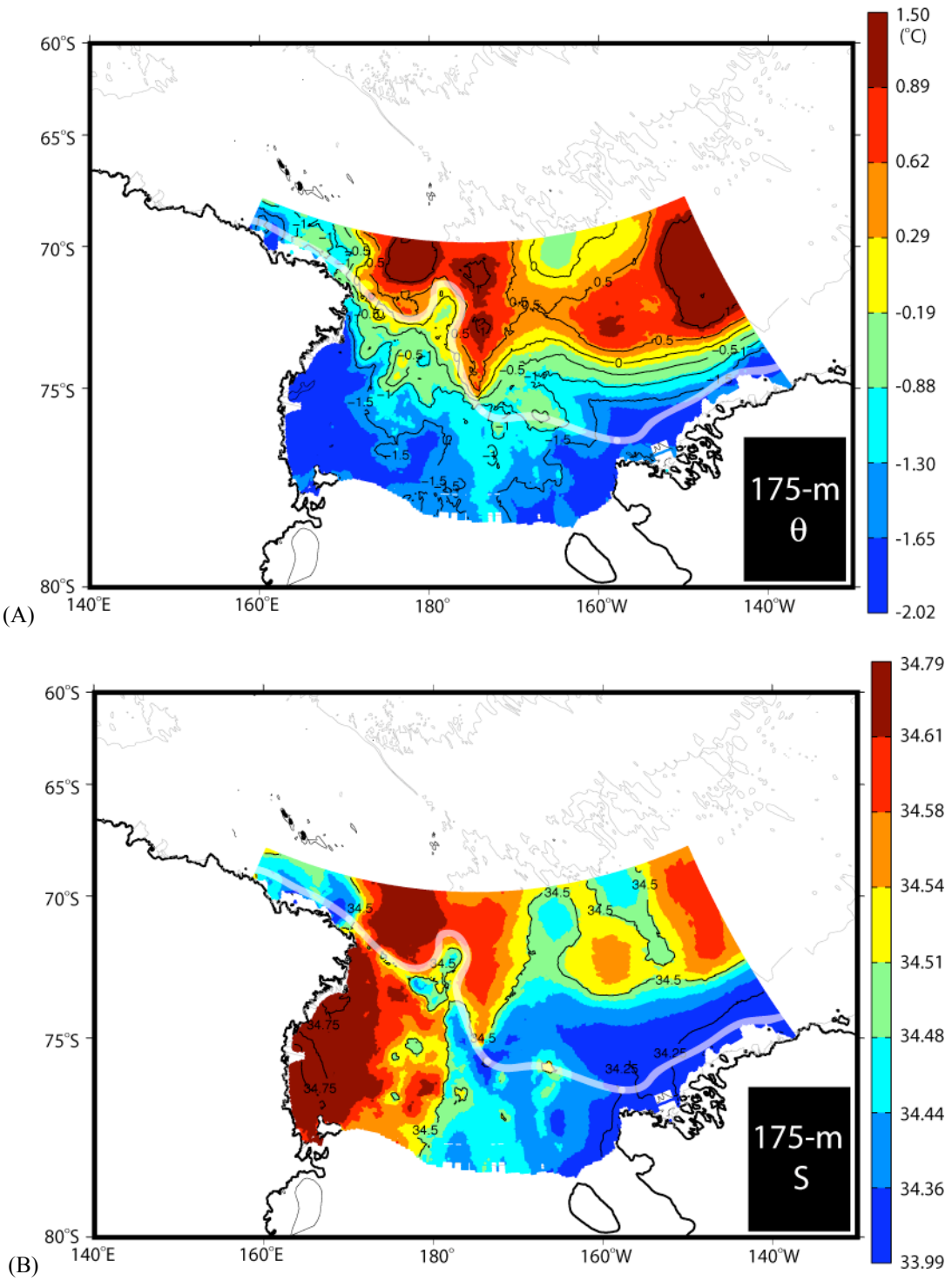

Figure 10. (A) Potential temperature, (B) salinity, and (C) neutral density at 175 m. Color distribution as in Figure 8. The two isobaths shown are the 1000-m (white line) and the 4000-m (gray line).

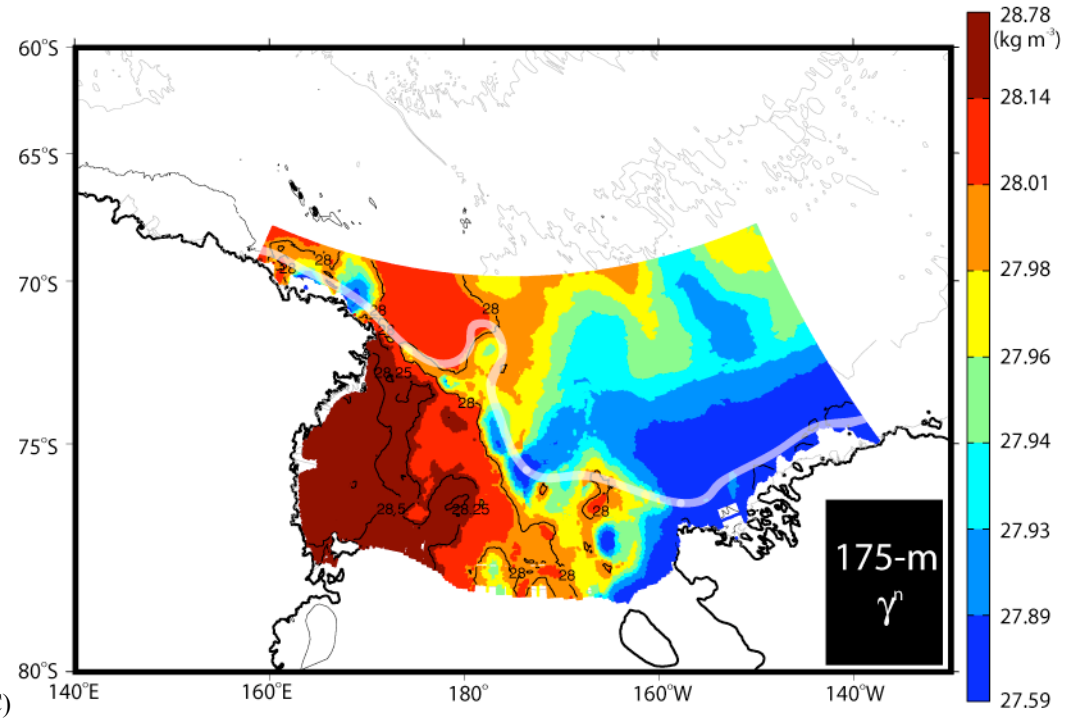

(C)

Figure 10. Continued.

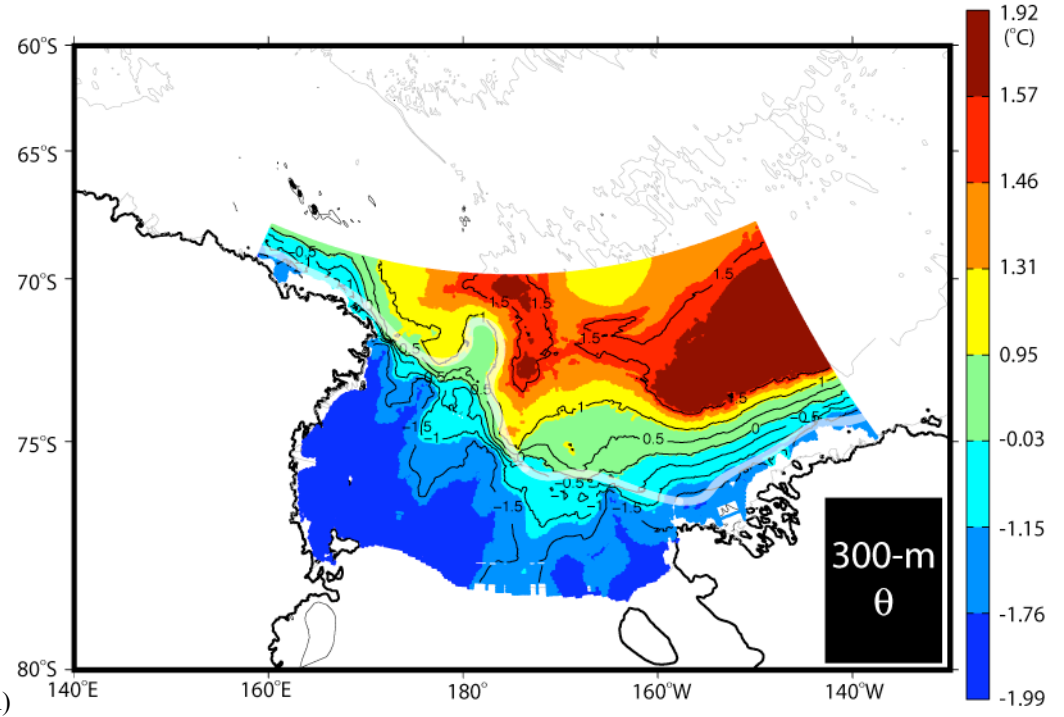

(A)

Figure 11. (A) Potential temperature, (B) salinity, and (C) neutral density at 300 m. Bathymetry and color distribution as in Figure 10.

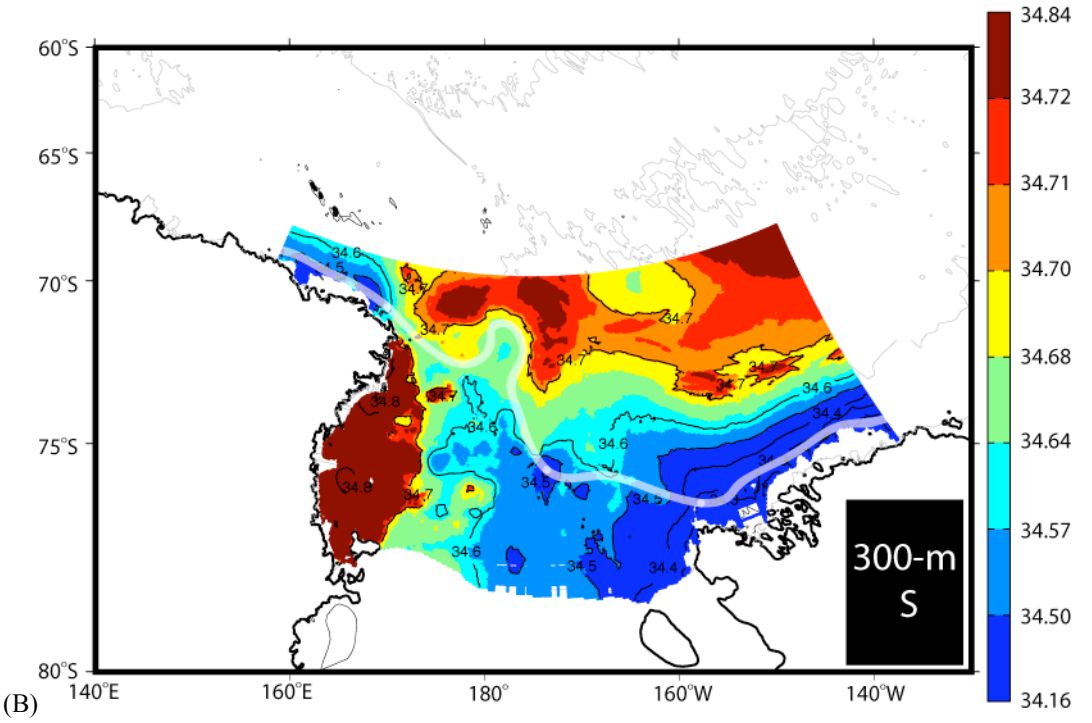

(B)

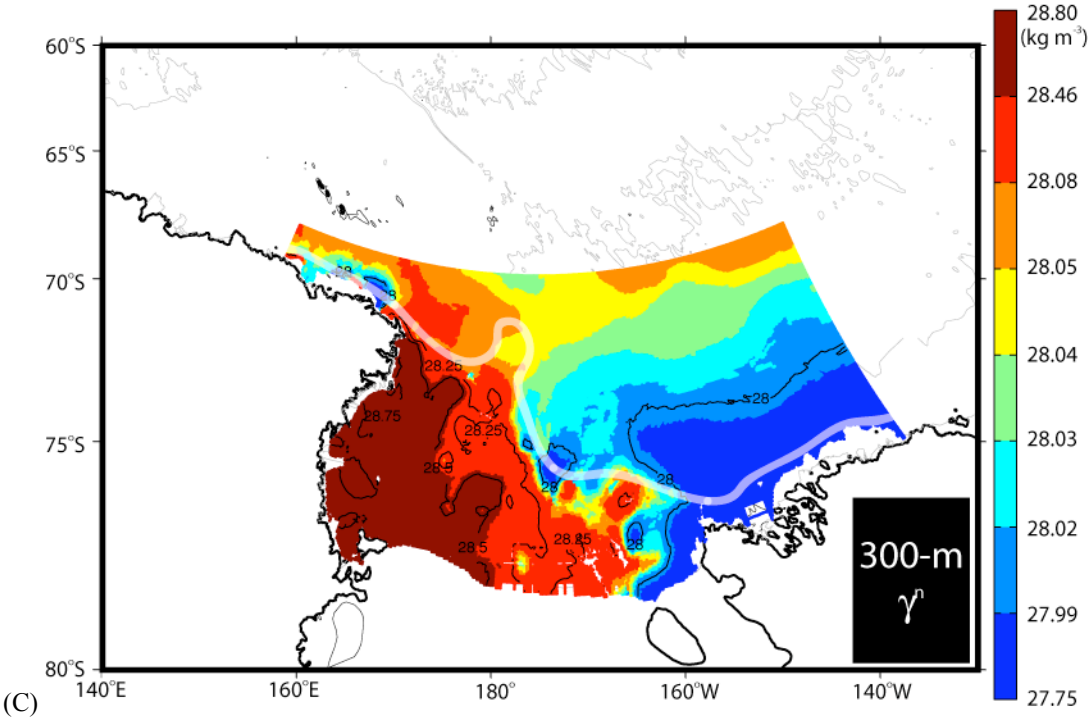

(C)

Figure 11. Continued.

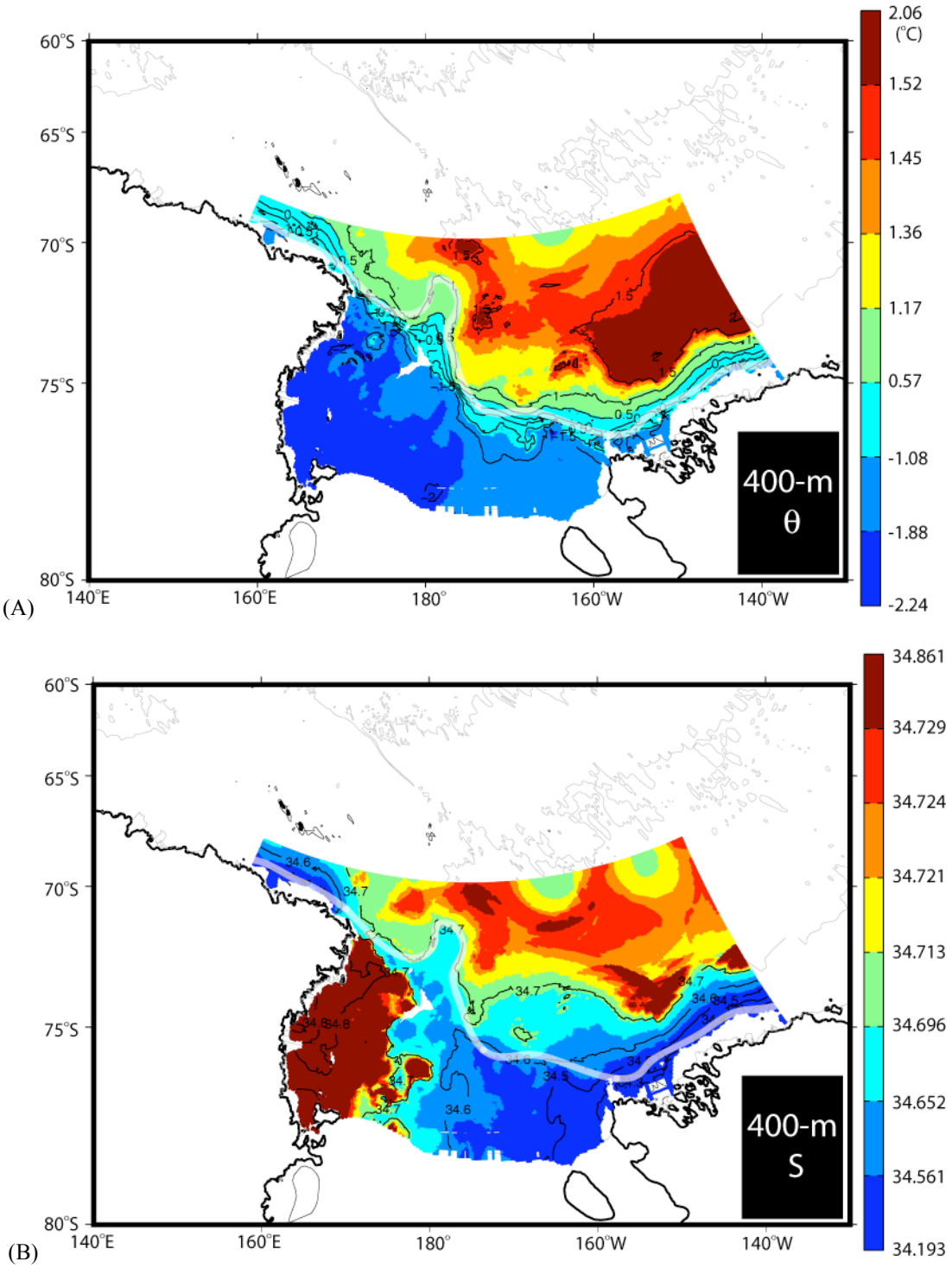

Figure 12. (A) Potential temperature, (B) salinity, and (C) neutral density at 400 m. Bathymetry and color distribution as in Figure 10.

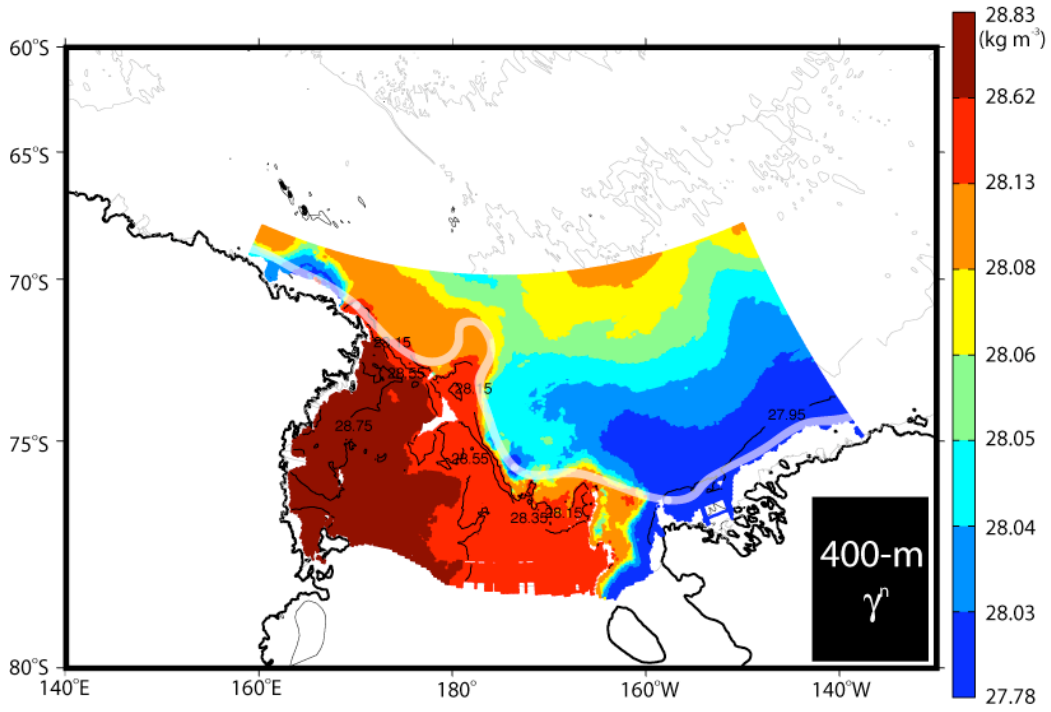

(C)

Figure 12. Continued.

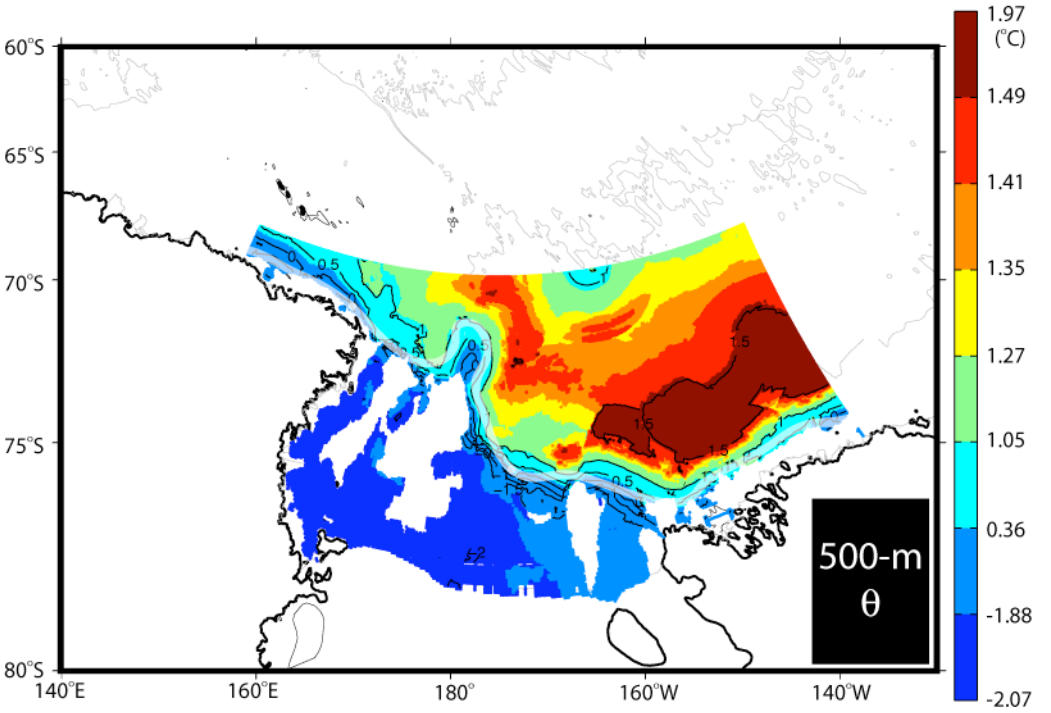

(A)

Figure 13. (A) Potential temperature, (B) salinity, and (C) neutral density at 500 m. Bathymetry and color distribution as in Figure 10.

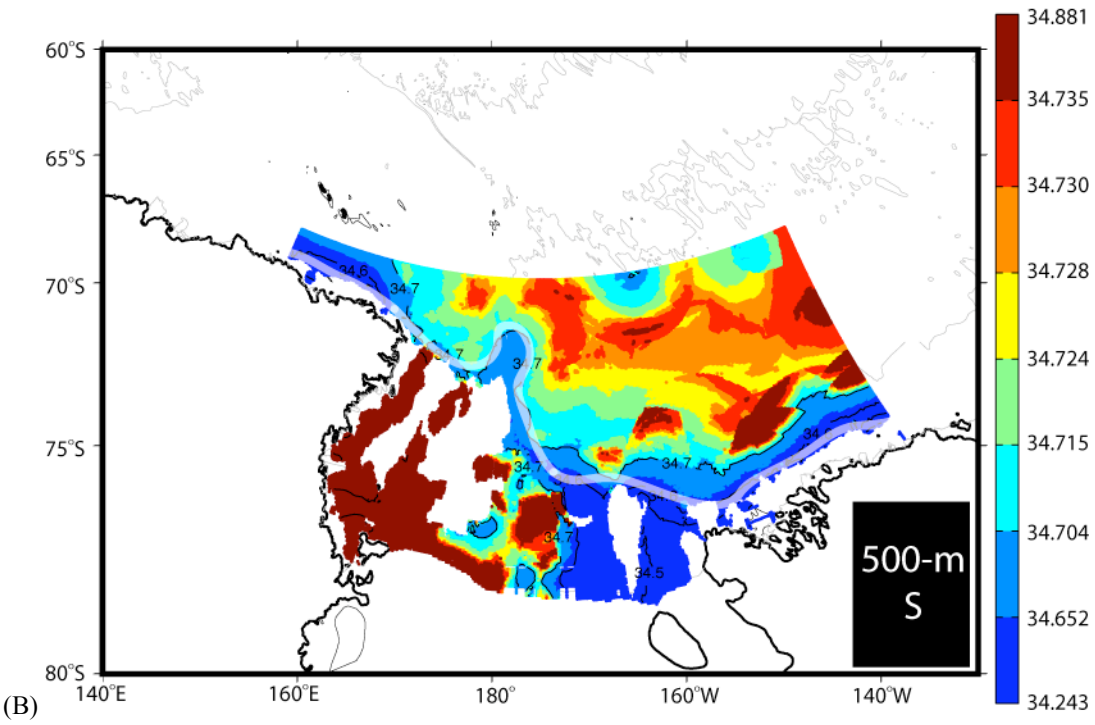

(B)

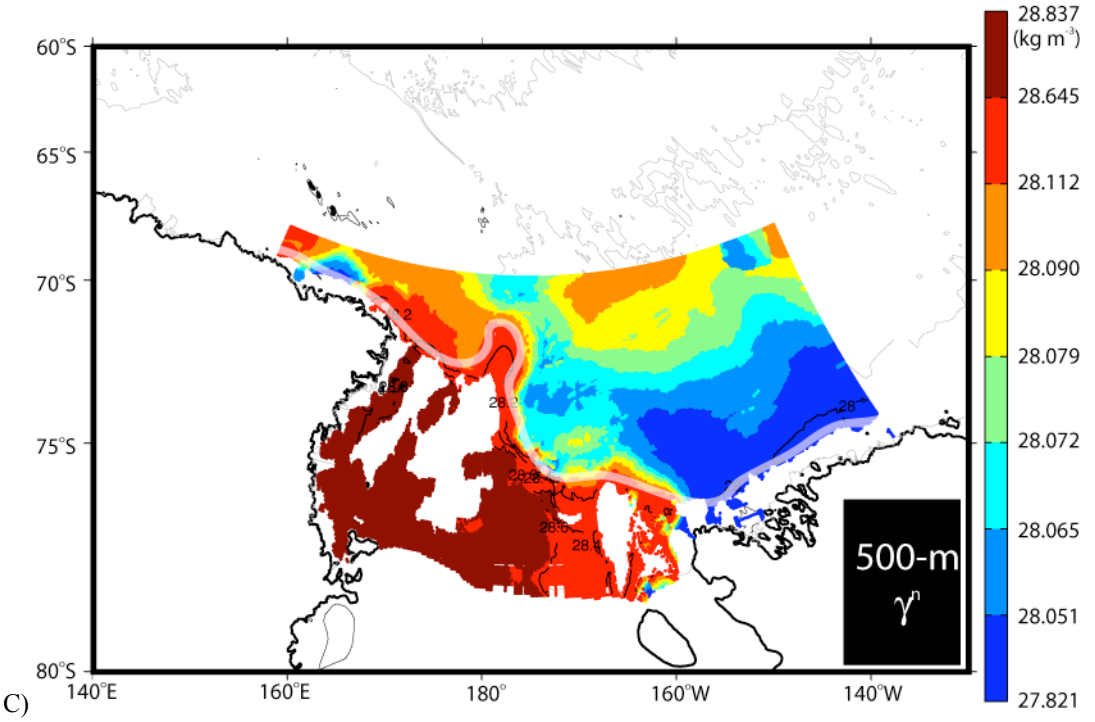

C)

Figure 13. Continued.

Antarctic Slope Front

Insights on the evolution of the Antarctic Slope Front along its transit through the Ross Sea can be gained from careful inspection of our new high-resolution climatology. Because the AASW layer is relatively thick at the Antarctic Slope Front, it is often seen separating CDW offshore with SW inshore. At the Front, the associated subsurface meridional property gradients (θ, S, γ^n) are expected to be somewhat larger than elsewhere in the deep oceanic and shallow shelf regimes. They will be used here to trace the Front's climatological distribution in the Ross Sea. For instance, at 300 m (Figure 11A-B) the relative fresh westward stream ($S < 34.685$) extending north of the Drygalski and Joides troughs clearly separates extremely cold ($\theta < -1.85°C$) and saline ($S > 34.70$) SW from offshore LCDW warmer than 0.50°C. A sharp thermal gradient band of at least 1°C is found throughout the 300 m level roughly tracing the entire length of the slope, and even along Saunders Coast where station sampling is less than desirable.

Due to the general westward shoaling of isopycnals throughout the study area, the Front's characteristic subsurface gradients are found at slightly different depths in different regions. The eastern sector of the ASF separates the thickest AASW from LCDW, and their associated horizontal gradients are the largest at depths between 400 m and 600 m. In the central region they lie between 300 m and 500 m deep, whereas the largest gradients are shallowest (100 m – 300 m) in the western sector.

The path of the ASF along the upper slope of the Ross Sea can be approximated fairly well by following the 0°C isotherm on maps of potential temperature at 500 m between 140°W and 160°W (Figure 13A), at 400 m from 160°W to 175°W (Figure 12A), and at 175 m west of 175°W (Figure 10A). This trace of the ASF, on average, follows the 800-m isobath. West of Cape Adare there is a steep southward dive of all isotherms similar to that seen off of Saunders Coast. Therefore, further tracing of the ASF in this region requires inspection of property maps at levels deeper than 175 m. In this region, the ASF appears to follow the 0°C isotherm, as well as the 800-m isobath, at a depth of 500 m (Figure 13A), horizontally separating the AASW inshore from the offshore LCDW.

Shallow Cross Frontal Exchange

Much of the relatively large variability in the physical properties of the AASW found within the Ross Sea can be inferred from the maps of layer-mean potential temperature and salinity (Figure 9B-C). The warmest regions of AASW ($\theta > -0.7°C$) are found in the slope regime near the Iselin Bank, due to mixing with the LCDW below. The next section will show that AASW and LCDW are in close proximity in this region, enhancing their mixing. The saltiest regions are found in the southwestern portion of the shelf, where considerable volumes of sea-ice are thought to form within the Ross Ice Shelf Polynya.

Two relatively warm and saline signals seem to connect the slope with the southern edges of the Ross Sea. One extends along 174°W, where relatively thick ($H \approx 175$ m) AASW seems to flow inshore as indicated by a tongue of relatively salty ($S > 34.35$) and warm ($\theta = -1.05°C$) water reaching toward the Ross Ice Shelf. Another southward inflow of similarly salty ($S > 34.35$), but warmer ($\theta = -0.50°C$) AASW can be inferred from the mouth of Drygalski Trough towards Ross Island.

Input of Lower Circumpolar Deep Water

Warm ($\theta > 1.5°C$) and saline ($S > 34.70$) LCDW flows cyclonically within the Ross Gyre beneath AASW (Figures 11-13). The westward-flowing southern limb of the gyre enters the study area south of about 71°S. LCDW is brought onto the shelf break at least at two major sites and is more clearly indicated on property maps at 300 m (Figures 11) and along the 28.05 kg m^{-3} isopycnal surface (Figure 14). The first inflow is located near 174°W, where a warm ($\theta \approx 1.50°C$) and salty ($S \approx 34.70$) southward tongue extends east of Iselin Bank. The second entrance of LCDW into the Ross Sea is inferred at around 178°E. It also represents a source of heat ($\theta \approx 1.0°C$) and salt ($S \approx 34.75$) relative to the mean shelf characteristics.

Inside the Ross Sea, i.e. at water depths less than 2000 m, the largest volume of LCDW (~1500 m thick) is found offshore of the 700-m isobath (Figure 15A). A rapid thinning of this source water to a thickness of only ~500 m is already evident near the shelf break. Farther inshore, the general patterns of mean properties for the middle

density layer (Figure 15B-C) are very similar to those described for the AASW layer above. The MCDW layer, a result of AASW mixing with LCDW, also thins out from east to west, from a thickness of about 400 m at 160°W to only 50 m near 170°E, eventually outcropping west of 165°E. Circulation patterns of MCDW on the continental shelf of the Ross Sea do not seem to be blocked by any topographic feature, but rather guided along the major banks and shoals.

Southward extension of the MCDW signals is evident in the eastern Ross Sea (Figure 15). A relatively thick ($H \approx 175$ m), warm ($\theta \approx -1$°C), and salty ($S \approx 34.50$) tongue approaches the Ross Ice Shelf along 174°W, only slightly cooling ($\Delta\theta = 1.25$°C) and freshening ($\Delta S = 0.05$) during its southward transit. Here the base of the MCDW layer lies at about 250 m, deep enough for some volume to flow under the glacier. Its further local cooling underneath the ice may contribute to a local type of ISW, i.e. super-cooled MCDW. In contrast, a net freshwater input from basal melting would form AASW with temperatures below the surface freezing point, i.e. super-cooled AASW.

Another major inflow of MCDW is indicated in the western Ross Sea, between 172°E and 178°E, extending along two separate routes. Both appear as tongues of relatively warm ($\theta \approx 0.5$°C) and salty ($S \approx 34.60$) characteristics. Although MCDW extends over the shelf regime of the eastern Ross Sea, it does not appear to flood onto the shelf as speculated by Dinniman, *et al.* (2003).

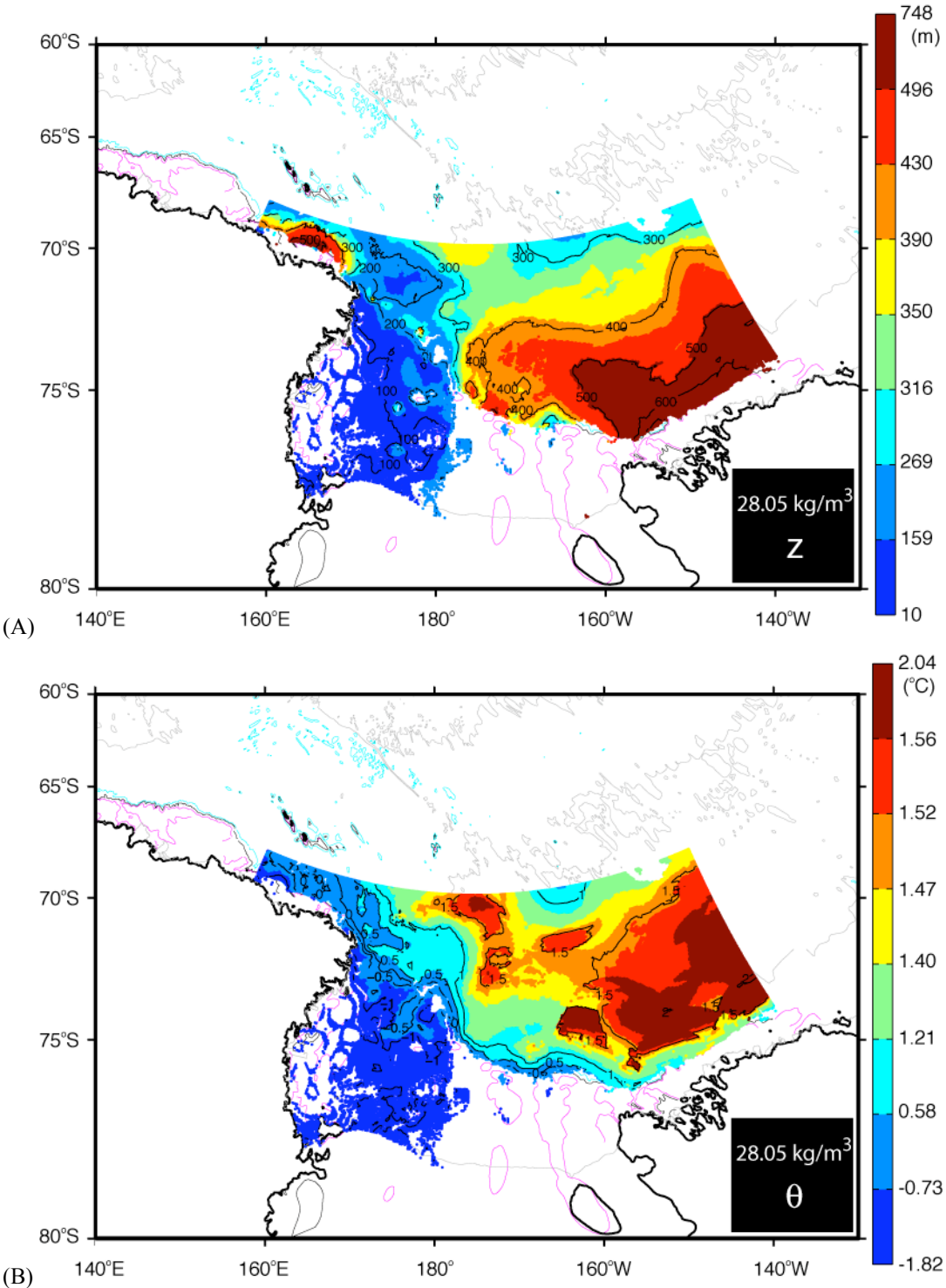

Figure 14. (A) Depth, (B) potential temperature, and (C) salinity on the 28.05 kg m^{-3} neutral density surface. Bathymetry and color distribution as in Figure 8.

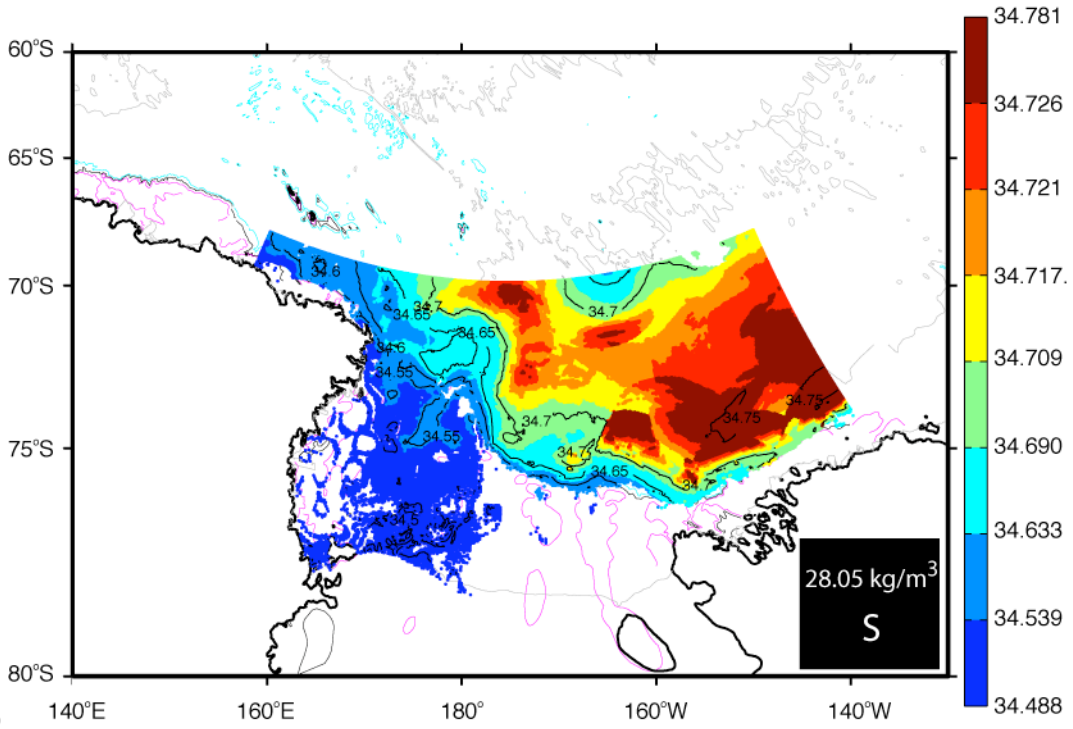

(C)

Figure 14. Continued.

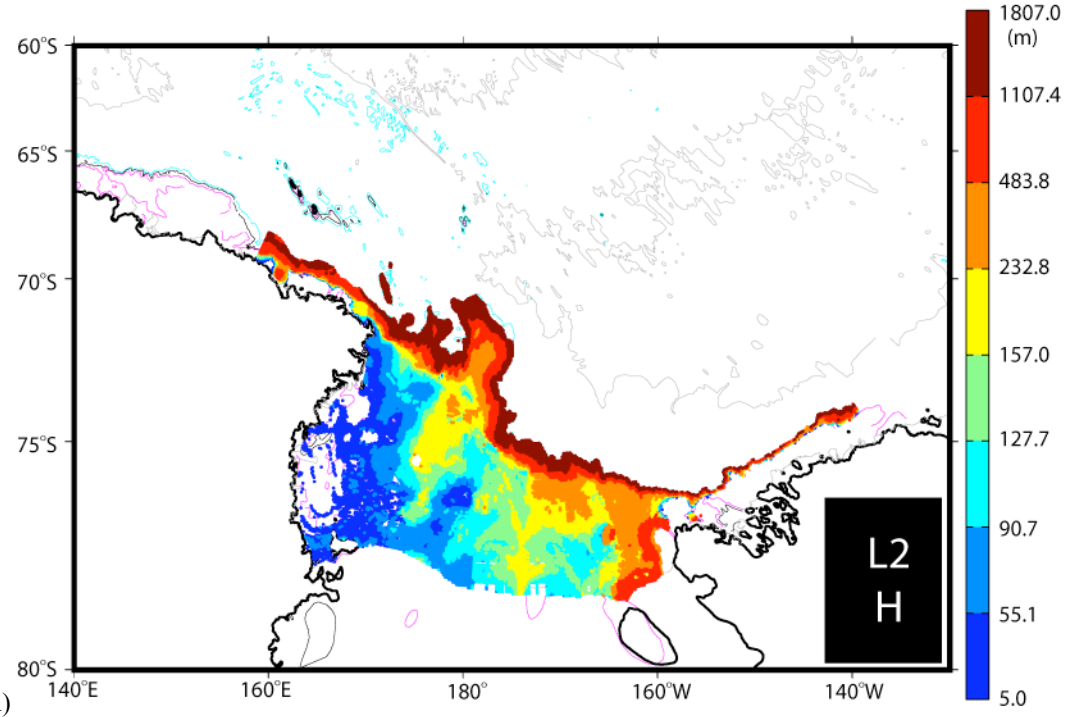

(A)

Figure 15. (A) Thickness, volume weighted (B) potential temperature, and (C) salinity of the middle layer (L2: 28 kg m^{-3} > γ^n<=28.27 kg m^{-3}) representing MCDW and LCDW. Bathymetry and color distribution as in Figure 8.

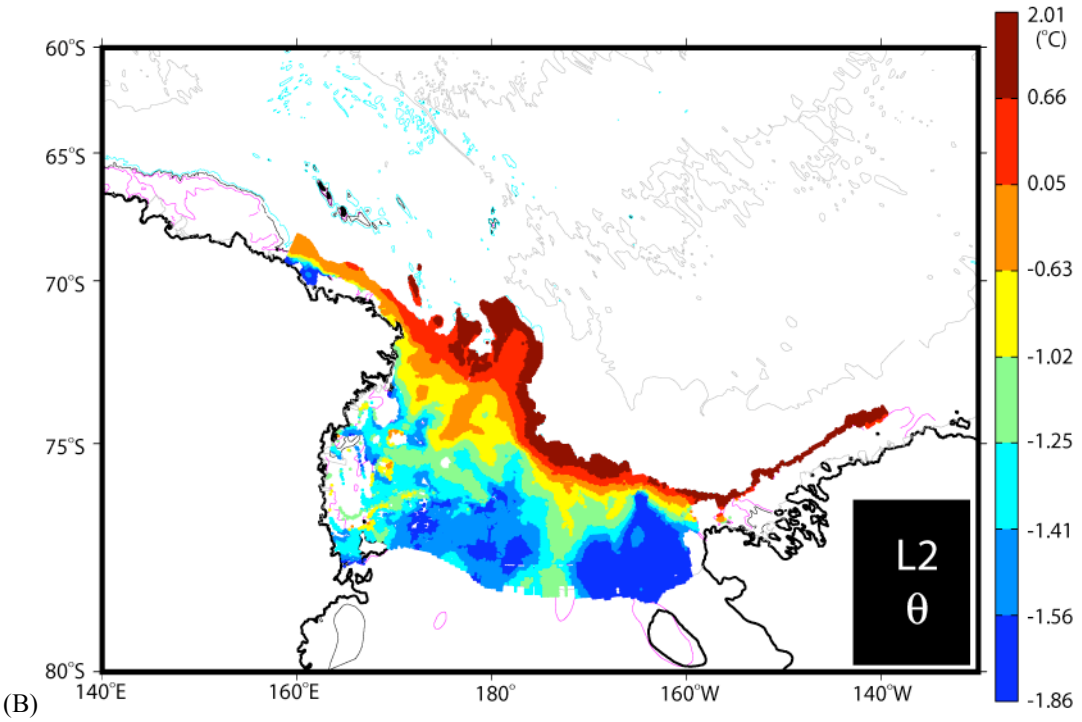

(B)

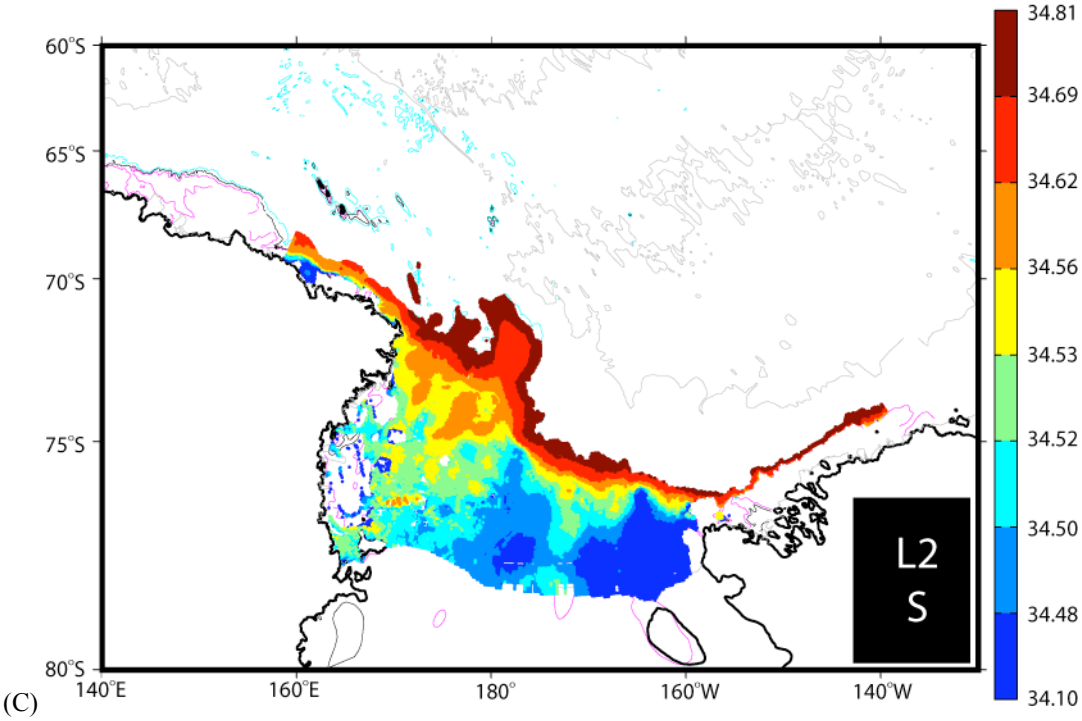

(C)

Figure 15. Continued.

Outflow of New Bottom Water

The bottom density layer spans all of the volumes of AABW (offshore of the 700-m isobath), SW and MSW (inshore of the 700-m isobath) found below the 28.27 kg m^{-3} neutral density surface. Unlike the middle and top density layers, the circulation patterns for the bottom layer are heavily influenced by the sea floor topography of the Ross Sea, e.g. flow into its eastern end, east of 160°W, is totally obstructed. The general thinning of this layer is toward the east; the opposite direction of the two layers above. The thickest regions are the southern portions of the Drygalski, Joides, and Glomar Challenger troughs, and much thinner layers are seen over the eastern Whales and Little America troughs. Ultimately, the bottom density layer runs aground at about 158°W (Figure 16A). On average, the bottom layer of the latter trough is also the coldest (θ < -1.85°C) and freshest (S < 34.67) of all. However, only the continental slope off Cape Adare shows evidence of a major outflow of new AABW (θ < -0.5°C, S < 34.71), likely supplied from both of the two westernmost troughs. Elsewhere there is no bottom layer found offshore of the 700-m isobath.

Salty Shelf Water Products

HSSW (γ^n > 28.27 kg m^{-3}, $\theta \leqslant$ -1.85°C, S > 34.7) spreads over the western and central regions of the Ross Sea (Figure 17), extending eastward to about 175°W. It shows a general thinning in that direction (Locarnini, 1994; Orsi *et al.*, 1999) being thicker than 700 m in the southern Drygalski Trough, but less than 200 m thick in the Glomar Challenger Trough. The Drygalski Trough hosts the saltiest HSSW (S > 34.80). Cyclonic circulation of HSSW within each of these sub-basins is inferred from the year-mean velocity fields produced by the most recent high-resolution numerical model of the Ross Sea (Dinniman *et al.*, 2003).

The mean dissolved oxygen map (Figure 17D) provides additional insight on the main production sites of HSSW. The Terra Nova Bay Polynya, located near 75°S, 165°E, is the site of HSSW oxygen concentrations above 300 μmol kg^{-1}. Well-ventilated HSSW is also found along the Ross Ice Shelf between 165°E and 178°E, within the reoccurring Ross Ice Shelf Polynya.

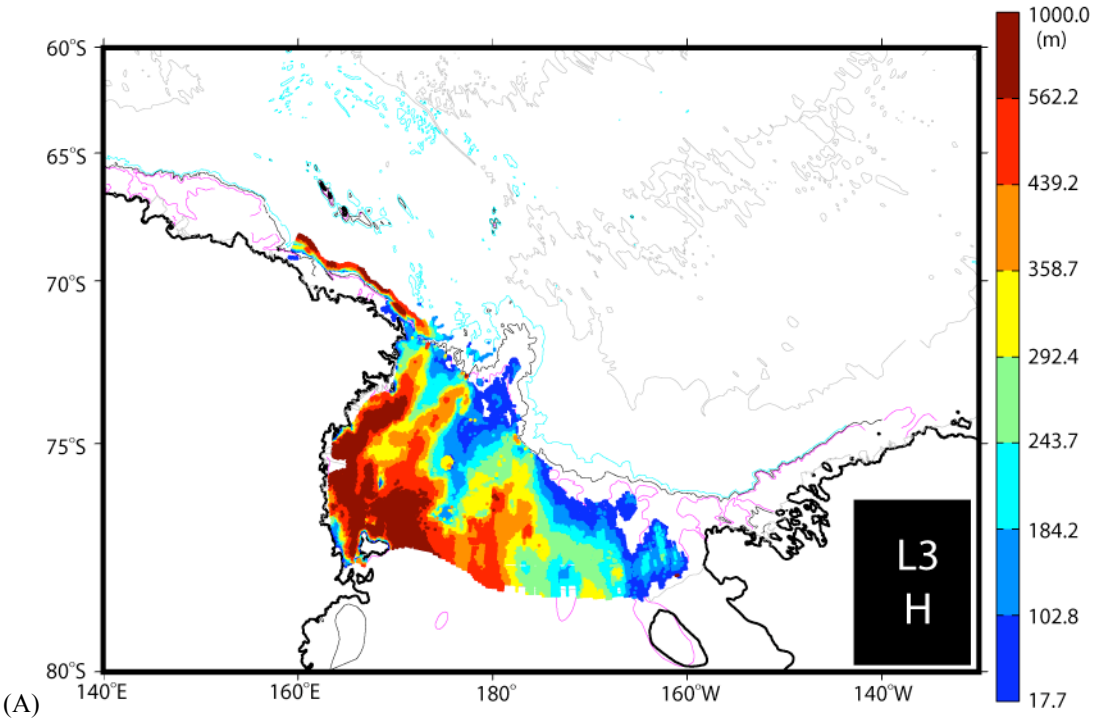

(A)

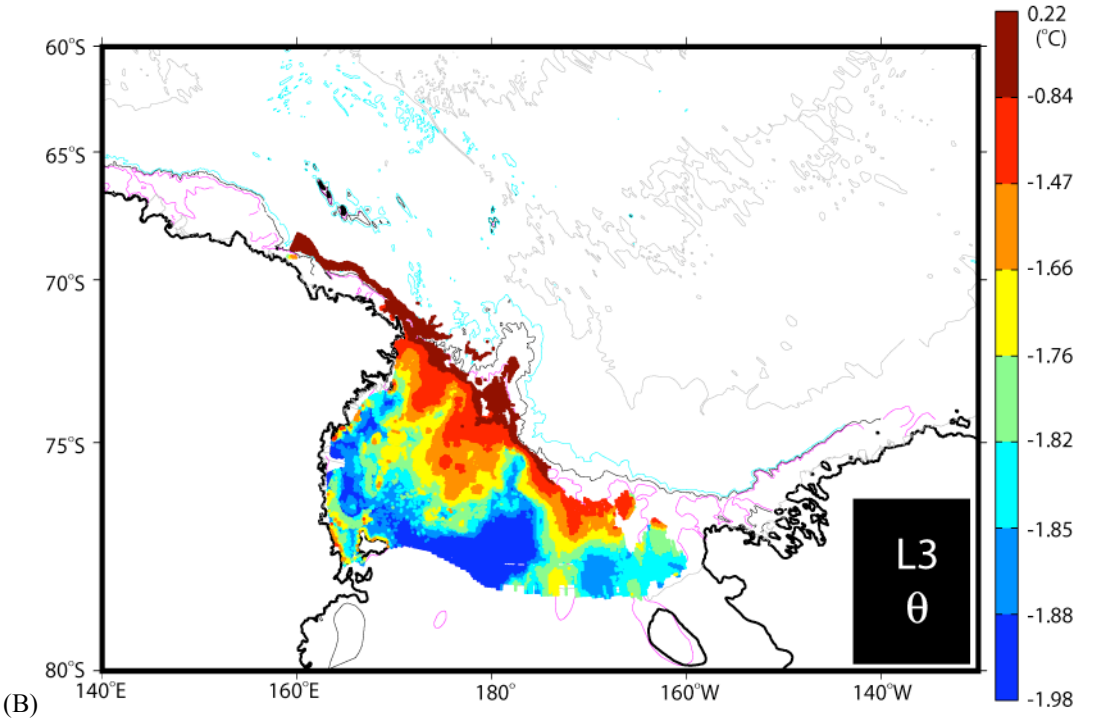

(B)

Figure 16. (A) Thickness, volume weighted (B) potential temperature, and (C) salinity of the bottom layer (L3: γ^n>28.27 kg m^{-3}) representing SW, MSW, and AABW. Bathymetry and color distribution as in Figure 8.

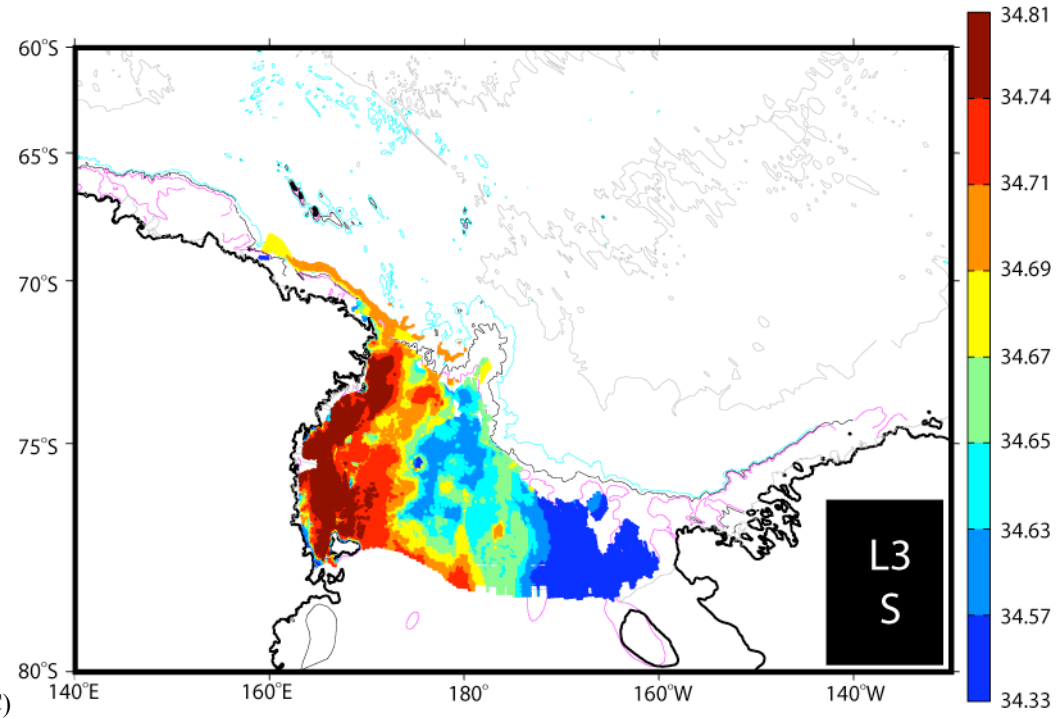

(C)

Figure 16. Continued.

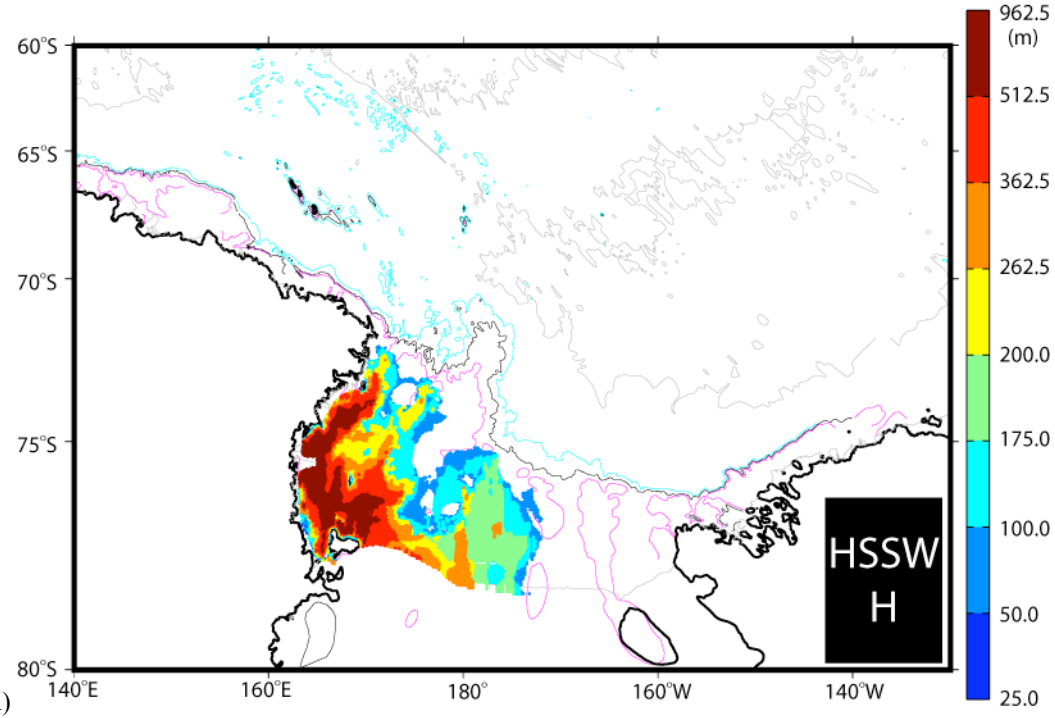

(A)

Figure 17. (A) Thickness, volume weighted (B) potential temperature, (C) salinity, and (D) dissolved oxygen of HSSW. Bathymetry and color distribution as in Figure 8.

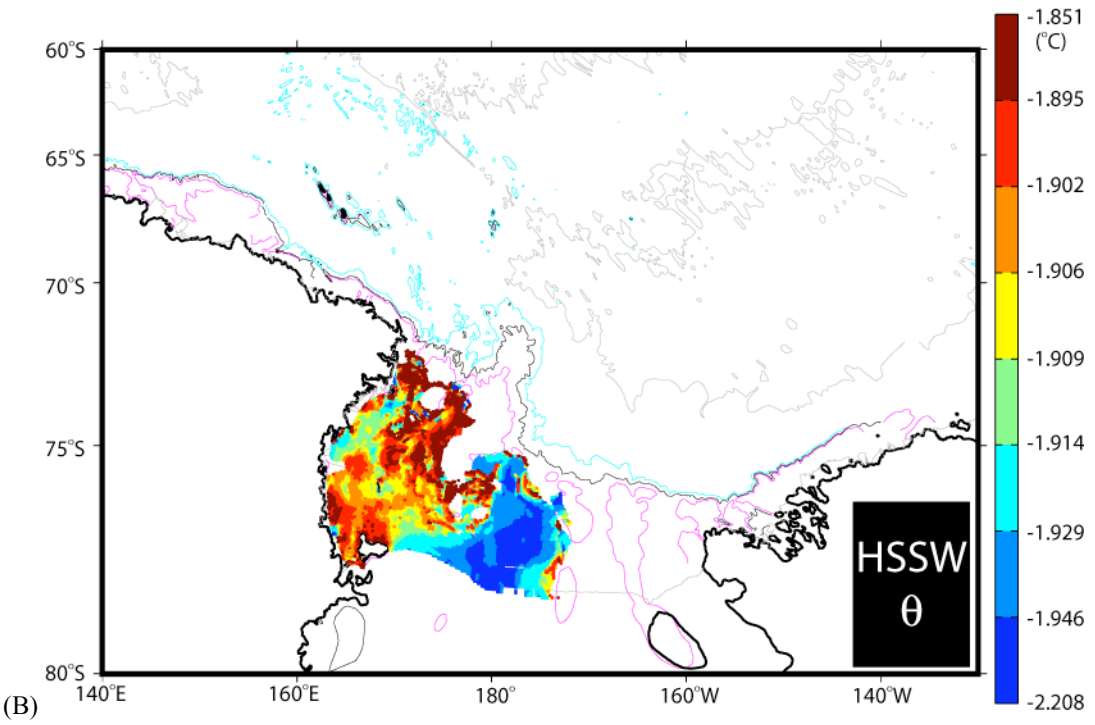

(B)

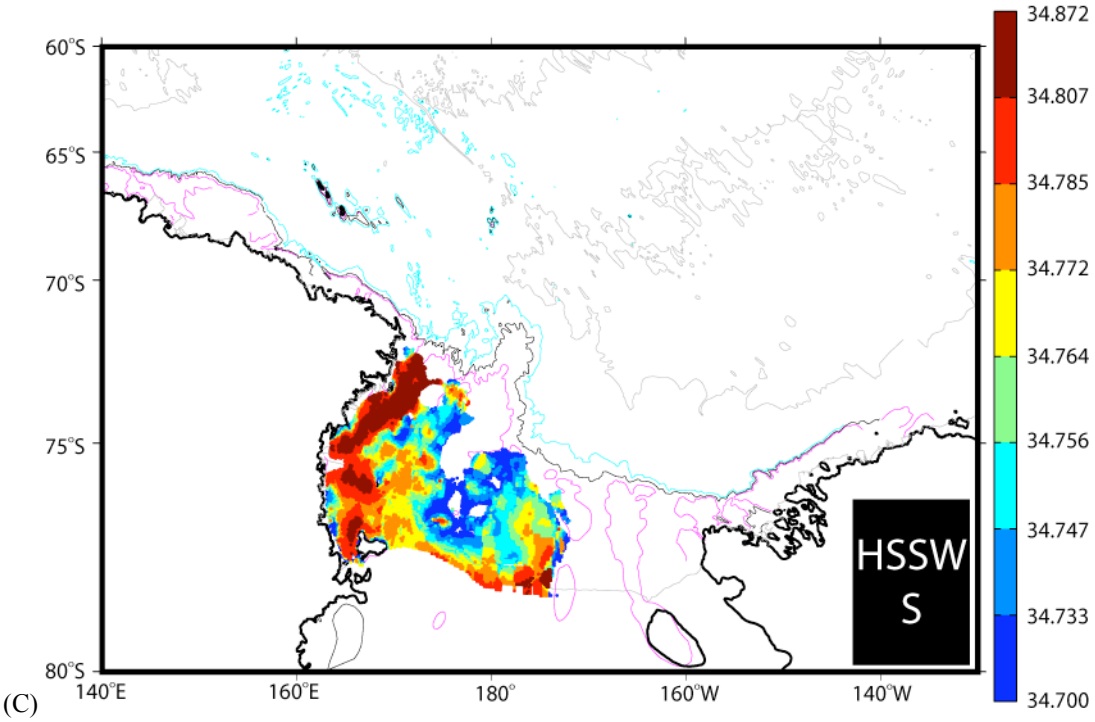

(C)

Figure 17. Continued.

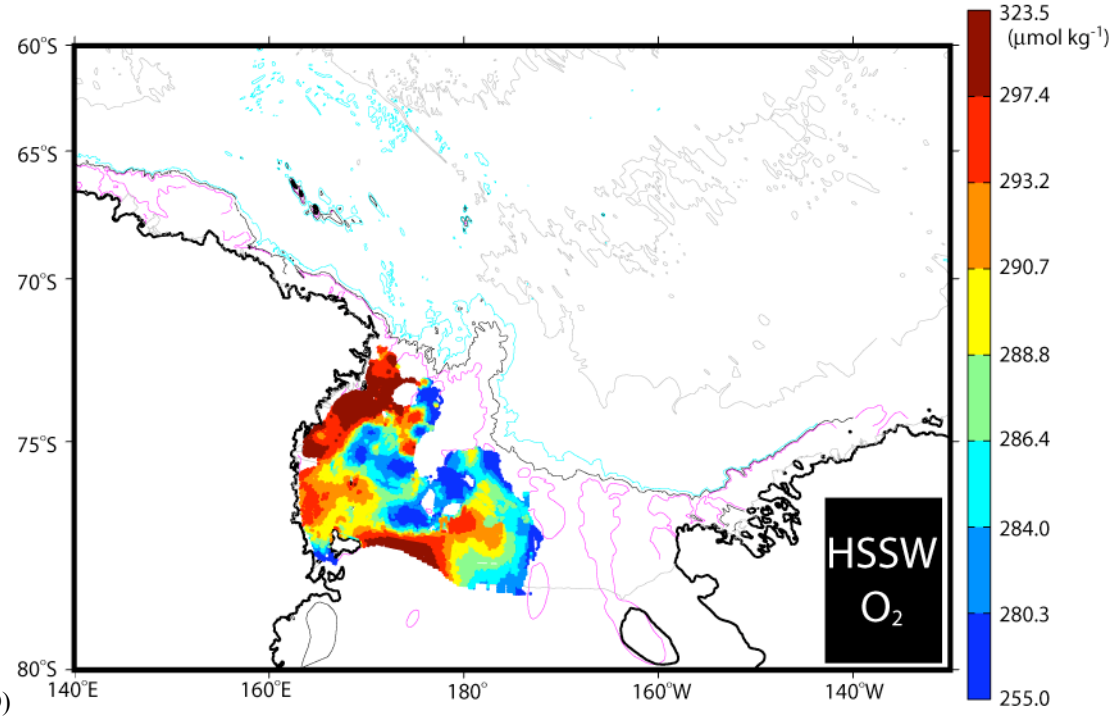

(D)

Figure 17. Continued.

It is speculated that some of the HSSW formed in the Terra Nova Bay Polynya flows southeast around Ross Island, and is able to sneak underneath the Ross Ice Shelf. This inflow eventually turns northeastward escaping around 180° into the Glomar Challenger Trough as ISW. This route is indicated by the relatively thick (H ≈ 300 m in Figure 17A) tongue of water extending northward along 180° with potential temperatures colder than -1.95°C (Figure 17B) and salinities around 34.75 (Figure 17C). Productive locations of new salty MSW are likely to show HSSW and MCDW readily available to mix with each other across isopycnals. Source water inflows (Figure 15) reveals that the three main input paths of MCDW (Drygalski, Joides, and Challenger troughs) coincide with HSSW flowing northward against the western flanks of those troughs. The warm influence of MCDW on HSSW is seen on the mean potential temperature map where the warmest (θ ≈ -1.85°C) HSSW is found north of 75°S and west of 175°E. A less prominent vertical mixing of MCDW and HSSW is inferred over the interior of the Glomar Challenger Trough, where potential temperatures remain

colder than -1.90°C due to additional cooling from its mixing with ISW found in between.

Over the shelf regime, the mixing product of HSSW and MCDW is hereafter referred to as High Salinity Modified SW (HSMSW: $\gamma^n > 28.27$ kg m^{-3}, $\theta > -1.85$°C, $S > 34.70$). It is found throughout the Drygalski Trough, over the northern Joides Trough, and some traces are also indicated near the sill of the Glomar-Challenger Trough (Figure 18). This water layer is the thickest ($H > 150$ m) and warmest ($\theta > -1.6$°C) at the northern edge of the western Ross Sea, within about 100 km of the shelf break. Additionally, a band also showing relatively high salinities ($S > 34.75$) and low oxygen concentrations ($O_2 < 280$ μmol kg^{-1}) is observed. Consistent with previous descriptions (Jacobs *et al.*, 1970), this HSMSW feeds the export of relatively saline ($S > 34.71$) AABW revealed offshore of the 700-m isobath directly north of the mouths of Drygalski (173°E) and Joides (177°E) troughs.

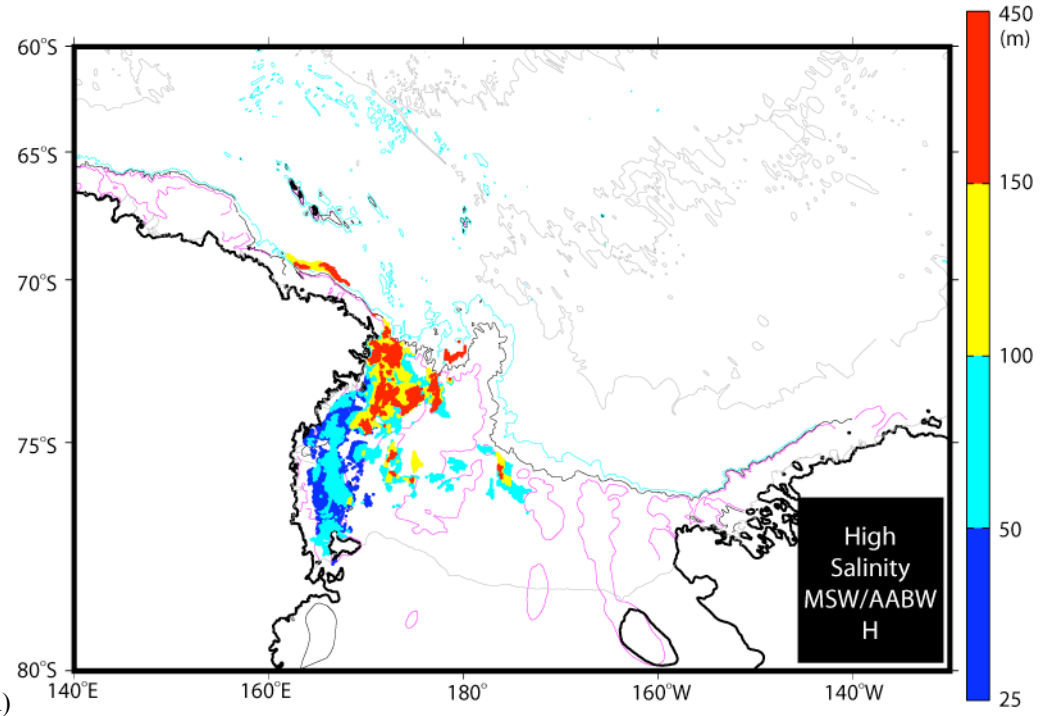

(A)

Figure 18. (A) Thickness, volume weighted (B) potential temperature, (C) salinity, and (D) dissolved oxygen of high-salinity MSW and AABW. Bathymetry and color distribution as in Figure 8.

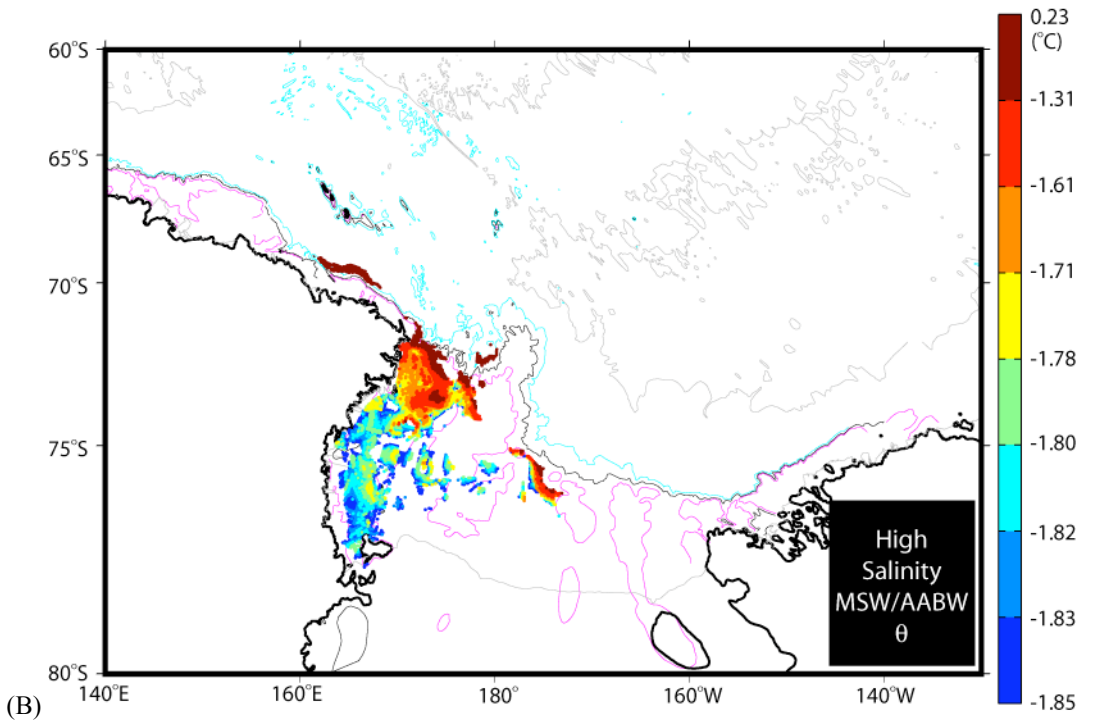

(B)

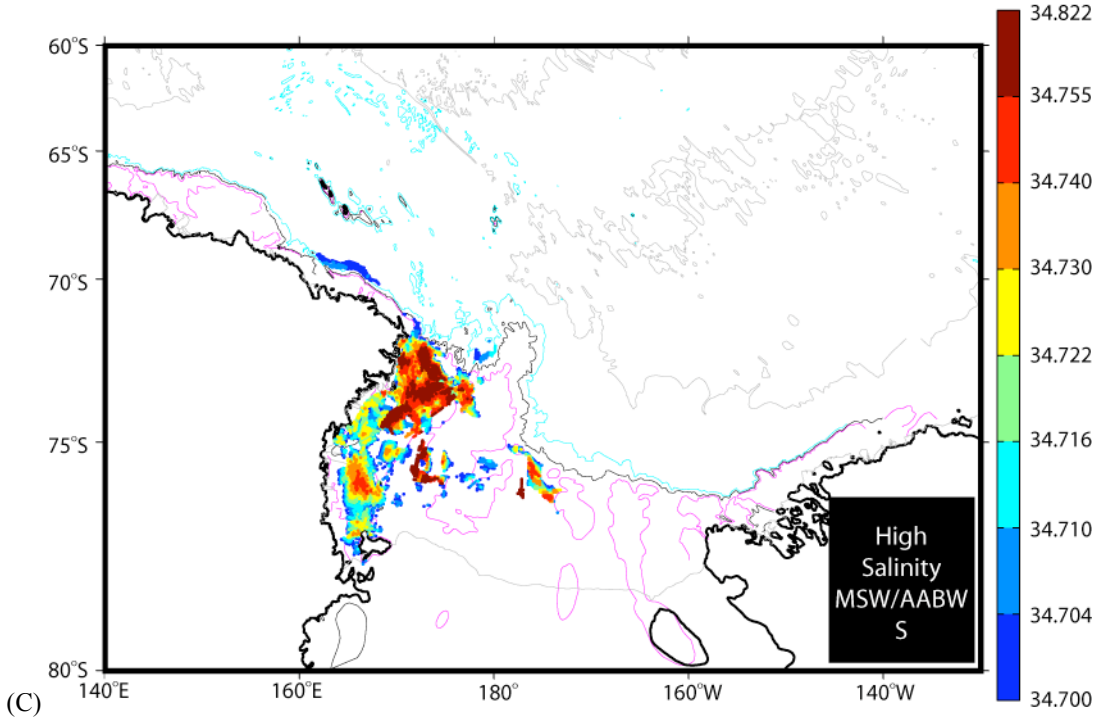

(C)

Figure 18. Continued.

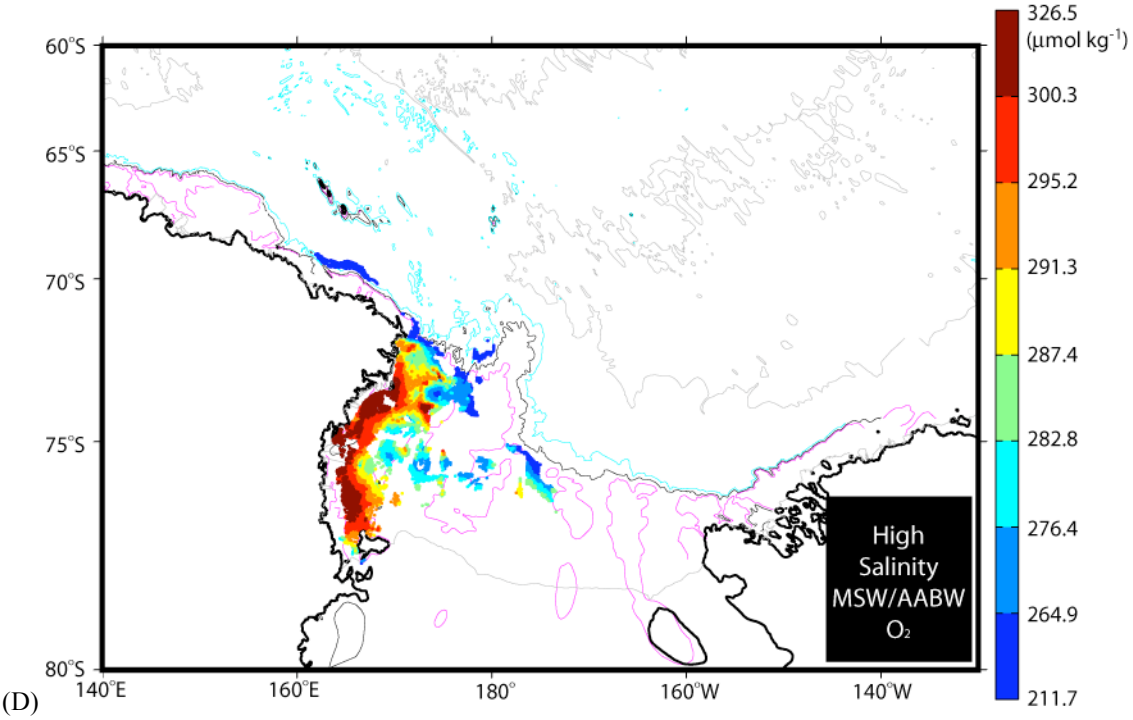

(D)

Figure 18. Continued.

Fresh Shelf Water Products

LSSW ($\gamma^n > 28.27$ kg m^{-3}, $\theta \leq -1.85$°C, $S \leq 34.7$) extends over the central and eastern regions of the Ross Sea (Figure 19), although a small volume of LSSW is also seen off of Victoria Land south of 76°S. LSSW colder than -1.95°C in the Challenger Trough most likely corresponds to the ISW that originates from the diluted HSSW exiting the Ross Ice Shelf to the north near 180°. Low-oxygen ($O_2 < 287$ µmol kg^{-1}) and low-salinity ($S < 34.63$) signals are consistent with an outflow of ISW and also in agreement with recent model results (Dinniman *et al.*, 2003) and CFC measurements (Smethie and Jacobs, 2005). LSSW tends to flow cyclonically hugging the western flank of the Challenger Trough. Formation of LSSW is also suggested in the Ross Ice Shelf Polynya, between Ross Island and 180°, by the relatively high dissolved oxygen concentrations ($O_2 > 292$ µmol kg^{-1}).

LSSW in the Whales Trough is relatively warm ($\theta > -1.87$°C) and fresh ($S <$ 34.55), and it likely derives from near-freezing AASW ($S < 34.35$) that enters the Ross

Sea along the Antarctic coastal current and gains salt during winter sea-ice formation. The warm influence from the MCDW above is more evident along the eastern half of the Whales Trough, where potential temperatures are near -1.85°C.

Low Salinity Modified SW (LSMSW: $\gamma^n > 28.27$ kg m^{-3}, $\theta > -1.85$°C, $S < 34.70$) is found throughout Ross Sea continental shelves. This water spans more than 150 m of the water column at some locations of the eastern, central, and western basins (Figure 20). West of 175°W the LSSW is relatively warm ($\theta > -1.40$°C), salty ($S > 35.65$), and low in oxygen content ($O_2 < 266$ μmol kg^{-1}) along the outer shelf. Farther inshore the signal from mixing with the MCDW above are clearly inferred in the broad relatively warm ($\theta > -1.6$°C) tongues extending southward in the western and central Ross Sea. Minimal mixing of MCDW with LSSW is inferred in the Whales Trough, where LSMSW is the coldest ($\theta < -1.82$°C) and freshest ($S < 34.52$).

Because LSSW is scarce in the Drygalski and Joides troughs, the relatively high salinities (34.65 to 34.70) of LSMSW over the western Ross Sea instead point to a HSSW parent. It is important to note that although the western Ross Sea is mainly thought to supply HSMSW, a seemingly substantial thickness ($H \approx 150$ m) of LSMSW resides above it. A more apparent outflow of this less saline water is observed in the mean dissolved oxygen map (Figure 20D) where a narrow tongue of relatively well-ventilated ($O_2 \approx 290$ μmol kg^{-1}) water approaches the shelf break off of the Drygalski Trough. This pattern sheds new light on a more complex mixing history between MCDW and SW in the Ross Sea.

A particularly interesting observation is that the western Ross Sea (Drygalski and Joides troughs) displays both flavors of MSW. One is the HSMSW, which forms where more plentiful and extremely saline ($S > 34.80$) HSSW is available to mix vertically with MCDW near the shelf break. The other is the LSMSW, which is a mixture of HSSW ($S \approx 34.72$) and relatively fresher and colder MCDW over most of the inner shelf regions. In contrast, the central and eastern basins of the Ross Sea only host the LSMSW, which in those regions results from vertical mixing of the local freshest LSSW with MCDW entering the shelves east of Iselin Bank.

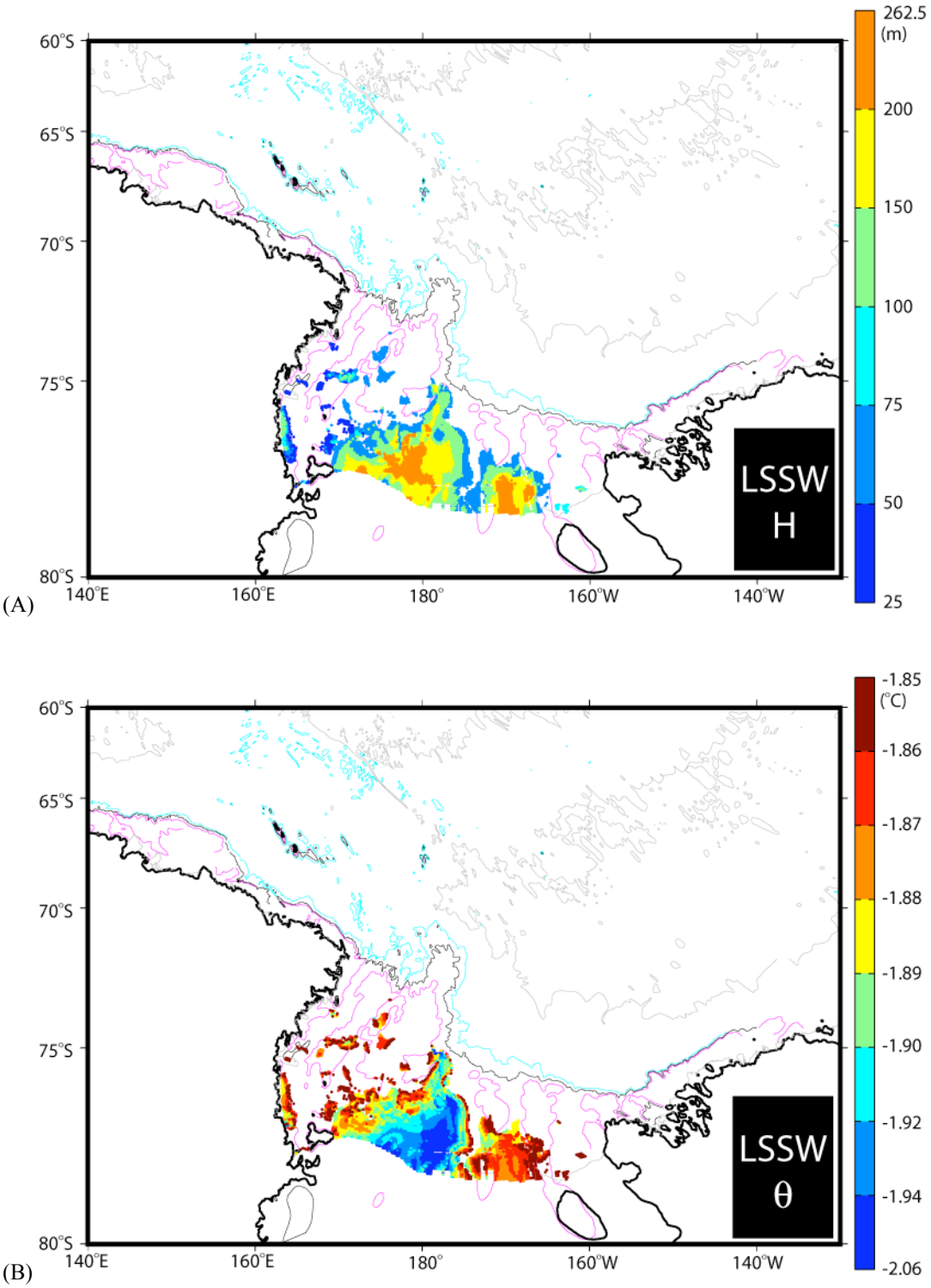

Figure 19. (A) Thickness, volume weighted (B) potential temperature, (C) salinity, and (D) dissolved oxygen of LSSW. Bathymetry and color distribution as in Figure 8.

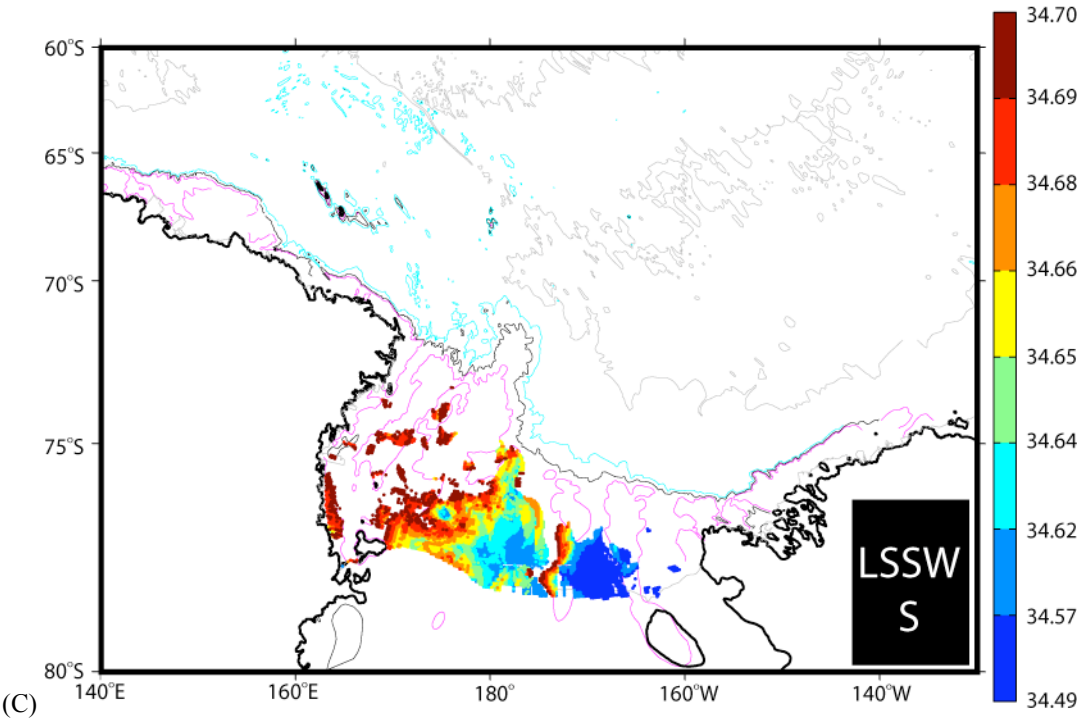

(C)

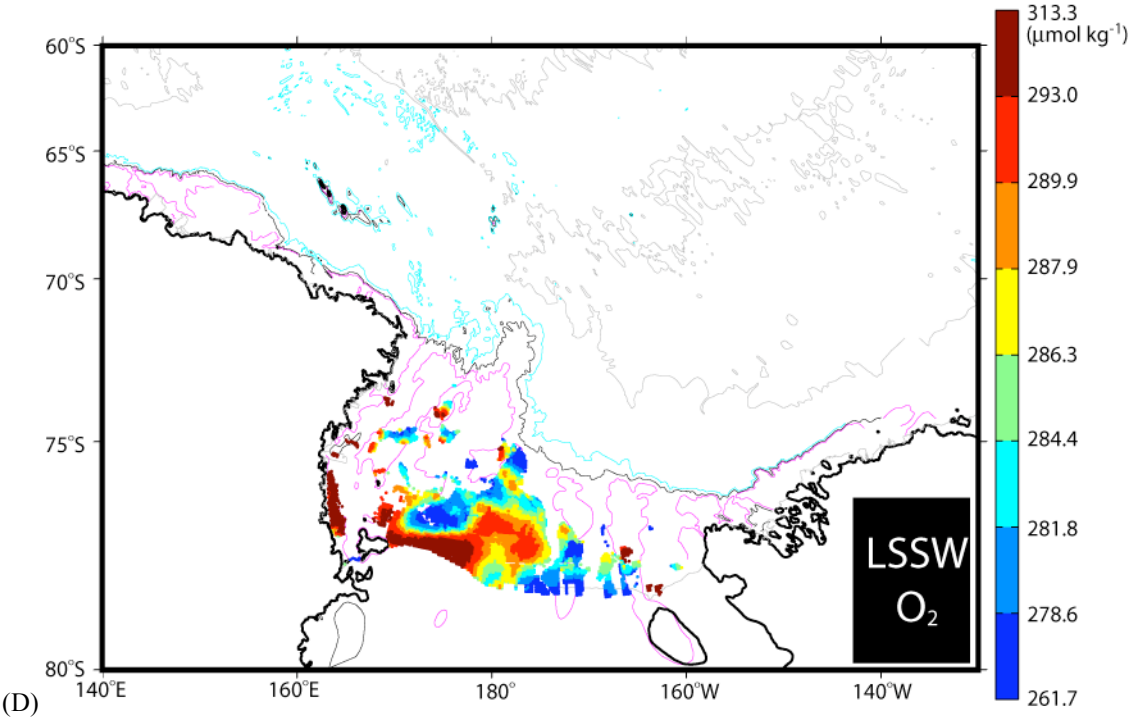

(D)

Figure 19. Continued.

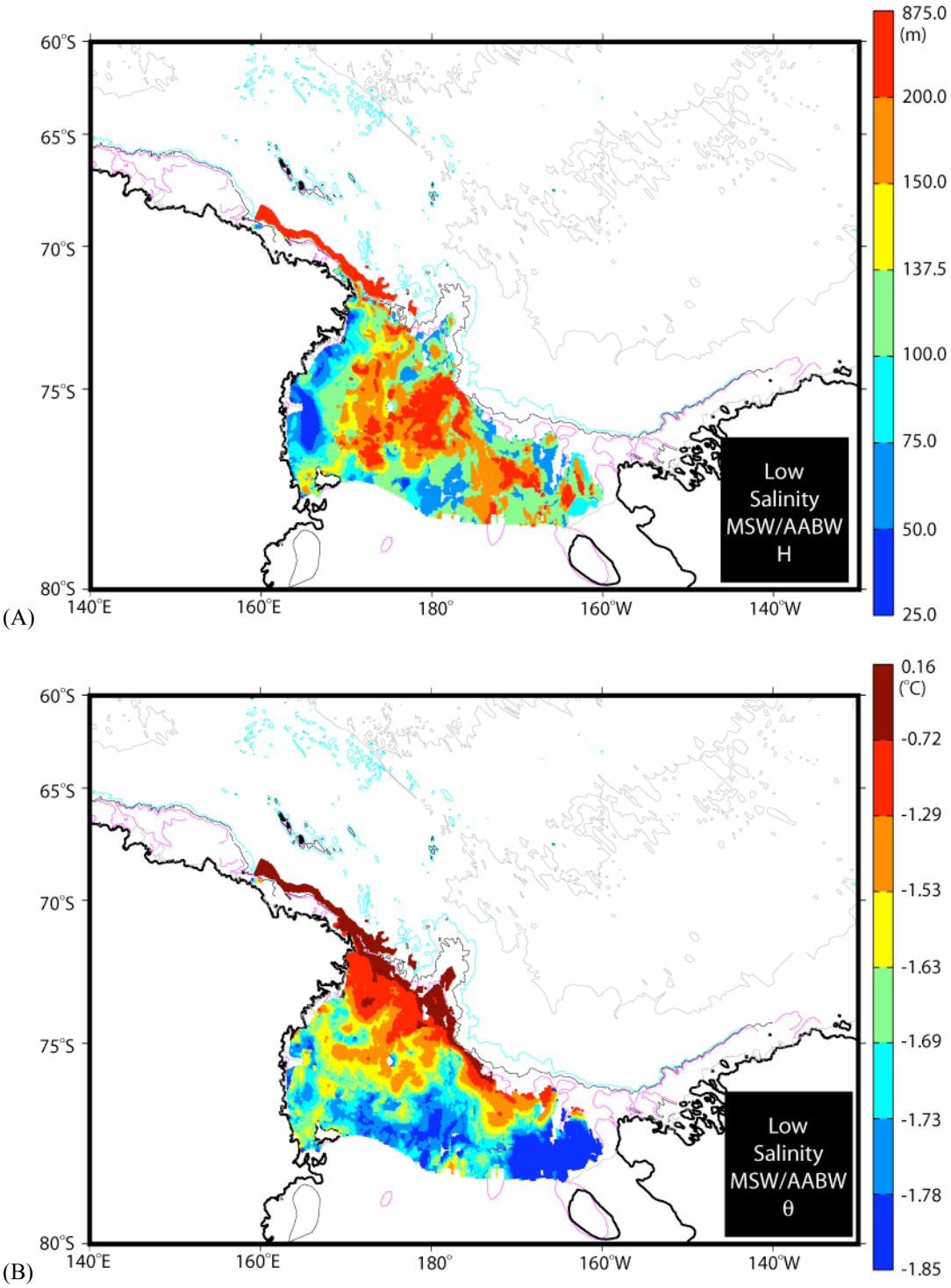

Figure 20. (A) Thickness, volume weighted (B) potential temperature, (C) salinity, and (D) dissolved oxygen of low-salinity MSW and AABW. Bathymetry and color distribution as in Figure 8.

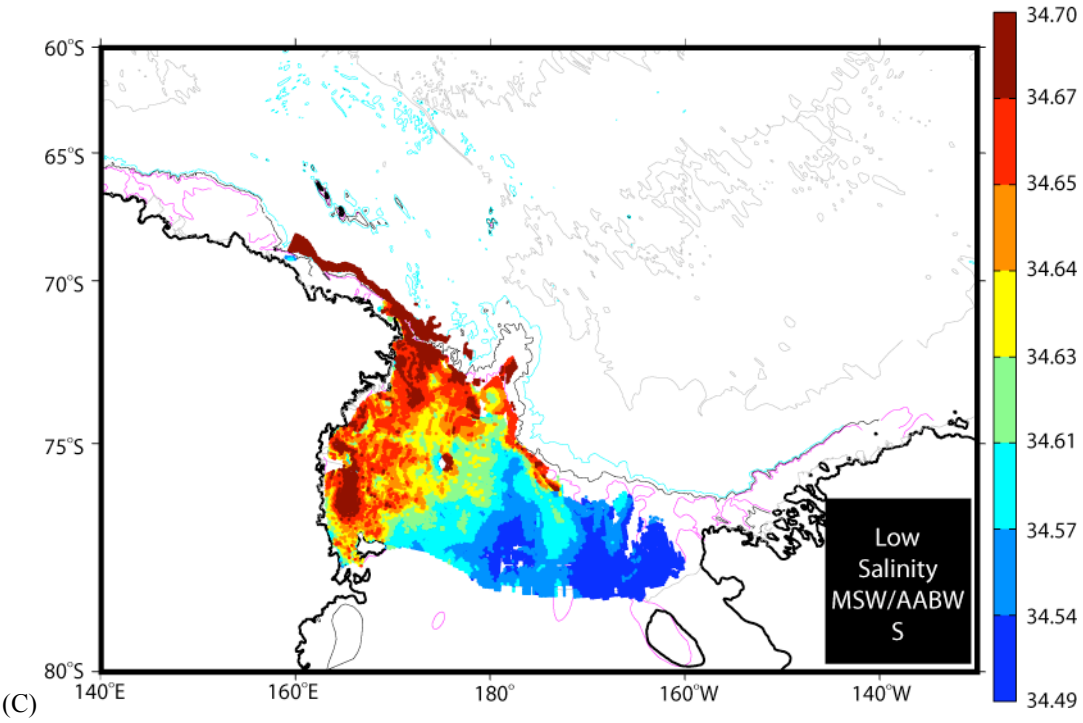

(C)

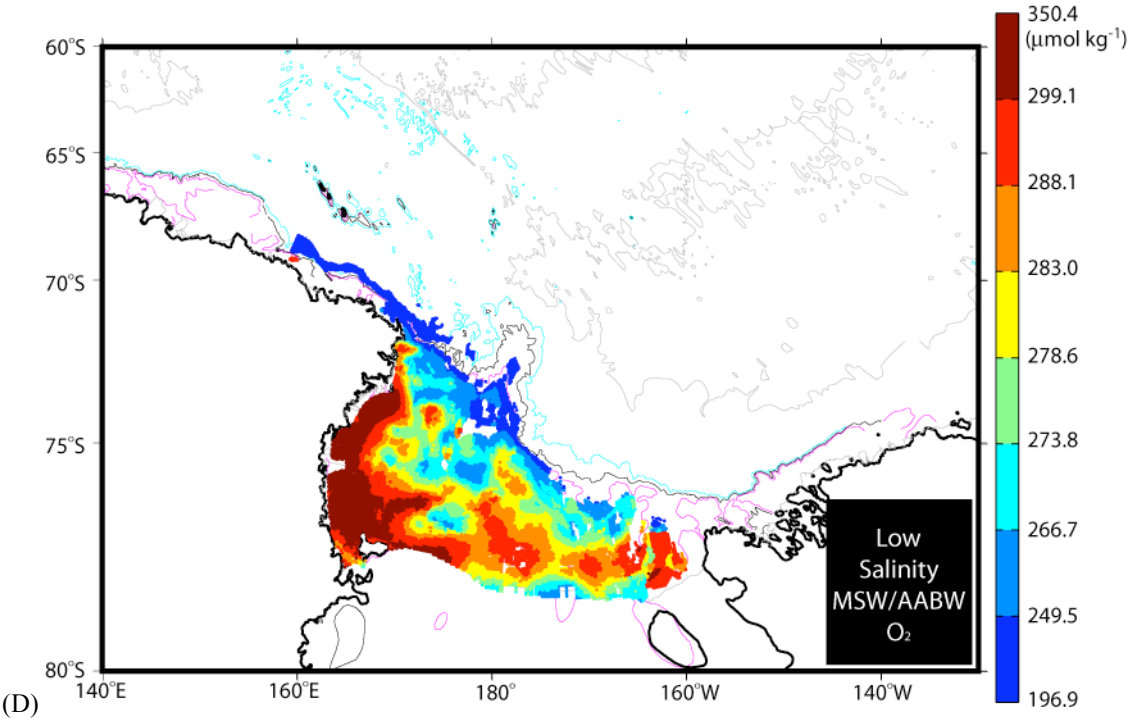

(D)

Figure 20. Continued.

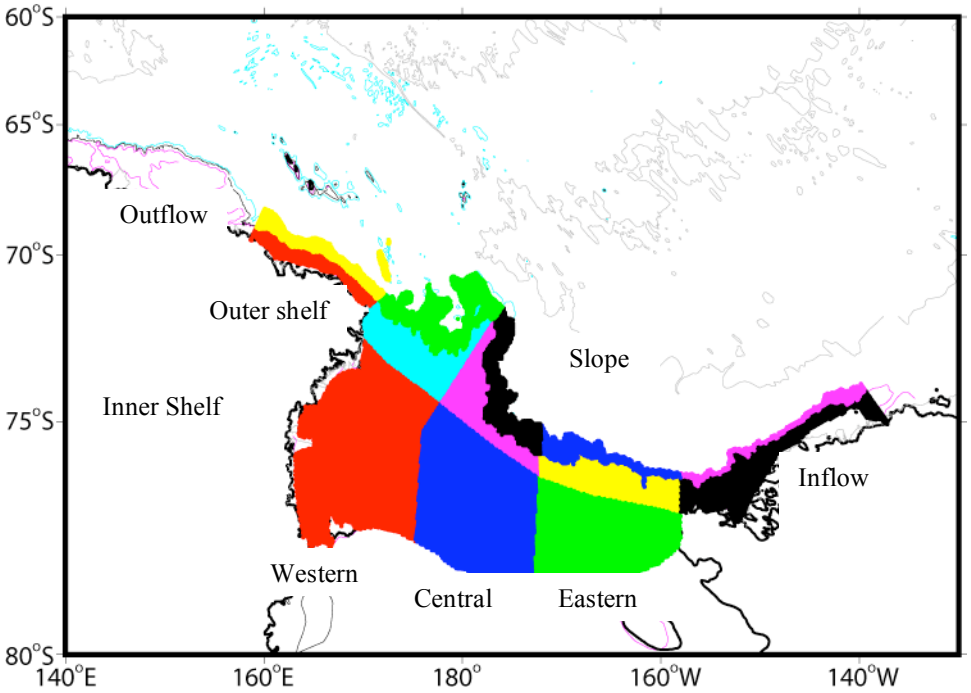

Figure 21. Selected geographical sub-regions of the Ross Sea. Inner shelf regions are the southernmost red (western), blue (central), and green (eastern) areas. The outer shelf regions are found between the 700-m isobath to 100-km south and are the red (outflow), cyan (western), magenta (central), yellow (eastern), and black (inflow) regions just north of the inner shelf. Slope regions are the remaining northernmost yellow (outflow), green (western), black (central), blue (eastern), and magenta (inflow). The coastline (thick black line), 500-m isobath (magenta line), 1000-m isobath (thin black line), 2000-m isobath (cyan line), and 4000-m isobath (gray line) are represented on the diagram.

NEW ACCOUNT OF ROSS SEA WATERS

The diverse circulation patterns and spatial distributions of all Ross Sea water masses described above inspires regional quantitative analyses of their volumes and mixing histories. Thus, the Ross Sea inshore of the 2000-m isobath, between Cape Adare and Cape Colbeck, is divided into several geographical regions as shown in Figure 21. The 700-m isobath along the shelf break was utilized to distinguish volumes of water masses found only over the slope, e.g. LCDW and AABW, from those over shelf regime, e.g. SW, MSW, and MCDW. Furthermore, because significant water mass modifications are inferred to occur along the shelf break, an arbitrary zonal demarcation extending approximately 100 km inshore of the 700-m isobath is used to distinguish between the outer and inner shelf regimes. Although the area of the slope and outer shelf regimes combined amounts to 2.22×10^5 km^2 (39%; Table 2A), about half (52%) of the entire volume of the Ross Sea is found there (Table 2B).

The Ross Sea was further split into eastern, central, and western regions, roughly along the 175°W and 175°E meridians. The 175°E demarcation seems appropriate because it isolates the two easternmost southern inflows of AASW observed on property maps for the top isopycnal layer. The western and central regions are delineated to separate the two major outflows of shelf waters (HSSW and ISW), as well as the two major inflow paths of MCDW. Since the circulation of the bottom density layer is largely inhibited by the bottom topography, eastward bend was used north of 75°S to separate western and central types of SW, approximately following the Ross, Pennell, and Iselin banks (Figure 2). Altogether the volumes in all the western regions represent exactly half of the Ross Sea total volume (Table 2B), and the combined areas are also roughly half of the Ross Sea total area (Table 2A). In turn, the western inner shelf region holds roughly as much volume (23%) as the central and eastern counterparts combined (25%).

Outside the Ross Sea domain inflow, mainly of AASW, and outflow, mainly of AABW, regimes were considered to the east of 158°W and to the west of 175°W, each also split into slope and outer shelf regions. Waters in these source and sink regions

were not considered during the Ross Sea quantitative comparisons that follow, but are discussed in subsequent section(s).

Table 2
Division of Ross Sea area, volume, and mean depth by geographical regions.

(A)

ROSS SEA AREA (in x10^5 km^2 _ **% of Ross Sea)**

REGION	WEST	CENTRAL	EAST	TOTAL
SLOPE	0.5265_ **9**	0.3025 _ **5**	0.1578 _ **3**	0.9868 _ **17**
OUTER SHELF	0.5745 _ **10**	0.3450 _ **6**	0.3128 _ **6**	1.2323 _ **22**
INNER SHELF	1.6188 _ **29**	1.1095_ **20**	0.7080 _ **12**	3.4363 _ **61**
TOTAL	2.7198 _ **48**	1.7570 _ **31**	1.1785 _ **21**	5.66 _ **100**

(B)

ROSS SEA VOLUME (in x10^4 km^3 _ **% of Ross Sea)**

REGION	WEST	CENTRAL	EAST	TOTAL
SLOPE	7.6809 _ **20**	3.9663 _ **10**	2.2003 _ **6**	13.848 _ **36**
OUTER SHELF	2.7467 _ **7**	1.7384 _ **5**	1.6142 _ **4**	6.0993 _ **16**
INNER SHELF	8.9961 _ **23**	6.2147 _ **16**	3.6335 _ **9**	18.844 _ **48**
TOTAL	19.424 _ **50**	11.919 _ **31**	7.448 _ **19**	38.792 _ **100**

(C)

ROSS SEA MEAN DEPTH (m)

REGION	WEST	CENTRAL	EAST	ALL
SLOPE	1459	1311	1394	1403
OUTER SHELF	478	504	516	495
INNER SHELF	555	561	513	548
ALL	714	678	632	685

Volumetric θ-S Census

A new volumetric θ-S census is calculated for the Ross Sea using high-resolution bins: $\Delta\theta = 0.1°C$, $\Delta S = 0.01$ (Worthington, 1981). Volume contours for the entire Ross Sea θ-S space are displayed in Figure 22A. The listing of the largest one hundred individual bin-volumes is provided in Appendix A. Regional division of the census (Figure 22B-J) provides further details of the water mass distribution in the Ross Sea.

A bimodal distribution is observed for the entire Ross Sea (Figure 22A) with the largest volumes corresponding to LCDW ($\theta = 0.75°C$, $S = 34.72$) and HSSW ($\theta = -1.9°C$, $S = 34.78$). A high-volume lobe (0.03×10^4 km^3 black contour) extends over the LSSW domain ($\theta = -1.9°C$, $S = 34.6$) and continuously over the coldest portions of the MCDW layer ($\theta = -1.2°C$, $S = 34.5$). A mode with volumes larger than 0.01×10^4 km^3 is in Figure 22A encompassing MCDW and LCDW. In contrast, a volume gap ($\theta = 0°C$ to $-1.5°C$, $S \geq 34.7$) exists in the θ-S domain between LCDW and HSSW. Additionally, the entire triangular θ-S space between MCDW and LSSW/HSSW (0.005×10^4 km^3 blue contour) lacks any volume gaps (Figure 22A). Another continuous triangular θ-S space, also within the 0.005×10^4 km^3 blue contour, but with $\gamma^n < 28$ kg m^{-3}, incorporates the lighter AASW. Within the AASW domain, the θ-min layer ($\theta = -1.4°C$, $S = 34.4$) shows the largest volume ($> 0.03 \times 10^4$ km^3).

Along the inner shelf region (Figure 22B-D) characteristics of the SW mode become predominantly fresher from west to east: 34.7 – 34.85 in the western and central and 34.5 in the eastern. Moreover, HSSW shows smaller volumes in the central inner shelf than in the western counterpart, indicating the origin of that water mass. In the eastern inner shelf, the bulk SW ($\theta = -1.9°C$, $S = 34.5$) is not much saltier than the θ-min mode ($\theta = -1.9°C$, $S = 34.4$). This proximity suggests that the formation of LSSW in the eastern Ross Sea is likely the result of θ-min water undergoing a relatively small salinity increase.

Along the slope regions (Figure 22H-J), LCDW shows remarkable homogeneity compared to SW. All three regions show volumes greater than 0.01×10^4 km^3 at potential temperature between 0°C and 1.5°C and salinities near 34.70. How LCDW

mixes with AASW is evident by the boomerang-like shape of the 0.003 x 10^4 km^3 black contour to the 0.01 x 10^4 km^3 purple contour in all three slope regimes. Slightly fresher and smaller (< 0.005 x10^4 km^3) amounts of water within the same density layer begin to reveal the more variable properties of MCDW. The western and central outer shelf regimes (Figure 22E-F) have the largest volumes (> 0.01 x10^4 km^3) of MCDW, with roughly the same θ-S properties. These characteristics are observed at 300 to 500 m, and are nearly identical to those of the MCDW found at much deeper levels (z > 1400 m) in the adjacent offshore slope regimes (θ = 0.1°C, S = 34.67). Such regional similarities over the western and central Ross Sea demonstrate the effective northward export of "inner shelf-like" thermocline water to the oceanic (slope) regime along isopycnals (γ^n = 28.10 kg m^{-3} to 28.27 kg m^{-3}). Note also the clearly connected high-volume ridges (0.003 x 10^4 km^3 black contour) in each of the three outer shelf regions, which all seem to parallel isopycnals (γ^n = 28.25 kg m^{-3} in the western and central, γ^n = 28.15 kg m^{-3} in the eastern).

Preliminary analysis of AnSlope time series data indicates that the coldest LCDW migrating poleward with every diurnal shift of the ASF is warmer than θ ≈ 0.3°C. At the outer shelf, the bottom half of the MCDW layer is "inner shelf-like" thermocline water (θ = -0.5°C, S = 34.6) and much colder than any water imported from the slope; therefore it must have originated over the inner shelf domain. Because there is not much volume of relatively warm MCDW (θ > 0°C) in the eastern outer shelf region (Figure 22G), the lateral replenishment of LCDW offshore with the colder inshore MCDW (θ < 0°C) is missing. Therefore, LCDW does not seem to be directly ventilated along isopycnals over the eastern Ross Sea.

The two major source regions of new AABW show very different patterns. A clear high-volume ridge (0.005 x10^4 km^3 green contour) connects the two parent water masses (MCDW and SW) only in the western outer shelf region (Figure 22E). This mixing path is less prominent for the central outer shelf region (Figure 22F), where a more patchy and less voluminous area is observed at γ^n > 28.27 kg m^{-3}. All of these

observations indicate that the western outer shelf is the most active producer of new AABW.

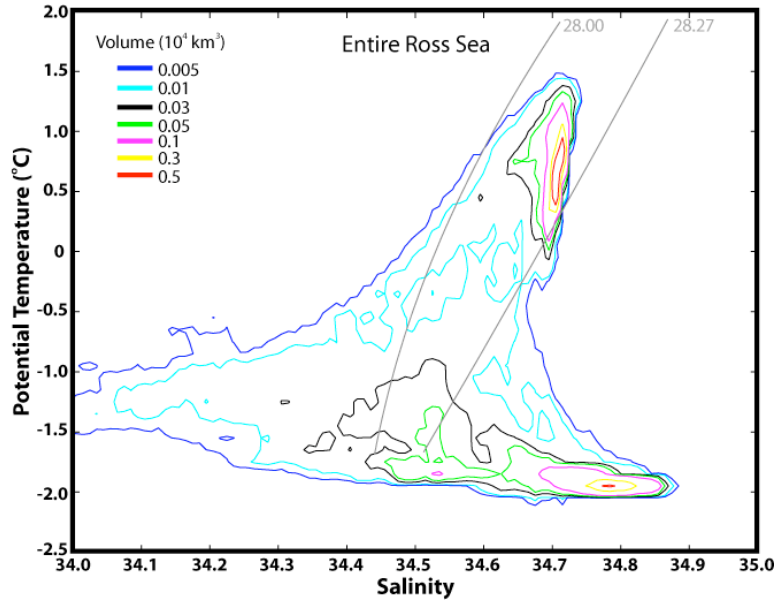

(A)

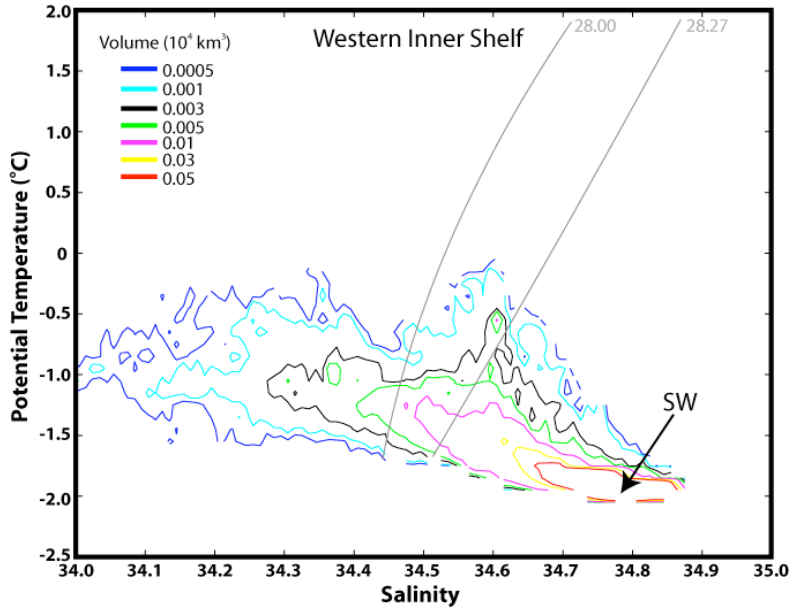

(B)

Figure 22. Volumetric census distribution in θ-S space. Results are displayed for (A) the entire Ross Sea; (B) western, (C) central, and (D) eastern inner shelves; (E) western, (F) central, and (G) eastern outer shelves; and the (H) western, (I) central, and (J) eastern slopes. Volumes are displayed in 10^4 km^3 and the γ^n = 28.00 kg m^{-3} and 28.27 kg m^{-3} isopycnals (gray lines) are shown.

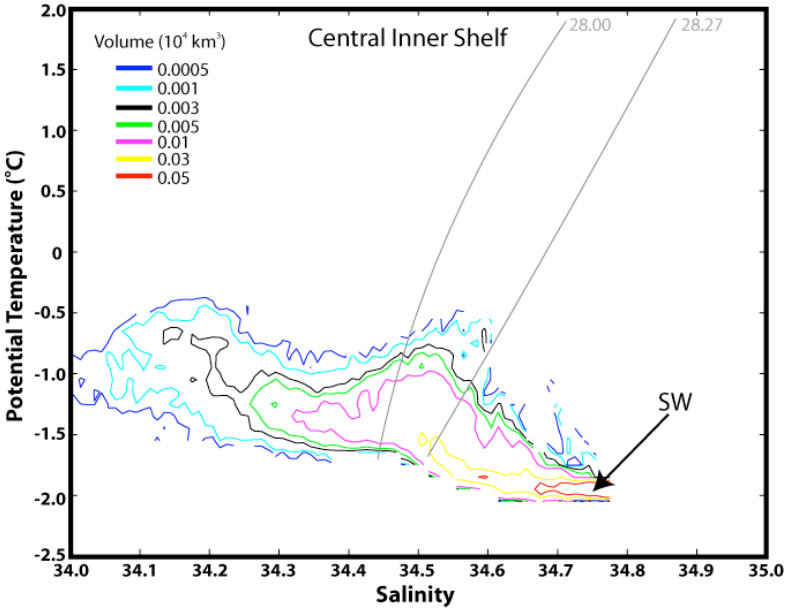

(C)

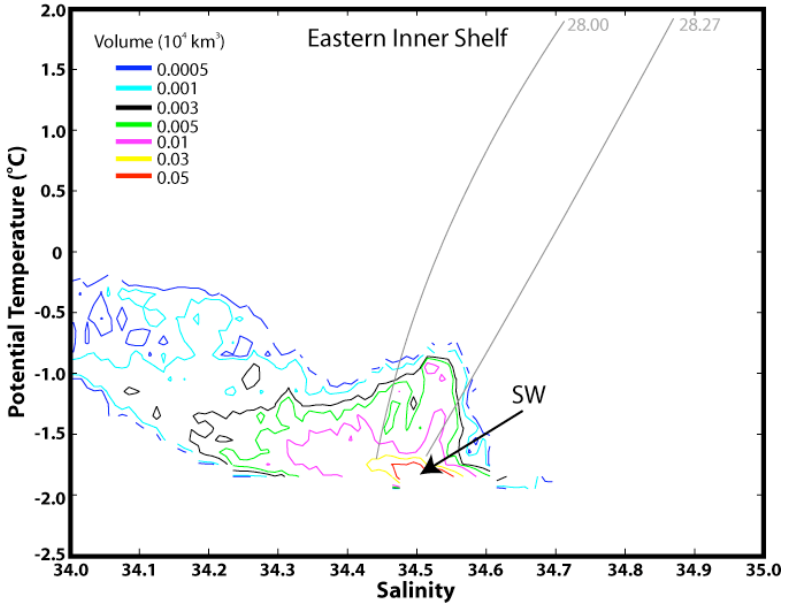

(D)

Figure 22. Continued.

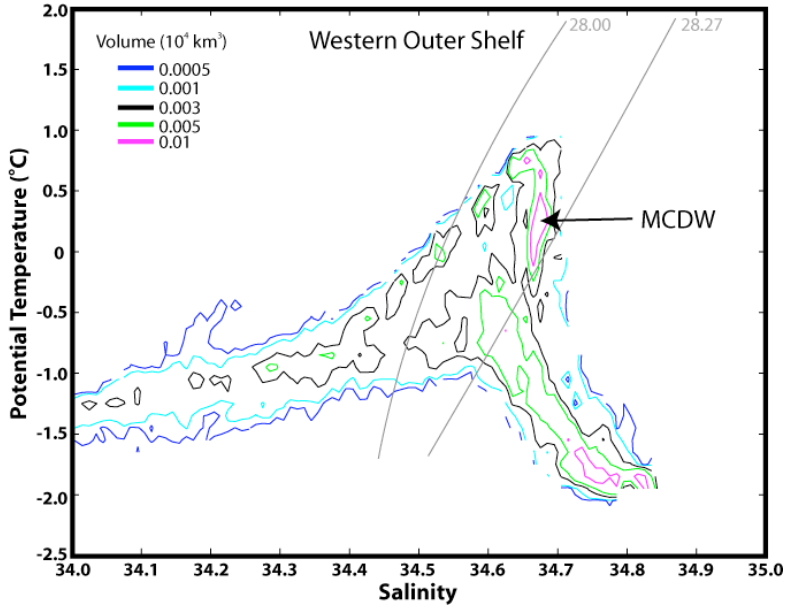

(E)

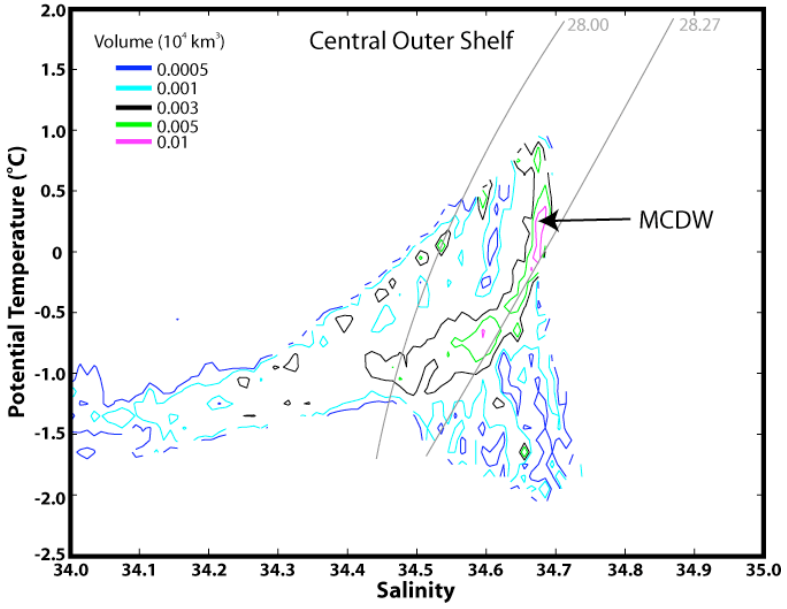

(F)

Figure 22. Continued.

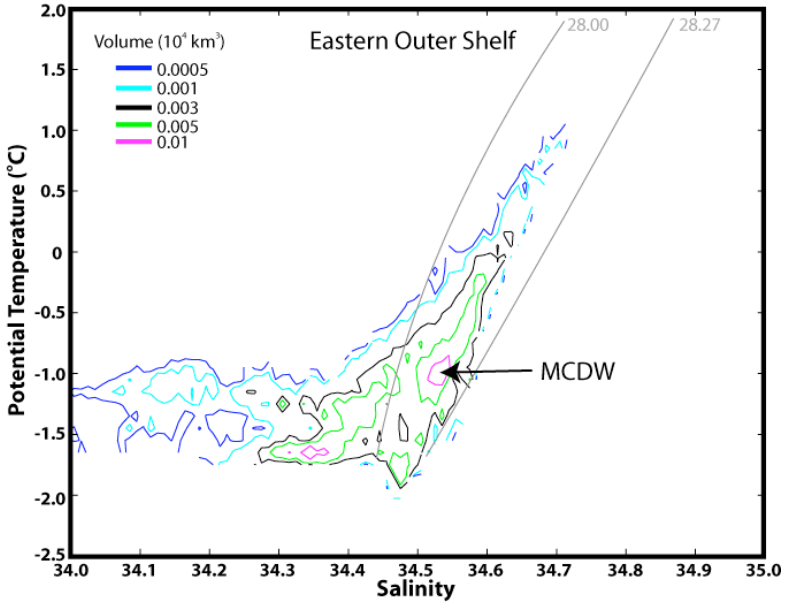

(G)

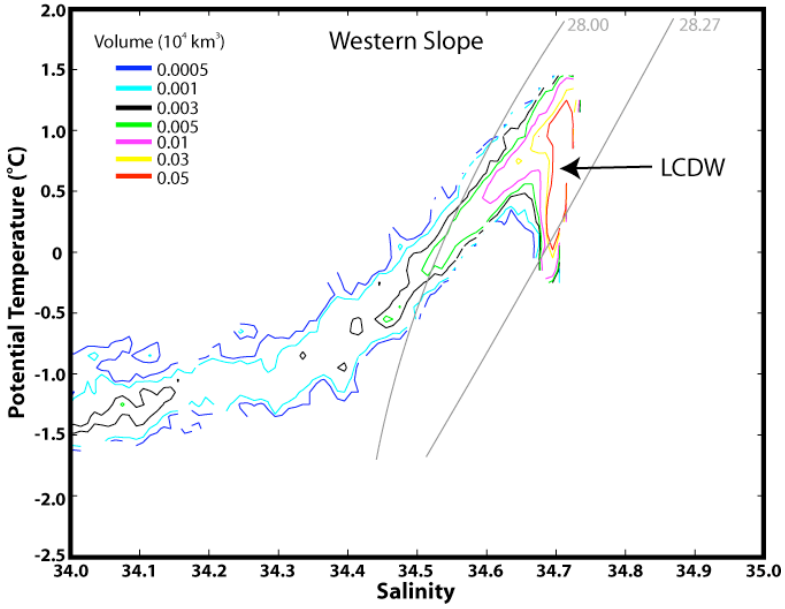

(H)

Figure 22. Continued.

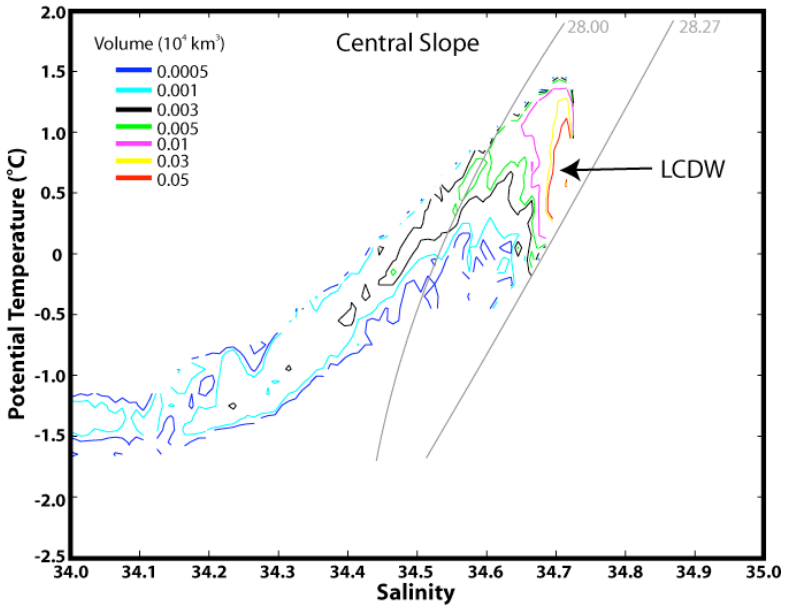

(I)

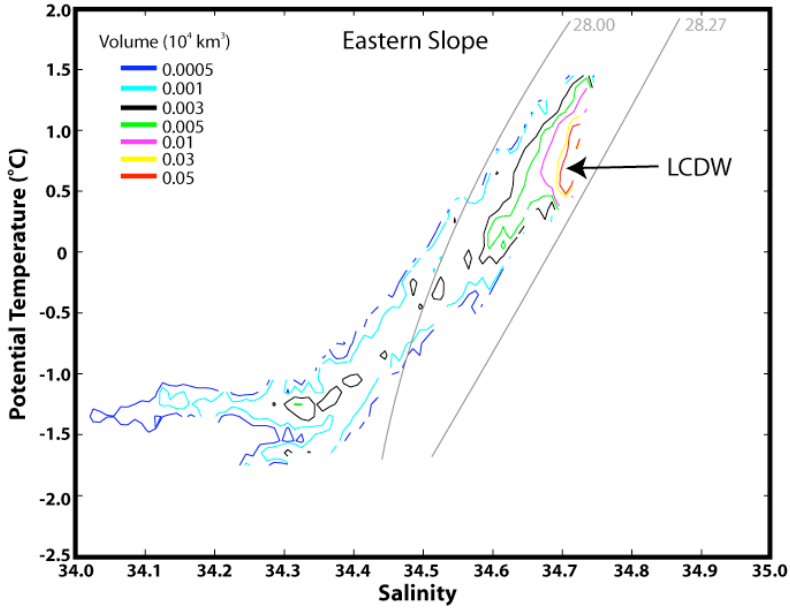

(J)

Figure 22. Continued.

Relative Abundance of Ross Sea Waters

The most volumetric water mass is LCDW (11.694 x 10^4 km^3), taking up about 30% of the Ross Sea (Figure 23; Table 3). The lightest water mass, AASW, has a volume (8.0988 x 10^4 km^3) very similar to the relatively denser near-freezing water mass, SW, about 20% of the Ross Sea. Also, almost 15% is occupied by each of the two modified water masses, MCDW and MSW, with volumes of 5.639 x 10^4 km^3 and 5.435 x 10^4 km^3.

Traces (0.2505 x 10^4 km^3) of AABW represent less than one percent of the Ross Sea. A much larger AABW volume (0.769 x 10^4 km^3) is found just downstream in the outflow region, while none is found upstream in the inflow region. There the Antarctic Coastal Current carries large volumes of AASW (1.7904 x 10^4 km^3), taking up about 98% of the shelf and 41% of the slope regimes. The shelf of the outflow region downstream of Cape Adare is mostly filled with AASW (55%) and MCDW (40%). A local source of AABW in either of the inflow or the outflow regions is precluded by the absence of SW. It is important to note that AABW is found at depths greater than 2000 m, outside of the study region.

As expected in the Ross Sea, which has been historically known for its saline SW, the volume of High Salinity SW (6.2941 x 10^4 km^3) is about four times larger than that of Low Salinity SW. Surprisingly in our classification, Modified SW reveals the opposite distribution, i.e. Low Salinity MSW (4.54824 x 10^4 km^3) is about five times larger than the salty type. Only a minor percentage (7.5%) of the total SW volume (7.67438 x 10^4 km^3) shows potential temperatures colder than -1.95°C, i.e. ISW.

The regional distribution (Table 4) of water mass volumes in the Ross Sea shows where new waters are likely produced. Most (80%) of the HSSW is found in the western shelf regions, whereas the LSSW is mainly concentrated in the central (60%) and eastern (21%) shelf regions. Their Modified varieties (MSW), however, are both more abundant in the western shelf: 94% of the High Salinity and 48% of the Low Salinity types of MSW. About 31% of the Low Salinity MSW is available in the central shelf region. The western slope region shows the largest fraction of LCDW (57%).

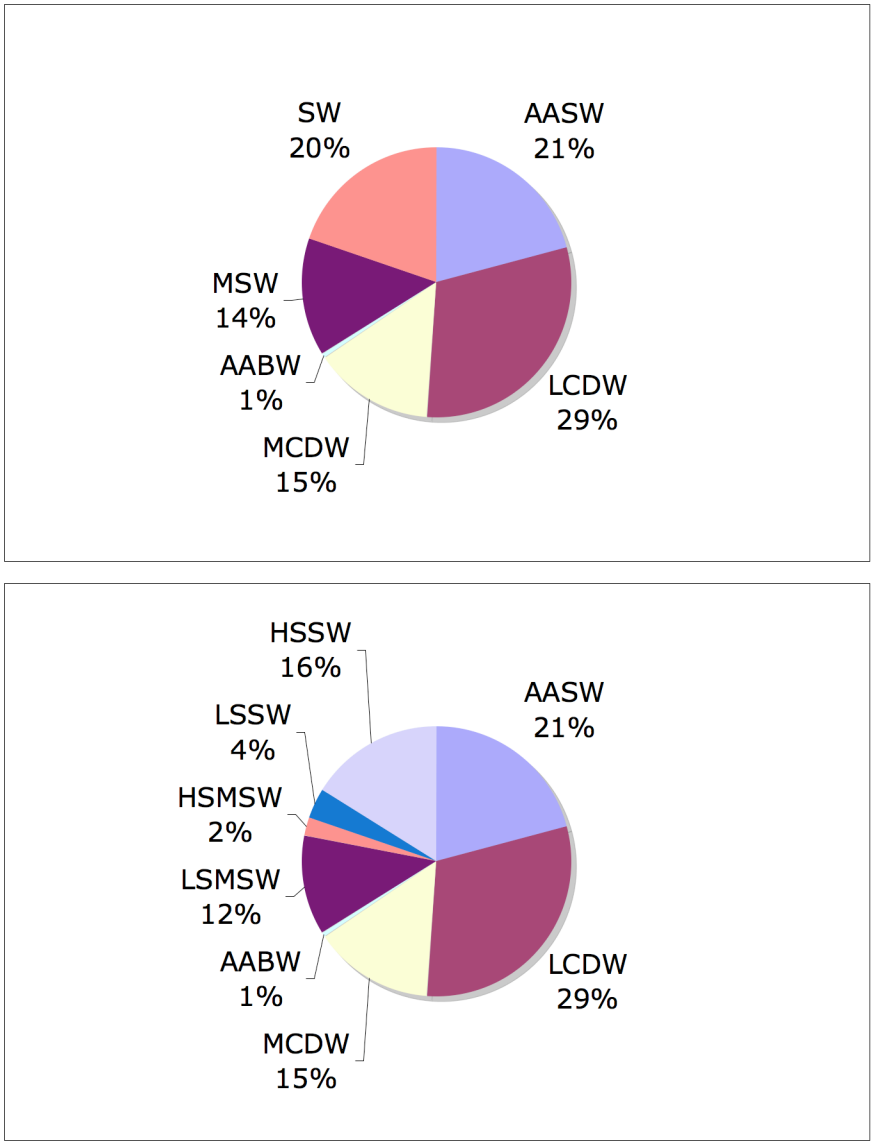

Figure 23. Relative abundance of Ross Sea water masses.

Table 3
Volumes (x10^4 km^3) of Ross Sea water masses by geographical regions.

VOL (x10^4 km^3) REGION		WEST	CENTRAL	EAST	TOTAL	INFLOW	OUTFLOW
	WATER				**38.791**		
SLOPE	**AASW**	0.754	0.730	0.420	1.904	0.563	0.625
SLOPE	**LCDW**	6.696	3.218	1.780	11.694	0.813	2.787
SLOPE	**AABW**	0.232	0.019	0.000	0.250		0.769
SLOPE	**Total**	7.681	3.966	2.200	13.847	1.376	4.182
OUTER SHELF	**AASW**	0.805	0.658	0.789	2.251	1.228	0.454
OUTER SHELF	**MCDW**	0.980	0.747	0.792	2.519	0.026	0.329
OUTER SHELF	**MSW**	0.801	0.312	0.033	1.146		0.029
OUTER SHELF	***LS***	*0.457*	*0.297*	*0.033*	*0.787*		
OUTER SHELF	***HS***	*0.344*	*0.015*	*0.000*	*0.359*		
OUTER SHELF	**SW**	0.161	0.023	0.000	0.184		
OUTER SHELF	***LS***	*0.001*	*0.012*		*0.013*		
OUTER SHELF	***HS***	*0.160*	*0.010*		*0.170*		
OUTER SHELF	**Total**	2.747	1.738	1.614	6.099	1.254	0.812
INNER SHELF	**AASW**	0.823	1.393	1.728	3.944		
INNER SHELF	**MCDW**	0.814	1.310	0.997	3.120		
INNER SHELF	**MSW**	2.199	1.472	0.619	4.289		
INNER SHELF	***LS***	*1.711*	*1.432*	*0.619*	*3.762*		
INNER SHELF	***HS***	*0.488*	*0.039*	*0.000*	*0.528*		
INNER SHELF	**SW**	5.160	2.041	0.290	7.491		
INNER SHELF	***LS***	*0.255*	*0.825*	*0.287*	*1.367*		
INNER SHELF	***HS***	*4.905*	*1.216*	*0.003*	*6.124*		
INNER SHELF	***I***	*0.049*	*0.526*	*0.000*	*0.575*		
INNER SHELF	**Total**	8.996	6.215	3.633	18.844		
	TOTAL	19.424	11.919	7.448	**38.791**		

Total Ross Sea	
AASW	8.099
LCDW	11.694
MCDW	5.639
AABW	0.250
MSW	5.435
LS	*4.548*
HS	*0.887*
SW	7.674
LS	*1.380*
HS	*6.294*
I	*0.575*
TOTAL	**38.791**

Table 4
Regional distribution of water mass volumes in the Ross Sea.

REGION		WEST	CENTRAL	EAST
	WATER	**%**	**%**	**%**
SLOPE	**AASW**	9.30	9.01	5.19
	LCDW	57.26	27.52	15.22
	AABW	92.54	7.46	0.00
OUTER SHELF	**AASW**	9.94	8.12	9.74
	MCDW	17.38	13.24	14.05
	MSW	14.74	5.73	0.61
	LS	*10.04*	*6.53*	*0.73*
	HS	*38.81*	*1.68*	*0.00*
	SW	2.10	0.29	0.00
	LS	*0.06*	*0.90*	
	HS	*2.54*	*0.16*	
INNER SHELF	**AASW**	10.17	17.20	21.33
	MCDW	14.43	23.22	17.68
	MSW	40.46	27.07	11.39
	LS	*37.61*	*31.49*	*13.61*
	HS	*55.08*	*4.44*	*0.00*
	SW	67.24	26.59	3.78
	LS	*18.50*	*59.74*	*20.80*
	HS	*77.93*	*19.32*	*0.04*
	I	*8.47*	*91.53*	*0.00*

Table 5
Percentage of Ross Sea region occupied by each water mass.

REGION		WEST		CENTRAL		EAST	
	WATER	VOLUME	**%**	VOLUME	**%**	VOLUME	**%**
		7.681		3.966		2.200	
SLOPE	**AASW**	0.754	**9.810**	0.730	**18.405**	0.420	**19.088**
SLOPE	**LCDW**	6.696	**87.172**	3.218	**81.124**	1.780	**80.912**
SLOPE	**AABW**	0.232	**3.018**	0.019	**0.471**	0.000	**0.000**
		3.548		1.738		1.614	
OUTER SHELF	**AASW**	0.805	**22.685**	0.658	**37.829**	0.789	**48.871**
OUTER SHELF	**MCDW**	0.980	**27.626**	0.747	**42.948**	0.792	**49.085**
OUTER SHELF	**MSW**	0.801	**22.575**	0.312	**17.928**	0.033	**2.044**
OUTER SHELF	***LS***	*0.457*	**12.874**	*0.297*	***17.073***	*0.033*	**2.044**
OUTER SHELF	***HS***	*0.344*	**9.701**	*0.015*	***0.856***	*0.000*	**0.000**
OUTER SHELF	**SW**	0.161	**4.538**	0.023	**1.294**	0.000	**0.000**
OUTER SHELF	***LS***	*0.001*	**0.025**	*0.012*	***0.712***	0.000	**0.000**
OUTER SHELF	***HS***	*0.160*	**4.514**	*0.010*	***0.582***	0.000	**0.000**
		11.195		6.215		3.633	
INNER SHELF	**AASW**	0.823	**7.354**	1.393	**22.413**	1.728	**47.552**
INNER SHELF	**MCDW**	0.814	**7.268**	1.310	**21.071**	0.997	**27.435**
INNER SHELF	**MSW**	2.199	**19.642**	1.472	**23.678**	0.619	**17.034**
INNER SHELF	***LS***	*1.711*	**15.280**	*1.432*	***23.045***	*0.619*	**17.034**
INNER SHELF	***HS***	*0.488*	**4.363**	*0.039*	***0.634***	*0.000*	**0.000**
INNER SHELF	**SW**	5.160	**46.093**	2.041	**32.838**	0.290	**7.978**
INNER SHELF	***LS***	*0.255*	**2.280**	*0.825*	***13.268***	*0.287*	**7.902**
INNER SHELF	***HS***	*4.905*	**43.813**	*1.216*	***19.570***	*0.003*	**0.076**
INNER SHELF	***I***	*0.049*	**0.435**	*0.526*	***8.466***	*0.000*	**0.000**

*Volumes in 10^4 km^3

The relative abundance of AASW in the Ross Sea diminishes from east to west along all three depth-regimes (Table 5). In the western slope region AASW occupies only 10% of the water column, but about 20% in each of the central and eastern sectors. The same general trend is observed in the relative volumes of MCDW. As much as 50% of the eastern shelf (both outer and inner) volume is taken up by AASW. MCDW is also progressively less abundant toward the west: along the outer and inner shelves, it occupies from 49% to 36% and from 27% to 9% of the local water column. The

opposite zonal tendency is observed in the relative abundance of the denser water masses below. Naturally, SW along the inner shelf regime is dramatically more abundant from east (8%) to west (57%). This is also the case for Modified SW along the outer shelf, whose fraction of the water column increases from 2% to 29%.

The maximum abundance of AASW along the outer shelf of the western and central Ross Sea, compared to the adjacent slope and inner shelf regimes, is a clear indication that this region is commonly the place showing a "V-shaped" expression of the ASF. This is more prominent in the western outer shelf region, where the AASW occupies about 23% of the water column and only 7% (10%) farther to the south (north). In contrast, all three western, central and eastern sectors of the Ross Sea show a progressively less dominant portion of the water column occupied by the source LCDW/MCDW toward the coast; and vice versa for the denser SW/MSW products.

Regional Water Mass Structure

To analyze the spatial distribution of the full stratification in the Ross Sea, mean θ-S curves and ± 1σ standard deviation envelopes were constructed for each of the selected regions. Two sets of mean relationships and variances were calculated, one using the source profile station data and the other taking advantage of the spatially uniform climatology data. Both sets are based on data interpolated to 21 standard neutral density surfaces (Table 2), rather than depth levels, since waters tend to mix primarily along isopycnals. Regional envelopes based on station data were already utilized to validate the climatology during its quality control. In turn we utilize the regional climatological envelopes to gain insights on the θ-S relationships in areas with poor station distributions.

Although in general both sets of mean regional characteristic diagrams are similar, the majority of the station envelopes are wider than the ones based on the new climatology. Most likely this is due to the preliminary spatial smoothing (within the radius of influence) applied during the optimal mapping of property fields.

Station and climatology based θ-S families (mean and envelopes) for all shelf regions (Figure 24A-C) agree remarkably well. Only the eastern inner shelf (Figure

24C) shows a prominent temperature minimum within the AASW layer. It is observed along the $\gamma^n = 27.95$ kg m^{-3} in both mean θ-S curves, which lie roughly at the same mean depth: 125 m (stations) and 142 m (climatology). On the other hand, the climatology created a slightly lighter ($\Delta\gamma^n = 0.15$ kg m^{-3}) and shallower ($\Delta z \approx 100$ m) mean temperature maximum at the eastern inner shelf; whereas the opposite discrepancy is seen at the central and western sectors. The regional depths of the climatological mean temperature maximum (θ-max: 79 m – western, 133 m – central, 195 m – eastern) indicate the general shoaling of MCDW observed from east to west.

Along the outer shelf regime (Figures 25A-C) the western region shows the warmest MCDW, its mean θ-max is warmer in both the climatological ($\theta \approx 0.22$°C) and station ($\theta \approx -0.08$°C) curves. The western mean θ-S curves are practically identical. The mean θ-max core is slightly warmer ($\Delta\theta \approx 0.23$°C) and deeper in the climatology

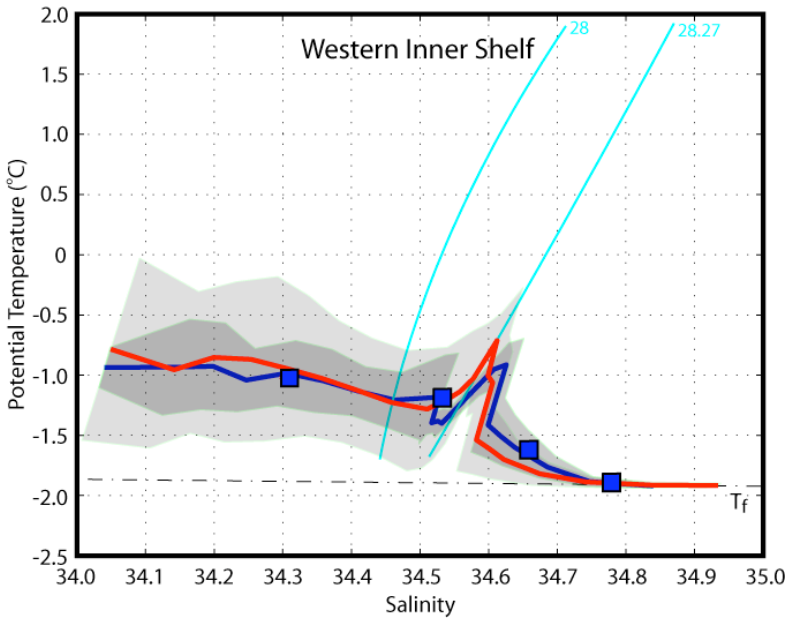

(A)

Figure 24. Mean θ-S curves (hydrographic stations: red line; climatology: blue line) and one-standard deviation envelopes (stations: light grey; climatology: dark gray) for the (A) western, (B) central, and (C) eastern inner shelf regions. Volume weighted mean θ-S properties for AASW, MCDW, MSW, and SW are indicated by the blue squares. Cyan lines represent the $\gamma^n = 28.00$ kg m^{-3} and 28.27 kg m^{-3} neutral density surfaces. The horizontal dashed line represents the freezing point temperature at the sea surface (T_f).

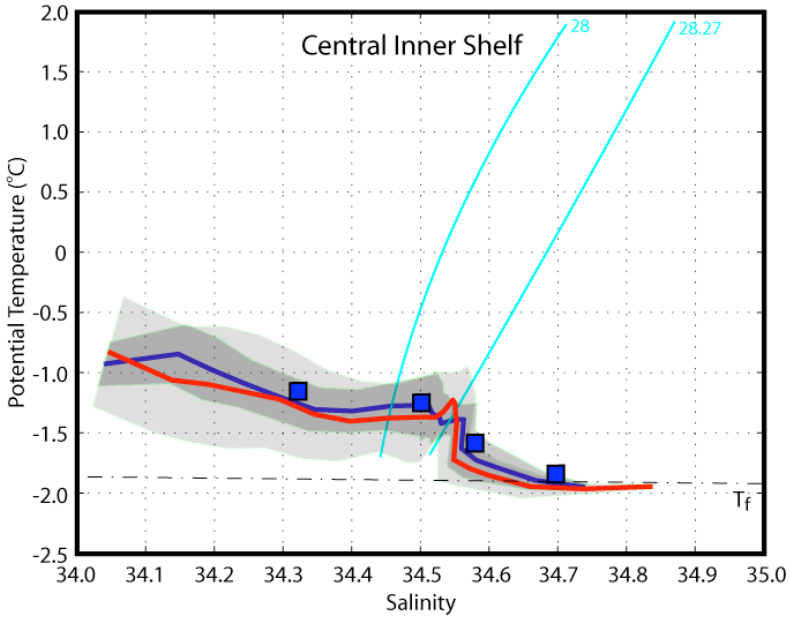

(B)

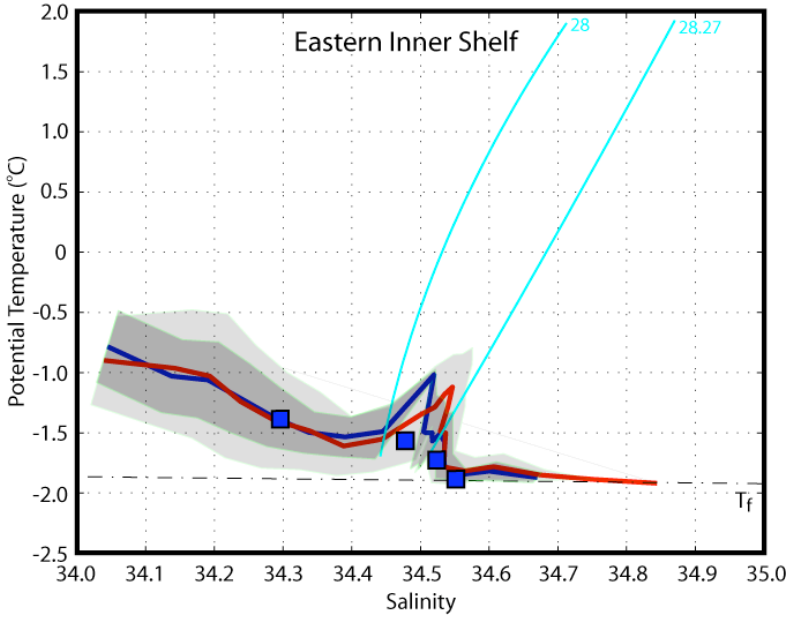

(C)

Figure 24. Continued.

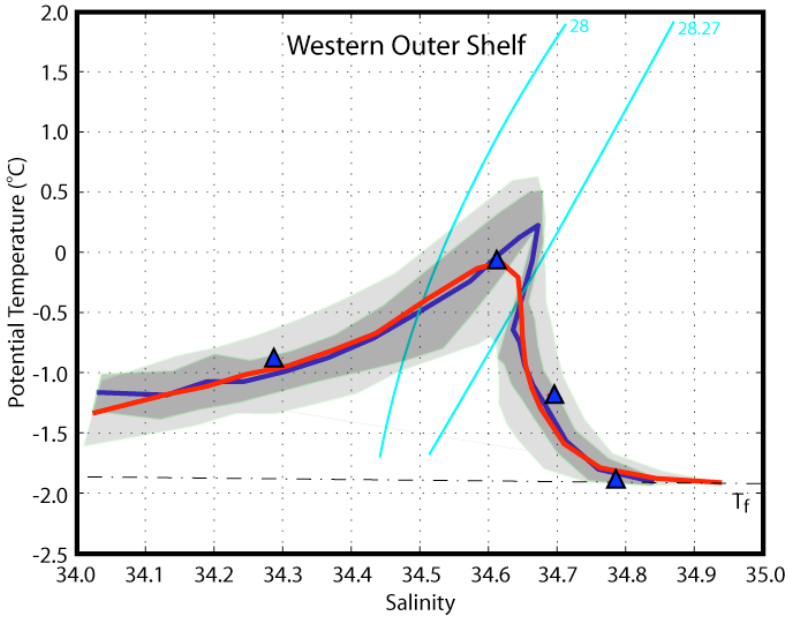

(A)

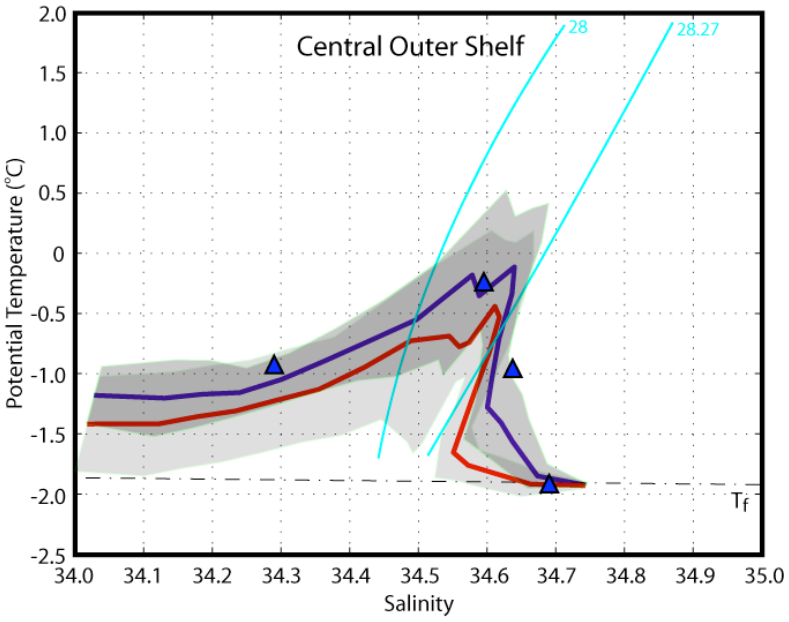

(B)

Figure 25. Mean θ-S curves (hydrographic stations: red line; climatology: blue line) and one-standard deviation envelopes (stations: light grey; climatology: dark gray) for the (A) western, (B) central, and (C) eastern outer shelf regions. Volume weighted mean θ-S properties for AASW, MCDW, MSW, and SW are indicated by the blue triangles. Cyan lines represent the γ^n = 28.00 kg m^{-3} and 28.27 kg m^{-3} neutral density surfaces. The horizontal dashed line represents the freezing point temperature at the sea surface (T_f).

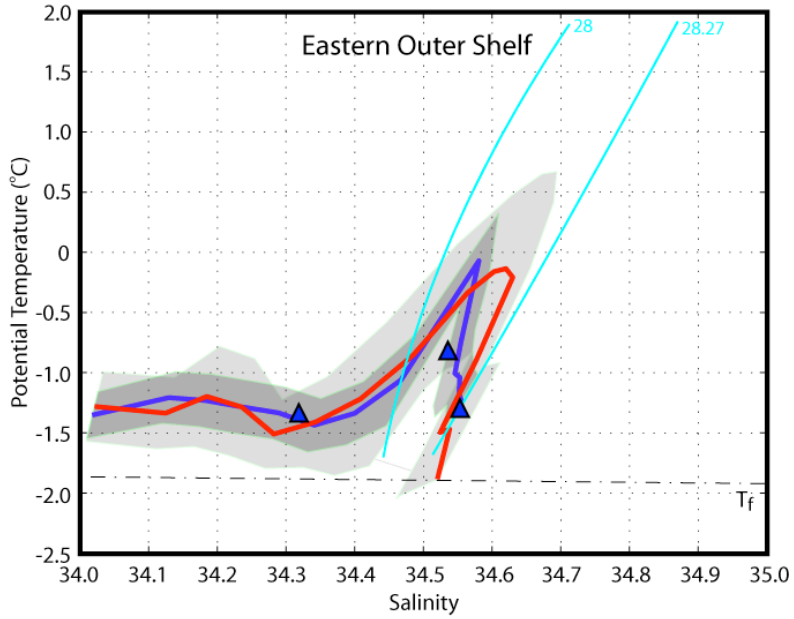

(C)

Figure 25. Continued.

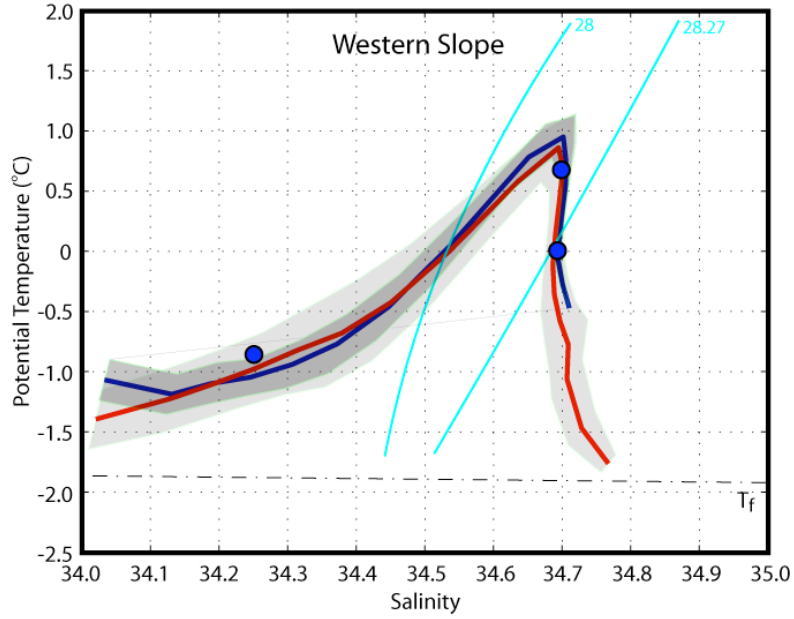

(A)

Figure 26. Mean θ-S curves (hydrographic stations: red line; climatology: blue line) and one-standard deviation envelopes (stations: light grey; climatology: dark gray) for the (A) western, (B) central, and (C) eastern slope regions. Volume weighted mean θ-S properties for AASW, LCDW, and AABW are indicated by the blue circles. Cyan lines represent the γ^n = 28.00 kg m^{-3} and 28.27 kg m^{-3} neutral density surfaces. The horizontal dashed line represents the freezing point temperature at the sea surface (T_f).

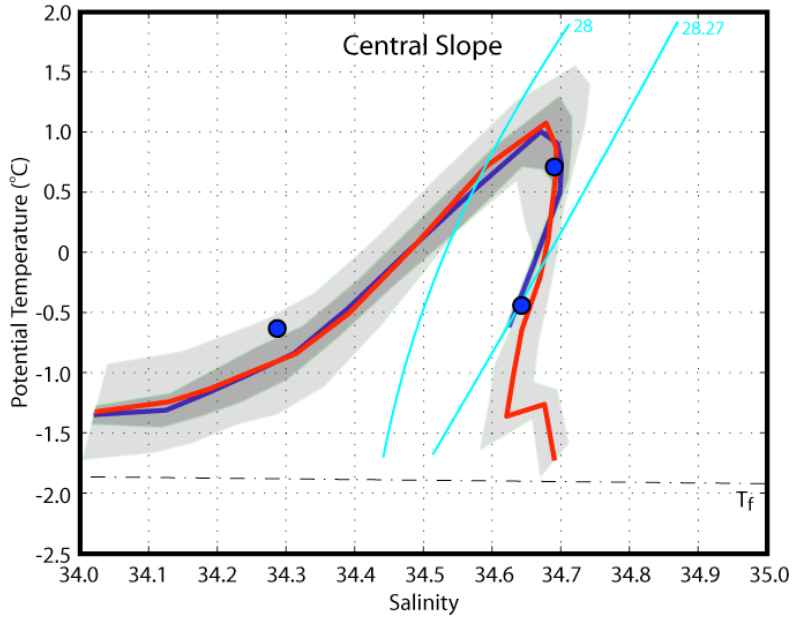

(B)

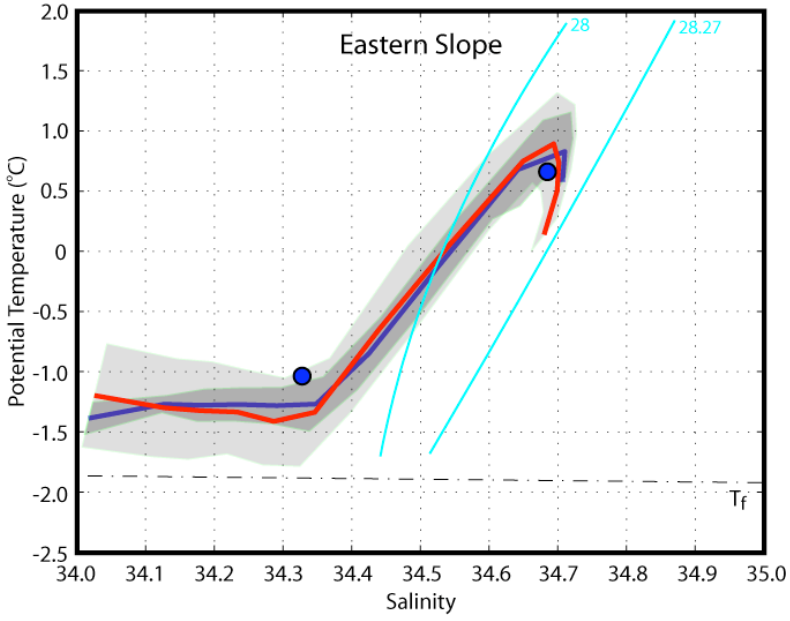

(C)

Figure 26. Continued.

Table 6
Volume weighted water mass potential temperature (°C) and salinity properties for each Ross Sea region.

REGION		WEST		CENTRAL		EAST		INFLOW		OUTFLOW	
		θ	Salinity	θ	Salinity	θ	Salinity	θ	Salinity	θ	Salinity
SLOPE	**AASW**	-0.85	34.25	-0.63	34.29	-1.02	34.33	-1.12	34.24	-1.30	34.29
	LCDW	0.68	34.70	0.71	34.69	0.68	34.69	0.92	34.70	-0.07	34.63
	AABW	0.00	34.69	-0.45	34.64	x	x	x	x	-0.09	34.69
OUTER SHELF	**AASW**	-0.89	34.29	-0.94	34.29	-1.34	34.32	-1.48	34.18	-1.33	34.31
	MCDW	-0.07	34.61	-0.26	34.60	-0.83	34.54	0.56	34.60	-1.13	34.51
	MSW	-1.18	34.69	-0.96	34.64	-1.31	34.55	x	x	-0.64	34.65
	SW	-1.90	34.79	-1.92	34.69	x	x	x	x	x	x
INNER SHELF	**AASW**	-1.02	34.31	-1.20	34.32	-1.40	34.30				
	MCDW	-1.19	34.53	-1.30	34.51	-1.56	34.48				
	MSW	-1.62	34.66	-1.65	34.59	-1.73	34.53				
	SW	-1.91	34.78	-1.93	34.71	-1.87	34.56				

over the western and central regions, but in the eastern region the climatology's θ-max is shallower and nearly as warm as the station-based mean.

Mean characteristic diagrams for the climatology and stations seldom deviated from one another along the slope regions (Figure 26A-C). LCDW's θ-max is found along roughly the same isopycnals in the western (γ^n = 28.10 kg m^{-3}) and central (γ^n = 28.05 kg m^{-3}) regions. Only a minor difference is seen at the eastern slope, where the climatology's θ-max is heavier (γ^n = 28.15 kg m^{-3}) and deeper (z = 940 m) than the station-based core (γ^n = 28.10 kg m^{-3}, z = 615 m), although both lie well below the average sill depth in the Ross Sea, thus indicating the inability of LCDW to flood the eastern shelf. In contrast, the mean depths of the western slope's θ-max (climatology: 448 m, stations: 407 m) and the central (climatology: 365 m, stations: 408 m) are shallow enough for LCDW to enter those shelves. In the western slope, both the mean climatology and station AABW characteristics point to a relatively High Salinity (S >

34.70) SW component. A relatively Low Salinity ($S \leq 34.70$) SW ingredient is indicated by the central slope mean curves. No evidence of newly formed AABW is found at the eastern slope.

Bulk Properties and Mixing Recipes

Volume weighted water mass properties were calculated for each Ross Sea region (Table 6) based on the new climatology. Fairly similar bulk characteristics are found in the AASW of Ross Sea regions, and only slightly fresher (colder) values appear in the upstream (downstream) regions. Almost identical mean characteristics ($\theta \approx 0.7°C$, $S \approx 34.69$) are estimated for the LCDW occupying the Ross Sea slope, whereas the inflow (outflow) region is somewhat warmer (colder). Regional differences within the Ross Sea are suggested in the mean properties of AABW: a relatively Low Salinity ($S \approx 34.64$) central AABW, and a somewhat saltier bulk average ($S \approx 34.69$) in the western and outflow regions.

Average properties of MCDW along the outer shelf do not show the same homogeneity seen in the offshore (slope) LCDW means. This variability is most likely due to the regional differences in the characteristics of the temperature minimum (θ-min) above, which is available to mix vertically with LCDW and form MCDW. The mean salinities for the western ($S \approx 34.78$) and central SW ($S \approx 34.70$) are considerably different, both in the inner and outer shelf regimes, but the eastern inner shelf SW shows an even fresher ($S \approx 34.56$) bulk salinity.

Bulk water mass properties show a clear pattern in the overall stratification of the Ross Sea: a progressive westward salinity increase. Even though only small variability is inferred in the AASW and LCDW of the Ross Sea, bulk salinities for each of the other water masses are lowest in the eastern regimes and highest in the western regimes. Moreover the whole volumetric mean θ-S relationship for the MCDW-MSW-SW structure uniformly shifts toward lower salinities from the western to the eastern Ross Sea sectors.

Combined with the corresponding mean regional θ-S curves, bulk water mass properties are useful to infer the dominant mixing processes producing new AABW in

the Ross Sea. For such process to take place it is required that all mixing ingredients coalesce, and only the western and central outer shelf regions satisfy that condition. Those two regions show that portions of MCDW and SW mix along straight lines in θ-S space, i.e. in the direction indicated by the gray envelopes in Figures 25A-B, roughly connecting the volumetric mean characteristics of the local MCDW, MSW and SW types.

Mean characteristics of the AABW at the central slope (θ = -0.45°C, S = 34.64, γ^n = 28.30 kg m^{-3}) fall exactly on that line, and at a point that indicates a composition from the diapycnal mixing of MCDW (75%) with SW (25%). In the western outer shelf, the climatological mean curve shows a sharp inflection point at the top of the MSW layer, near θ = -0.64°C and S = 34.64. This MSW has the same density of the mean AABW at the slope (θ = 0.0026°C, S = 34.69), thus it represents a potential source water after sinking downward along isopycnal surfaces. The composition of that source MSW would be the same as inferred in the central outer shelf, i.e. 75% and 25% of the local MCDW and SW types. Modified SW with these source characteristics (θ = -0.64°C, S = 34.64, γ^n = 28.30 kg m^{-3} and θ = -0.71°C, S = 34.62, γ^n = 28.30 kg m^{-3} along the mean θ-S curve) are found at 266 m in the western and at 360 m central regions near the shelf break (outer shelf) according to the mean θ-S curves. Offshore sinking along isopycnal surfaces would bring these waters down to the bottom of the slope.

Western MCDW at the outer shelf is composed of 30% θ-min water and 70% LCDW at the slope, but moving eastward, the θ-min water has a greater influence on MCDW. Its inferred contribution to the central MCDW increases to 40%. The eastern outer shelf region displays the greatest θ-min influence, of about 60%.

If one considers that "source" Modified Shelf Water is the mixing product of LCDW, θ-min water, and SW occurring over a relatively wider zonal band (outer shelf/slope regimes), then its composition would reflect the general eastward freshening of the AASW described before. Western MSW would be composed of 23% θ-min water, 52% LCDW and 25% SW, but central MSW would have more (30%) θ-min water, less (45%) LCDW, and equal (25%) amounts of SW.

AABW formation is not inferred near the eastern shelf break due to the lack of a SW component. However, the small presence of MSW there is most likely advected in from the central region.

DECADAL CHANGES IN ROSS SEA WATERS

Decadal variability in water mass characteristics was examined based on the source station data of the Ross Sea. Profile data were grouped to locate regions with adequate spatial sampling and large variance in properties interpolated to four isopycnal surfaces (AASW: γ^n = 27.95 kg m^{-3}, LCDW/MCDW: γ^n = 28.05 kg m^{-3} and 28.10 kg m^{-3}, HSSW: γ^n = 28.7 kg m^{-3}) and two depth levels (AASW: z = 200 m, MCDW: z = 500 m). All of the time series in these regions span at least 35 years and are derived from no fewer than 15 hydrographic stations. Five-year averages of interpolated potential temperature, salinity, and depth (or neutral density) were computed starting at 1950, in part to account for the relatively large uncertainty in older instrumentation and sampling methods used prior to the advent of high-resolution CTD recorders, but also to reduce the expected short-scale temporal and spatial aliasing in the historical data. The linear fit to the averaged data and the associated correlation coefficient (r^2) were calculated along with the standard deviation of the averaged data for each time series. Regions with robust linear fits and high variance, ought to provide insight on the sources and processes giving rise to the observed long-term trends. Inspection of inferred long-term property trends on selected isopycnals (depth levels) were then extended to the entire water mass layer.

Freshening of Antarctic Surface Water

The region with one of the largest freshening signals in the AASW layer is located at the inflow from the Antarctic Coastal Current, in an area located just northeast of Cape Colbeck (158°-140°W, Figure 27A). Here the entire water column is comprised of AASW, and the interpolated data at 200 m is deep enough to be unaffected by seasonal variability. The 38 hydrographic casts used in the construction of the time series for this area span over 40 years. A sizeable freshening (r^2 = 0.81) is indicated at 200 m where salinities (Figure 27B) in the 1960s (S $\approx$ 34.35) have steadily decreased to S $\approx$ 34.15 by the year 2000. The same general trend is consistently found between 100 m and 300 m in this region (Figure 27E). Potential temperatures, however, do not show

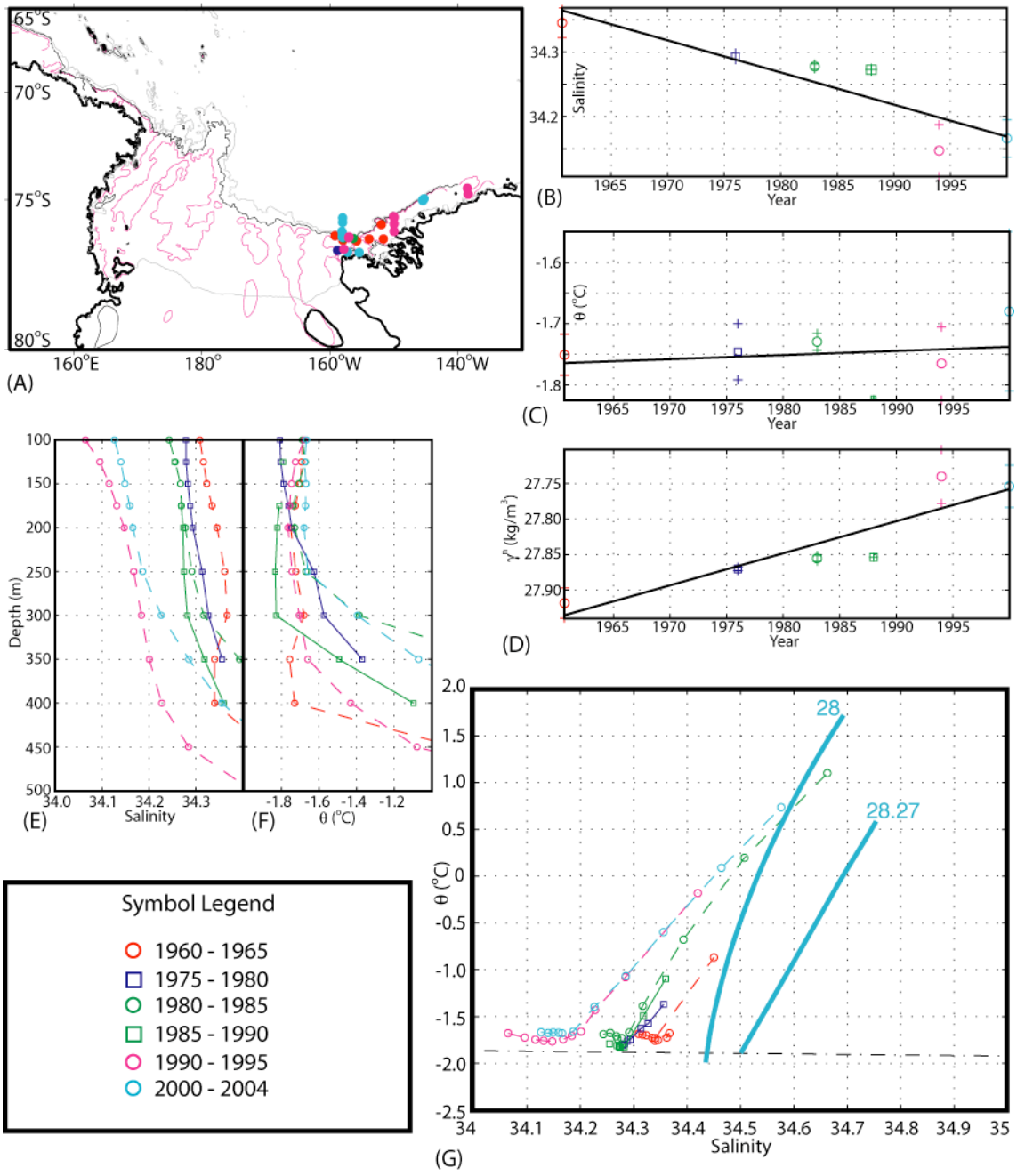

Figure 27. Temporal variability of inflowing AASW at 200 m. (A) Location of stations used to analyze AASW inflow variability. Five-year mean (B) salinity, (C) potential temperature, and (D) neutral density versus year for stations at 200-m depth with linear best-fit lines in black. Circles and squares represent mean value with error bars marked by plus signs above and below. Five- year mean (E) salinity and (F) potential temperature versus depth (z > 100 m) for stations shown in (A). (G) θ-S plot of 5-year mean values from (E) and (F).

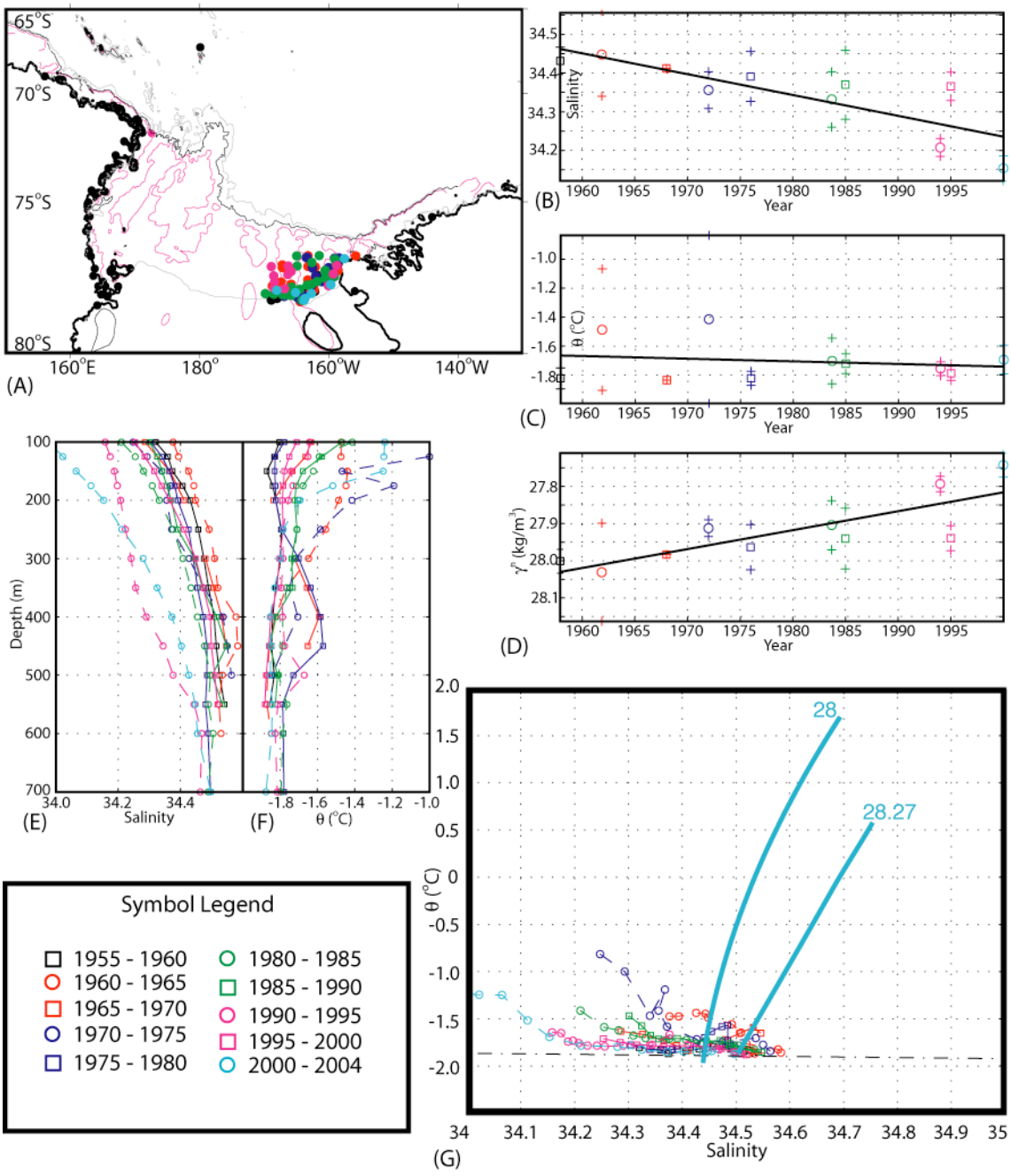

Figure 28. Temporal variability of eastern AASW at 200 m. (A) Location of stations used to analyze AASW inflow variability. Five-year mean (B) salinity, (C) potential temperature, and (D) neutral density versus year for stations at 200-m depth with linear best-fit lines in black. Circles and squares represent mean value with error bars marked by plus signs above and below. Five- year mean (E) salinity and (F) potential temperature versus depth for stations shown in (A). (G) θ-S plot of 5-year mean values from (E) and (F).

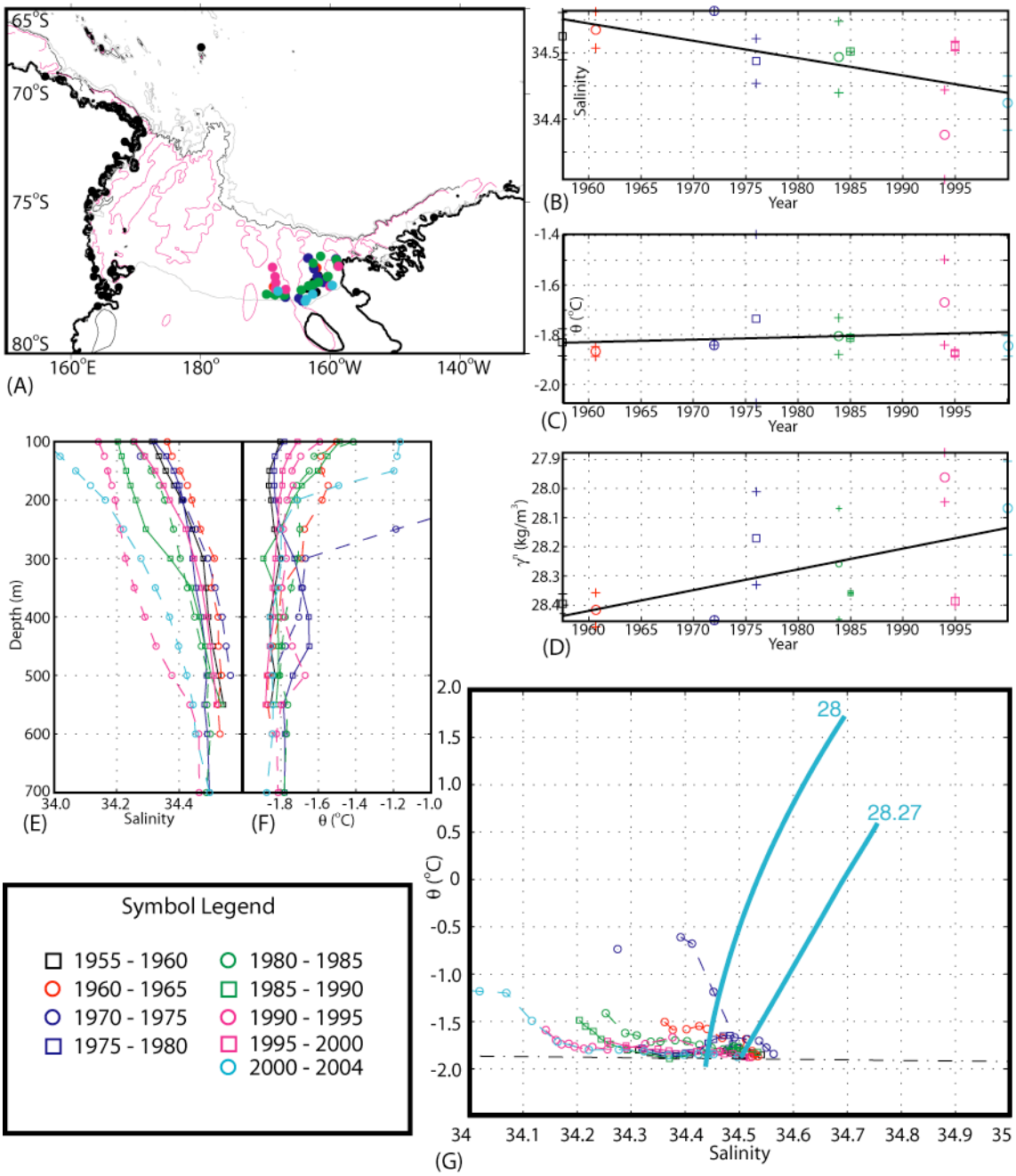

Figure 29. Temporal variability of eastern MCDW at 500 m. (A) Location of stations used to analyze MCDW variability. Five-year mean (B) salinity, (C) potential temperature, and (D) neutral density versus year for stations at 200-m depth with linear best-fit lines in black. Circles and squares represent mean value with error bars marked by plus signs above and below. Five- year mean (E) salinity and (F) potential temperature versus depth for stations shown in (A). (G) θ-S plot of 5-year mean values from (E) and (F).

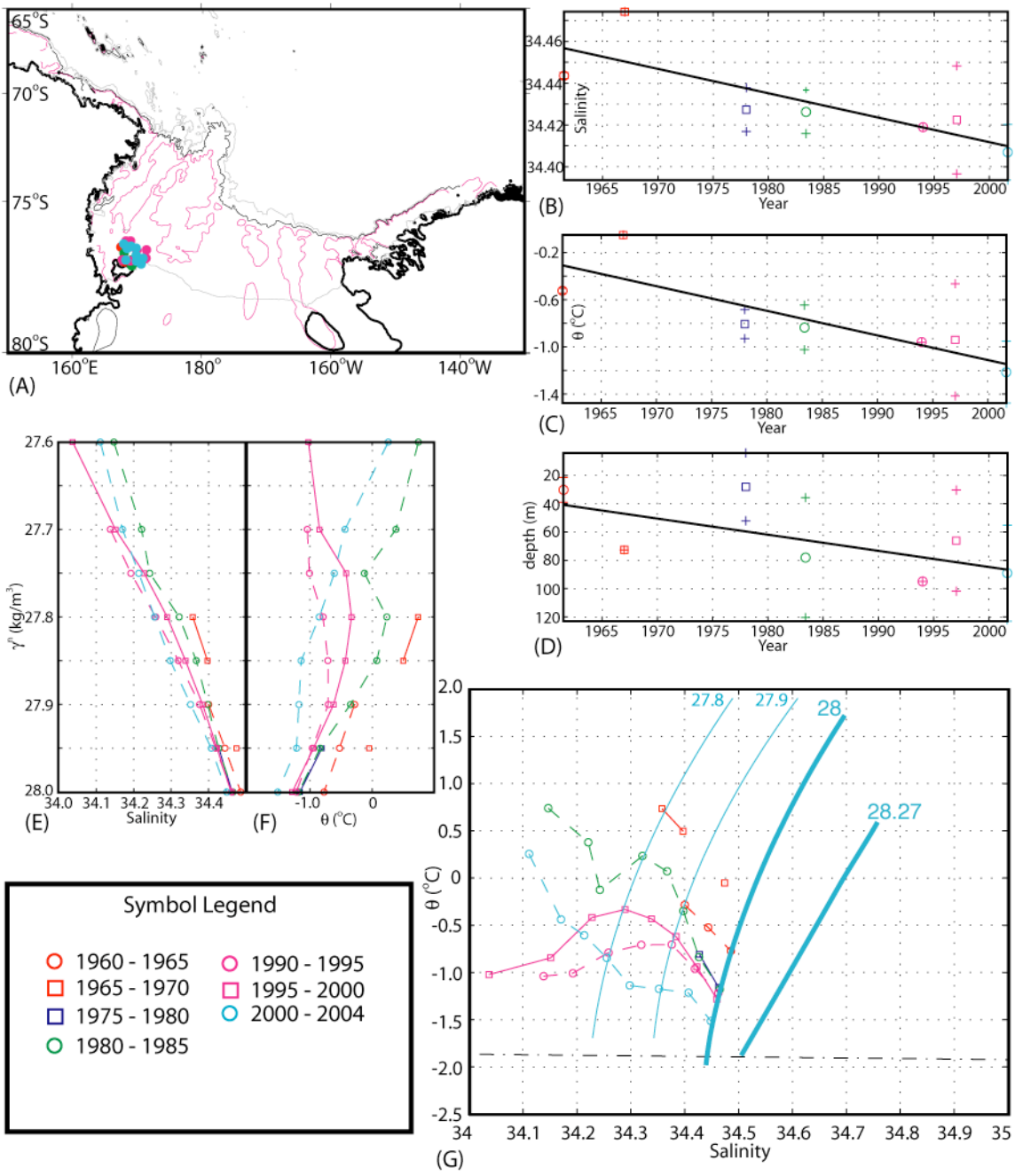

Figure 30. Temporal variability of AASW on the 27.95 kg m^{-3} neutral density surface near Ross Island. (A) Location of stations used to analyze AASW variability. Five-year mean (B) salinity, (C) potential temperature, and (D) depth versus year for stations along the 27.95 kg m^{-3} neutral density surface with linear best-fit lines in black. Circles and squares represent mean value with error bars marked by plus signs above and below. Five-year mean (E) salinity and (F) potential temperature versus depth for stations shown in (A). (G) θ-S plot of 5-year mean values from (E) and (F).

any major warming or cooling ($r^2 = 0.04$) at 200 m (Figure 27C), nor in the upper 300 m (Figure 27F), where a nearly homogeneous temperature of about $\theta = -1.75°C$ has been measured during this 40-year time period. Nonetheless, the observed freshening was large enough to change the overall density at 200 m in this region, from $\gamma^n = 27.95$ kg m^{-3} to a much lighter AASW with $\gamma^n = 27.75$ kg m^{-3}. In fact Figure 27G reveals that there was a dramatic freshening ($\Delta S = 0.2$) not only of the local temperature minimum but also in portions of the upper thermocline water as well.

Similar salinity trends in the AASW are found inside the eastern Ross Sea south of 77°S (170°-160°W, Figure 28A). The 146 hydrographic casts used in this area were taken over 45 years. AASW considerably freshens ($r^2 = 0.67$) from $S \approx 34.45$ in the 1950s and 1960s to $S \approx 34.15$ by the year 2000. Figure 28D shows that such salinity change was large enough to transform what we classify as MCDW ($28 < \gamma^n > 28.27$ kg m^{-3}) to lighter AASW ($\gamma^n = 27.75$ kg m^{-3}). Data from the stations (75) reaching deeper than 500 m in this same region (Figure 29A) shows basically the same long-term tendency toward lower salinities seen at 200 m. There is a seemingly considerable ($r^2 = 0.47$) freshening (Figure 29B) from about $S \approx 34.55$ in the 1950s to $S \approx 34.40$ in 2000. The relatively low r^2 for the 500-m salinity time series is probably due a lower number of stations at this location. Such reduction in salinity (density) implies that local waters at 500 m used to be as dense as LSSW ($\gamma^n = 28.40$ kg m^{-3}), but now constitute relatively lighter MCDW ($\gamma^n = 28.10$ kg m^{-3}). This suggests that near the eastern Ross Ice Shelf the general freshening trend is clearly robust between 100 m and 500 m (Figure 29E).

In the southwestern corner of the Ross Sea, just north of Ross Island (Figure 30A), there is another region with a similar temporal variance in the local AASW. The 53 stations nearby indicate a less pronounced freshening trend over the past 40 years ($\Delta S = 0.05$, $r^2 = 0.68$) along the $\gamma^n = 27.95$ kg m^{-3} surface (Figure 30B), which lies at the base of the AASW layer. In contrast to the lack of any temperature trends at the 200-m level in the other two regions, there is a dramatic ($r^2 = 0.73$) cooling ($\Delta\theta \approx 1.0°C$) in the AASW along this isopycnal (Figure 30C). In turn this isopycnal appears to have

deepened about 50 m (Figure 30D) over that period of time, but still remaining within the upper 100 m. The high r^2 values are consistent with linear long-term trends observed along additional isopycnal surfaces (Figure 30G) above (γ^n = 27.80 kg m^{-3} to 27.90 kg m^{-3}) and below (γ^n = 28.00 kg m^{-3}).

Long-term salinity changes in the AASW has been reported recently by Jacobs (2002), who shows a widespread freshening of the temperature minimum over the southern and eastern portions of the Ross Gyre. The origin of this oceanic signal was speculated to be located in the Ross Sea, where the largest changes in the AASW salinity are found at the entrance of the Antarctic Coastal Current, i.e. the ultimate source of the freshwater anomaly. He found sizeable 40-year freshening trend near the two ends of the Ross Ice Shelf, the western of which coincides with one of the areas described above.

Warming of Lower Circumpolar Deep Water

Jacobs (2002) reported changes in the characteristics of the oceanic source water of the opposite trend to those observed in the AASW. They were inferred from a decadal warming and salinity increase of the subsurface temperature maximum. Here the reported trends are investigated further near the inflows of LCDW to the Ross Sea, i.e. where the eastern limbs of the Ross (Figure 31A) and Balleny gyres (Figure 32A) approach the continental slope. Although no stations are available in these areas between 1975 and 1985, an apparent warming of LCDW is also inferred along two isopycnals lying near the top of this source water layer.

Properties from 43 deep stations (water depths > 700 m) located just northeast of Cape Colbeck (158°-140°W, Figure 31A) reveal a long-term salt (ΔS = 0.04, r^2 = 0.58) and heat ($\Delta\theta$ = 0.4°C, r^2 = 0.58) gain on the γ^n = 28.05 kg m^{-3} (Figures 31B-C), which lies approximately at the local subsurface temperature maximum (Figure 31F). Examination of the entire LCDW layer in this region (Figure 31E-G) confirms these trends along γ^n = 28.00 kg m^{-3} and 28.10 kg m^{-3}. Jacobs (2002) analysis at the 200-m to 400-m levels also shows that the largest warming occurs in the southeastern limb of the Ross Gyre, versus the changes in the northwestern limb.

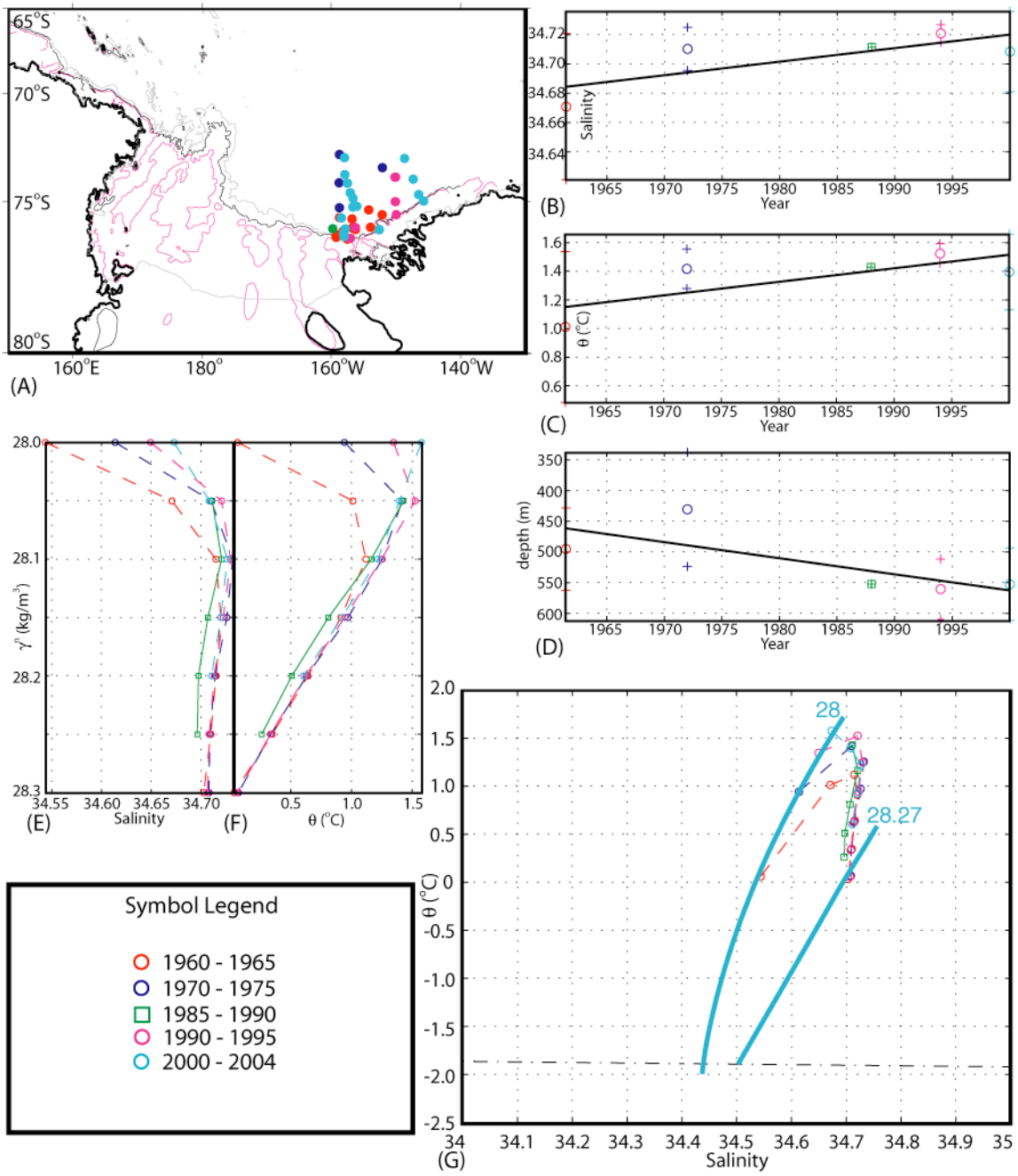

Figure 31. Temporal variability of inflowing LCDW from the Ross Gyre on the 28.05 kg m^{-3} neutral density surface. (A) Location of stations used to analyze inflowing LCDW variability. Five-year mean (B) salinity, (C) potential temperature, and (D) depth versus year for stations along the 28.05 kg m^{-3} neutral density surface with linear best-fit lines in black. Circles and squares represent mean value with error bars marked by plus signs above and below. Five- year mean (E) salinity and (F) potential temperature versus depth for stations shown in (A). (G) θ-S plot of 5-year mean values from (E) and (F).

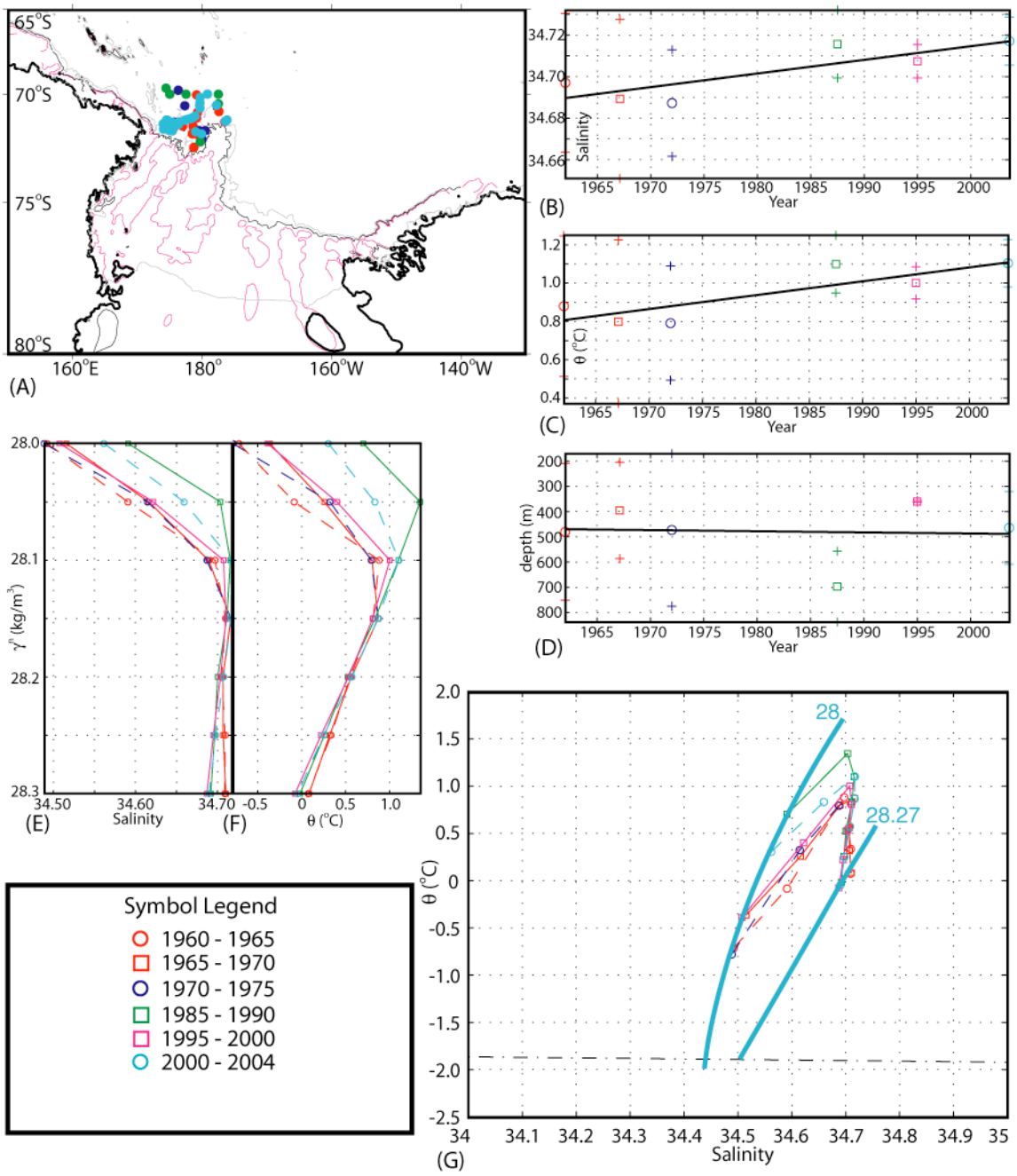

Figure 32. Temporal variability of inflowing LCDW from the Balleny Gyre on the 28.1 kg m^{-3} neutral density surface. (A) Location of stations used to analyze inflowing LCDW. Five-year mean (B) salinity, (C) potential temperature, and (D) depth versus year for stations along the 28.10 kg m^{-3} neutral density surface with linear best-fit lines in black. Circles and squares represent mean value with error bars marked by plus signs above and below. Five- year mean e) salinity and f) potential temperature versus depth for stations shown in (A). g) θ-S plot of 5-year mean values from (E) and (F).

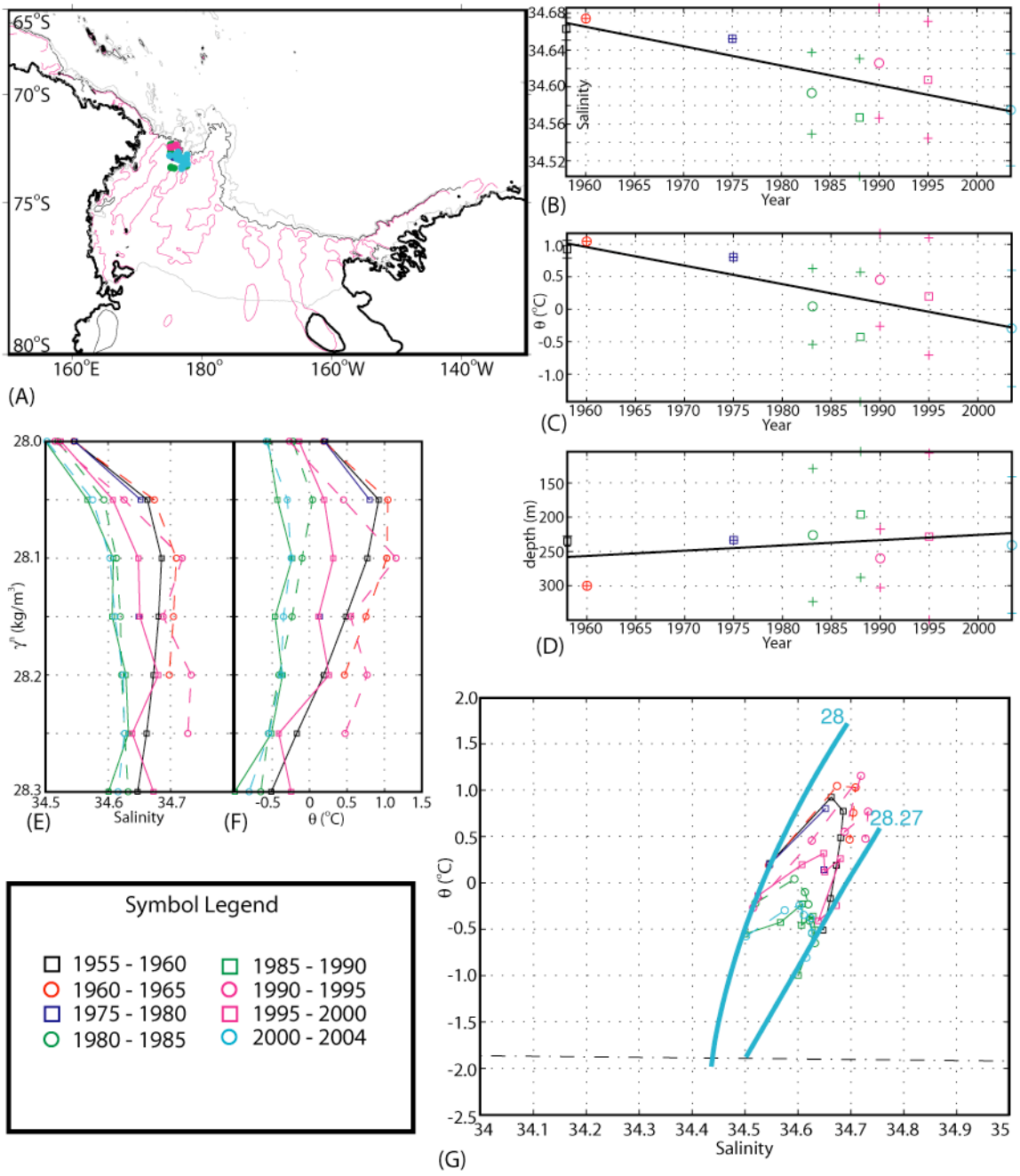

Figure 33. Temporal variability of MCDW on the 28.1 kg m^{-3} neutral density surface in the western Ross Sea. (A) Location of stations used to analyze inflowing MCDW variability. Five-year mean (B) salinity, (C) potential temperature, and (D) depth versus year for stations along the 28.05 kg m^{-3} neutral density surface with linear best-fit lines in black. Circles and squares represent mean value with error bars marked by plus signs above and below. Five- year mean (E) salinity and (F) potential temperature versus depth for stations shown in (A). (G) θ-S plot of 5-year mean values from (E) and (F).

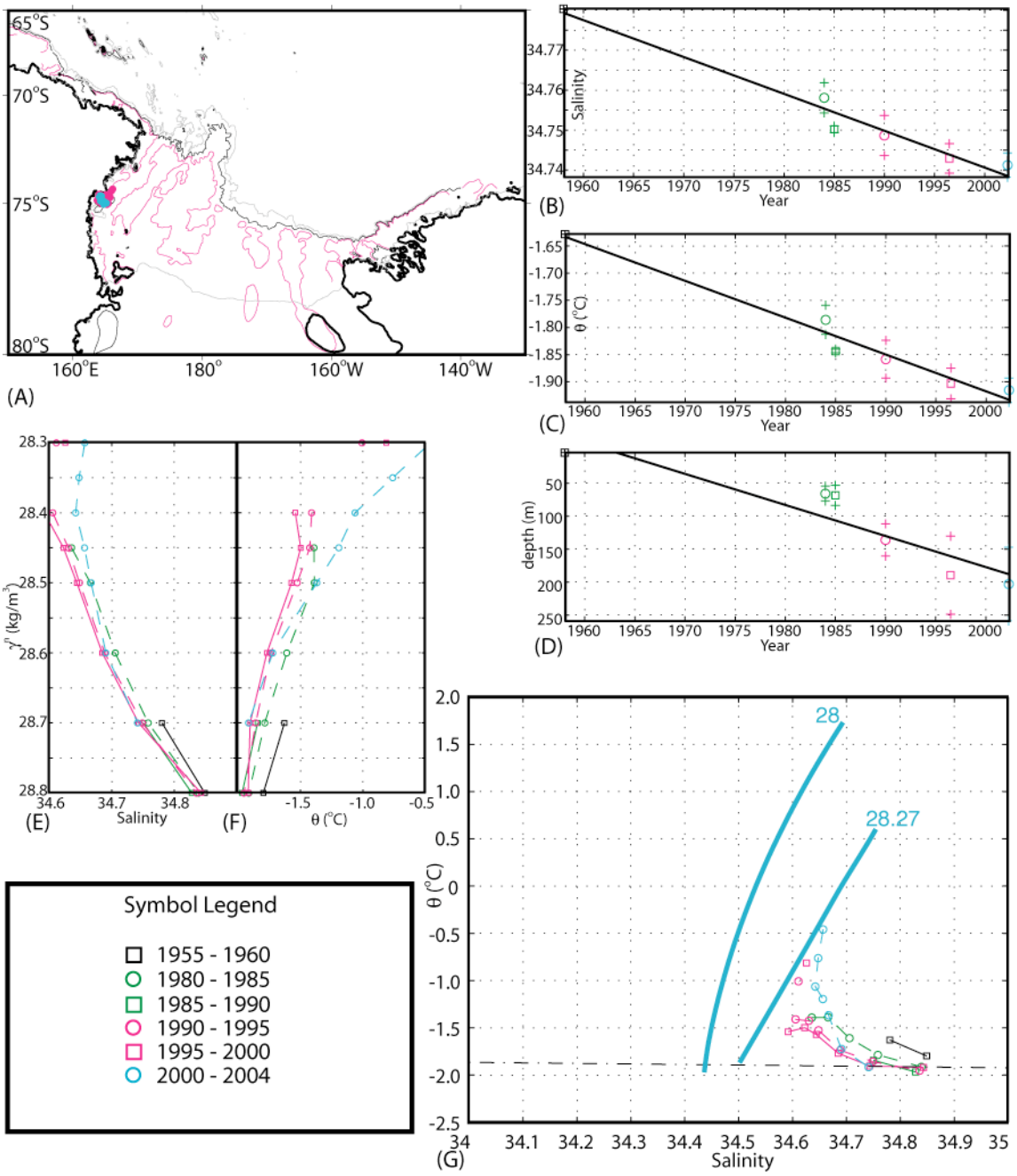

Figure 34. Temporal variability of HSSW on the 28.70 kg m^{-3} neutral density surface near the Terra Nova Bay polynya. (A) Location of stations used to analyze HSSW variability. Five-year mean (B)salinity, (C) potential temperature, and (D) depth versus year for stations along the 28.70 kg m^{-3} neutral density surface with linear best-fit lines in black. Circles and squares represent mean value with error bars marked by plus signs above and below. Five- year mean (E) salinity and (F) potential temperature versus depth for stations shown in (A). (G) θ-S plot of 5-year mean values from (E) and (F).

The 76 stations available at the western inflow region just west of Pennell Bank (Figure 32A) show very similar 40-year trends along $\gamma^n = 28.10$ kg m^{-3}. A 0.03 salinity increase ($r^2 = 0.71$) and 0.3°C warming ($r^2 = 0.72$) is indicated by the local time series (Figures 32B-C). As in the eastern inflow region (Figure 31), these trends extend through upper LCDW layer, between $\gamma^n = 28.00$ kg m^{-3} and 28.10 kg m^{-3} (Figure 32E-G).

Effects of Mixing Byproducts

The observed long-term changes in the characteristics of AASW and LCDW of the Ross Sea must inevitably bear some effect on the water mixtures produced by them. Assuming the mechanisms that mix AASW with LCDW across isopycnals near the shelf break remained the same during the past forty years, the resulting MCDW found near the inflow regions described above is likely to also reflect decadal variability in its property values. Only the outer shelf segment just west of Pennell Bank has adequate sampling and a large signal of property trends in the local MCDW.

Fifty-six stations located near the shelf break (water depths shallower than 700 m) between the Drygalski and Joides troughs (Figure 33A) are reasonably close to the progressively warmer and saltier LCDW inflow from the Balleny Gyre, but far downstream of the progressively fresher AASW inflow from the Antarctic Coastal Current off Cape Colbeck. The resulting ~45-year time series from their data interpolated to $\gamma^n = 28.05$ kg m^{-3} show a major ($r^2 = 0.71$) decrease in salinity (Figure 33B) from S = 34.68 to 34.57, as well as a prominent cooling (Figure 33C) of $\Delta\theta \approx$ 1.25°C ($r^2 = 0.69$). Similar cooling and freshening trends are found through the entire MCDW layer in this area, e.g. $\gamma^n = 28.00$ kg m^{-3} - 28.27 kg m^{-3} (Figure 33E-G).

The last area found with large decadal variability is located near the Terra Nova Bay Polynya (Figure 34A). Property time series along the near bottom $\gamma^n = 28.70$ kg m^{-3} isopycnal span about 45 years and are derived from 94 hydrographic casts. Long-term cooling ($r^2 = 0.97$) and freshening ($r^2 = 0.97$) is also found at this extremely dense isopycnal. The salinity decreases from S = 34.78 to 34.74 (Figure 34B), and potential temperature (Figure 34C) decreases from θ = -1.63°C (MSW) towards a pure HSSW (θ

= -1.92°C). This is consistent with the decadal changes observed in the MCDW near the western shelf break, all suggesting that a relatively warmer and saltier inflowing MCDW was available in the past. More importantly, Figure 34G indicates that the general trend toward cooler and fresher MSW is apparent throughout the MSW layer ($\gamma^n < 28.60$ kg m^{-3}).

Temporal variability of SW properties has been monitored for over a decade now. Hellmer and Jacobs (1994) reported a cooling of 0.4°C and freshening of 0.06 near Ross Island. Jacobs (2002) reported an extensive decrease of SW salinity in the western Ross Sea during the past four decades. It is speculated that a combination of processes can be attributed to the observed freshening in the Ross Sea, e.g. a reduction in the net brine rejection during winter sea-ice formation, an increase in the net melting rate of the West Antarctic Ice Sheet, an increase in regional precipitation rates (Hellmer and Jacobs, 1994; Jacobs, 2004), and a weaker inflow of MCDW (Hellmer and Jacobs, 1994). Since SW is a key component of AABW, its observed freshening is likely altering the characteristics and volumes of Ross Sea Bottom Water outflows (Jacobs and Giulivi, 1998). Such changes could ultimately influence the characteristics of the AABW filling the abyssal layer of the Australian-Antarctic Basin (Whitworth, 2002).

All of the trends described above can be combined to speculate on the water mass stratification within the Ross Sea. The concurrent salt and heat gain in the LCDW layer with the opposite trends in the AASW layer (loss of density) result in the development of a relatively stronger pycnocline over the years, not only becoming progressively less likely to overturn in the oceanic domain as Jacobs (2002) speculated, but also more (Figure 35) likely to reduce diapycnal mixing which produces MCDW near the shelf break. The general freshening and cooling observed in MCDW and SW must result in a freshening of the Ross Sea AABW outflows and possibly stop its bi-modal production of high and low salinity types to just Low Salinity Bottom Waters, much like the Weddell Sea has operated during the past forty years.

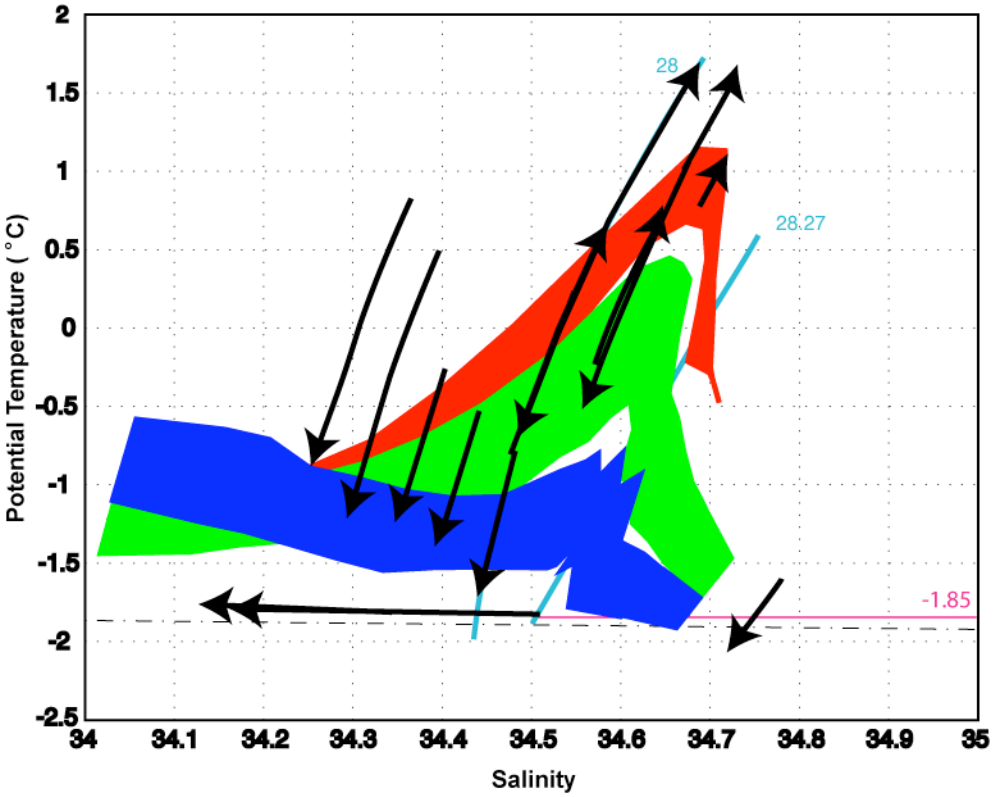

Figure 35. θ-S schematic of variability found in all inspected Ross Sea regions. Slope (red area), outer shelf (green area), and inner shelf (blue area) mean θ-S envelopes are overlain with black arrows, which indicate decadal variability trends.

FUTURE WORK

Further analysis of the new Ross Sea climatology and its derived volumetric census are valuable first steps toward attaining more precise calculation of Ross Sea AABW production rates. Carmack (1977) estimated the annual global production of AABW (5 to 10 x 10^6 m^3s^{-1}) using a Shelf Water residence time of 3.5 to 7 years estimated by Gill (1973) for the Filchner Depression in the Weddell Sea. Additionally, independent global production rates of AABW based on CFC budgets are available (Orsi, et al., 1999). New climatologies and volumetric θ-S censuses can be created for other productive regions around Antarctica, like the Weddell Sea, to provide more detailed comparisons among all of the main AABW sources in the Southern Ocean.

Inferences and speculations on the characteristics of the Antarctic Slope Front are generally drawn from a small number of synoptic hydrographic crossings. Only general assumptions can be made in regions that lack sufficient hydrographic stations. The new Ross Sea climatology offers an exceptionally larger number of "gridded synoptic crossings" across the shelf break. A more detailed description of the evolution of the ASF through its transit over the Ross Sea will result from the analysis of those climatology-based vertical sections.

The observed long-term changes in Ross Sea waters suggest that separate climatologies constructed with data from just certain time frames e.g. different decades could reveal distinct modes of AABW production in the Ross Sea. Similar climatologies could be created for other basins of the Southern Ocean, leading to further decadal comparisons of water mass property trends between these basins. Envisioned works like these may point to the regions undergoing the greatest temporal changes in the Southern Ocean and ultimately indicate the possible sources of the dramatic current freshening of the AASW.

SUMMARY AND CONCLUSIONS

The creation of a new Ross Sea high-resolution climatology and volumetric θ-S census provides a more detailed description of water mass stratification and circulation within the Ross Sea. The climatology and census are constructed from all available hydrographic station data of the Southern Ocean Database, supplemented with new hydrography from the AnSlope and CLIMA programs. Property maps on neutral density surfaces and layers and several depth levels are created from the new climatology.

Maps associated with Antarctic Surface Water ($\gamma^n < 28.0$ kg m^{-3}) show a southwestward inflow stemming from the southern limb of the Ross Gyre. This inflow splits near Cape Colbeck, feeding a thick layer of relatively cold and fresh Surface Water heading south against the coastline to near the eastern end of the Ross Ice Shelf. The northern branch continues northwestward roughly following the 700-m isobath. Along this transit, two relatively salty and warm influences from the oceanic domain are observed at the mouths of the Challenger and Drygalski troughs. Over the western Ross Sea slope, the characteristic "V" shape of the Antarctic Slope Front is indicated by a relatively thick layer of Antarctic Surface Water. The Antarctic Surface Water layer shows a general shoaling from east to west. This shoaling is also evident in the horizontal property gradients associated with the Antarctic Slope Front separating the Circumpolar Deep Water offshore from the Antarctic Surface Water inshore.

Two separate inflow regions of relatively thick Circumpolar Deep Water (γ^n = 28.00 kg m^{-3} - 28.27 kg m^{-3}) found offshore originate from the Ross and Balleny gyres. These inflows are the sole suppliers of salt and heat to the Ross Sea inshore of the 700-m isobath. Two tongues of relatively warm and salty Modified Circumpolar Deep Water continue a great distance inshore along the axes of the Drygalski and Joides troughs. These southward tongues progressively thin and attenuate their signals as this Modified Circumpolar Deep Water mixes with Antarctic Surface Water above and Shelf Water below. A third and broader relatively warm and salty tongue of Modified Circumpolar Deep Water is observed over the Challenger Trough. No significant inflow is observed farther to the east over the Whales and Little America troughs.

Northward outflows of much denser Shelf Water ($\gamma^n > 28.27$ kg m^{-3}, $\theta \leq -1.85$°C) are observed along the Drygalski, Joides, and Challenger troughs. The saltiest and thickest Shelf Water is found against the western flanks of the Drygalski and Joides troughs.

Enhanced vertical mixing of outflowing Shelf Water types with inflowing Modified Circumpolar Deep Water is inferred near the sills of the Drygalski, Joides, and Challenger troughs. As a result, there is a localized layer with intermediate characteristics, which is defined as Modified Shelf Water ($\gamma^n > 28.27$ kg m^{-3}, $\theta > -1.85$°C). This mixing product is denser than Lower Circumpolar Deep Water, but shallow enough to clear the sills and feed the main outflows of new Antarctic Bottom Water ($\gamma^n > 28.27$ kg m^{-3}, $\theta > -1.85$°C). These are only observed off the Drygalski, Joides, and Challenger troughs.

Inferences to key mixing and production regions can be made when a distinction between "pure" and modified forms of Shelf Water are utilized according to their salinity. High Salinity Shelf Water ($S > 34.7$) with the highest dissolved oxygen concentrations ($O_2 > 300$ μmol kg^{-1}) points to the location of its sources (due to sea-ice formation) near the Terra Nova Bay and along the Ross Ice Shelf polynyas, where ventilation takes place each winter. Near Ross Island, High Salinity Shelf Water lies deep enough ($z > 200$ m) to sneak southward under the Ross Ice Shelf. Ultimately, it emerges northward as extremely cold ($\theta \leq -1.95$°C) and fresh Ice Shelf Water in the Challenger Trough. Mixing with poleward-flowing Modified Circumpolar Deep Water above is most evident near the sills of the Drygalski and Joides troughs, where the warmest ($\theta \approx -1.85$°C) High Salinity Shelf Water is found.

Unlike the salty component, Low Salinity Shelf Water ($S \leq 34.7$) appears to be produced by two different processes. Its volume in the Challenger Trough derives from diluted and super-cooled High Salinity Shelf Water (Ice Shelf Water) from its transit underneath the Ross Ice Shelf. In contrast, Low Salinity Shelf Water in the Whales Trough derives from Antarctic Surface Water that gains salt during winter sea ice formation all along coastal polynyas in front of the Ross Ice Shelf. It is important to note

that even though small in volume, Low Salinity Shelf Water is also found in the western Ross Sea, lying right above the High Salinity Shelf Water.

The source of high salinity Antarctic Bottom Water ($\gamma^n > 28.27$ kg m^{-3}, $S > 34.7$) is located along the outer edge of the western Ross Sea. Formation of less saline ($S \leq 34.7$) bottom water seems to be more widespread over the outer shelf regions by incorporating relatively colder and fresher types of Modified Circumpolar Deep Water.

A volumetric census is calculated in fine-scale θ-S bins ($\Delta\theta = 0.1°C$, $\Delta S = 0.01$). To better infer water mass conversions and mixing recipes, the census is further divided into nine sub-regions. On the whole, the most voluminous water is Lower Circumpolar Deep Water found over the slope regime. The bulk of outflowing Antarctic Bottom Water is found over the western slope. Its source water mass in the western shelf region of the Ross Sea, namely Modified Shelf Water, is largely of the low-salinity ($S \leq 34.7$) variety. This suggests that the outflow of low-salinity Antarctic Bottom Water is favored in the western Ross Sea. A smaller volume of outflowing Modified Shelf Water is found over the central region, mostly of the low-salinity type due to the predominance of resident Low Salinity Shelf Water. The eastern shelf break region lacks Antarctic Bottom Water, as well as its parent Shelf Water component.

Mixing recipes are derived based on the volume-weighted mean potential temperature and salinity relationships for each water mass region. A relatively larger (smaller) component of Lower Circumpolar Deep Water (temperature minimum water) in Modified Circumpolar Deep Water is inferred from east to west: from only 40% in the eastern region, to 60% in the central region, and 70% in the western Ross Sea. In contrast, equal portions of Modified Circumpolar Deep Water (75%) are deduced to form Modified Shelf Water in both the western and central regions. No Modified Shelf Water is formed in the eastern outer shelf region of the Ross Sea.

The characteristic properties of near surface Ross Sea waters are undergoing long-term changes (Jacobs, 2002). Inspection of historical profile data interpolated to selected depth levels and isopycnal surfaces indicates regions with the largest decadal variability in potential temperature and salinity. The inflow of Antarctic Surface Water

to the eastern Ross Sea has become considerably fresher ($\Delta S = 0.2$ to 0.3) over the last 40 years. During the same time, Antarctic Surface Water near Ross Island has also freshened ($\Delta S = 0.05$) and cooled ($\Delta\theta = 1.0°C$). Opposite to this during the same time frame, Circumpolar Deep Water inflows from the southern limbs of the Ross and Balleny gyres have become relatively warmer ($\Delta\theta = 0.3°C$ to $0.4°C$) and saltier ($\Delta S =$ 0.03 to 0.04). These two observations indicate that a more stable pycnocline has developed throughout the Ross Sea in recent years.

Near the western shelf break, where intense mixing of these two water masses occurs, a consistent 40-year freshening ($\Delta S = 0.11$) and cooling ($\Delta\theta = 1.25°C$) trend is found in the local Modified Circumpolar Deep Water. Moreover, at its main production site in the Terra Nova Bay polynya, High Salinity Shelf Water shows a 45-year trend of freshening ($\Delta S = 0.04$) and cooling ($\Delta\theta = 0.29°C$). Over the years, it appears that the High Salinity Shelf Water variety is gradually changing toward the Low Salinity Shelf Water type ($S \leq 34.7$). The combined freshening and cooling of both Modified Circumpolar Deep Water and Shelf Water ingredients over the same period of time seem to result in the overall freshening of Antarctic Bottom Water produced in the Ross Sea. Ultimately, this would result in a long-term shift from the well-known bi-modal types of Antarctic Bottom Water production in the Ross Sea to a single low-salinity type, as it has been the case in the Weddell Sea.

REFERENCES

Budillon, G., Gremes Cordero, S., Salusti., E., 2002. On the dense water spreading off the Ross Sea shelf (Southern Ocean). Journal of Marine Systems 35, 207-227.

Carmack, E.C., 1977. Water characteristics of the Southern Ocean south of the Polar Front. In: Angel, M. (Ed.), A Voyage of Discovery: George Deacon 70th Anniversary, Pergamon, Oxford, pp. 15-41.

Deacon, G.E.R., 1937. The hydrology of the Southern Ocean. Discovery Reports 15, 3-122.

Deacon, G.E.R., 1984. The Antarctic circumpolar ocean. Studies in Polar Research Series, Cambridge University, Cambridge, pp. 180.

Dinniman, M.S., Klinck, J.M., Smith Jr., W.O., 2003. Cross-shelf exchange in a model of the Ross Sea circulation and biogeochemistry. Deep Sea Research Part II 50, 3103-3120.

Fichefet, T., Goosse, H., 1999. A numerical investigation of the spring Ross Sea polynya. Geophysical Research Letters 26, 1015-1018.

Foldvik, A., Gammelsrod, T., 1988. Notes on Southern Ocean hydrography, sea-ice and bottom water formation. Palaeogeography, Palaeoclimatology, Palaeoecology 67, 3-17.

Gill, A.E., 1973. Circulation and bottom water formation in the Weddell Sea. Deep-Sea Research 20, 111-140.

Goosse, H., Campin, J.-M., Tartinville, B., 2001. The sources of Antarctic bottom water in a global ice-ocean model. Ocean Modeling 3, 95-108.

Gordon, A.L., 1982. Weddell Deep Water variability. Journal of Marine Research, Supplement 40, 199-217.

Gordon, A.L., 1998. Western Weddell Sea thermohaline stratification. In: Jacobs, S.S., Weiss, R.F. (Eds.), Ocean, Ice and Atmosphere: Interactions at the Antarctic Continental Margin. Antarctic Research Series 75, AGU, Washington, D.C., pp. 215-240.

Gordon, L.I., 2000. Seasonal evolution of hydrographic properties in the Ross Sea, Antarctica, 1996-1997. Deep-Sea Research 47, 3095-3117.

Hellmer, H.H., Jacobs, S.S., 1994. Temporal changes in shelf-water of the southern Ross Sea. Antarctic Journal of the United States 29 (5), 123-124.

Jackett, D.R., McDougall, T.J., 1995. Minimal adjustment of hydrographic profiles to achieve static stability. Journal of Atmospheric and Oceanic Technology 12, 381-389.

Jacobs, S.S., Amos, A.F., Bruchhausen, P.M., 1970. Ross Sea oceanography and Antarctic Bottom Water formation. Deep Sea Research 17, 935-962.

Jacobs, S.S., 1989. Marine controls on modern sedimentation on the Antarctic continental shelf. Marine Geology 85, 121-153.

Jacobs, S.S., 1991. On the nature and significance of the Antarctic Slope Front. Marine Chemistry 35, 9-24.

Jacobs, S.S., Giulivi, C.F., 1998. Interannual ocean and sea ice variability in the Ross Sea. In: Jacobs, S.S., Weiss, R.F. (Eds.), Ocean, Ice and Atmosphere: Interactions at the Antarctic Continental Margin. Antarctic Research Series 75, AGU, Washington, D.C., pp. 135-150.

Jacobs, S.S., Giulivi, C.F., Mele, P.A., 2002. Freshening of the Ross Sea during the late 20th century. Science 297, 386-389.

Jacobs, S.S., 2004. Bottom water production and its links with the thermohaline circulation. Antarctic Science 16, 427-437.

Kim, S., Stössel, A., 2001. Impact of subgrid-scale convection on global thermohaline properties and circulation. Journal of Physical Oceanography 31, 656-674.

Levitus, S., 1982. Climatology atlas of the World Ocean. NOAA Prof. Paper No. 13, US Government Printing Office.

Locarnini, R.A., 1994. Water masses and circulation in the Ross Gyre and environs. Ph.D. Dissertation, Texas A&M University, unpublished.

Newsom, K., Francavillese, L., Tierney, J., 1965. Oceanography in Operation Deep Freeze 62, 1961-1962. Marine Geophysical Investigations, Technical Report TR-118, US Naval Oceanographic Office, Washington, DC, 8-38.

Orsi, A.H., Whitworth III, T., Nowlin Jr., W.D., 1995. On the meridional extent and fronts of the Antarctic Circumpolar Current. Deep-Sea Research, Part I 42, 641-673.

Orsi, A.H., Johnson, G.C., Bullister, J.L., 1999. Circulation, mixing, and production of Antarctic Bottom Water. Progress in Oceanography 43, 55-109.

Orsi, A.H., Smethie, W., Bullister, J.L., 2002. On the total input of Antarctic waters to the deep ocean: A preliminary estimate from chlorofluorocarbon measurements. Journal of Geophysical Research 107 (31), 1-14.

Smethie Jr., W.M., Jacobs, S.S., 2005. Circulation and melting under the Ross Ice Shelf: estimates from evolving CFC, salinity and temperature fields in the Ross Sea. Deep Sea Research Part I 52, 959-978.

Whitworth III, T., Orsi, A.H., Kim, S.-J., Nowlin Jr., W.D., 1998. Water masses and mixing near the Antarctic Slope Front. In: Jacobs, S.S., Weiss, R.F. (Eds.), Ocean, Ice and Atmosphere: Interactions at the Antarctic Continental Margin. Antarctic Research Series 75, AGU, Washington, D.C., pp. 1-27.

Whitworth III, T., 2002. Two modes of bottom water in the Australian-Antarctic Basin. Geophysical Research Letters. 29 (17), 1-3.

Worthington, L.V., 1981. The water masses of the World Ocean: Some results of a fine-scale census. In: Warren, B.A., and Wunsch, C. (Eds.), Evolution of Physical Oceanography. MIT Press, Cambridge, pp. 42-69.

Wüst, G., 1935. Schichtung und Zirkulation des Atlanticschen Ozeans, Die Stratosphare. Wissenschaftliche Ergebnisse der Deutschen Atlantischen Expedition auf dem Forschungs- und Vermessungsschiff "Meteor" 6(1), 99-188.

APPENDIX A

Appendix A. Listing of the largest one hundred individual θ-S bin-volumes from the volumetric census.

Rank	Pot. Temp (°C)		Salinity		Volume (km^3)	% of Ross Sea West	Cent	East
1	0.5	0.6	34.70	34.71	8476.9	56.2	29.9	13.9
2	0.6	0.7	34.70	34.71	8005.0	54.3	29.8	15.9
3	0.4	0.5	34.70	34.71	7266.3	75.6	21.0	3.4
4	0.8	0.9	34.71	34.72	6994.4	67.1	20.4	12.5
5	0.7	0.8	34.70	34.71	5640.0	62.4	27.4	10.2
6	0.7	0.8	34.71	34.72	5486.3	54.8	30.3	14.9
7	-2.0	-1.9	34.78	34.79	5373.8	80.2	19.8	0.0
8	-2.0	-1.9	34.77	34.78	5177.2	69.7	30.3	0.0
9	0.9	1.0	34.71	34.72	5013.1	62.2	21.5	16.3
10	-2.0	-1.9	34.79	34.80	4824.4	88.2	11.8	0.0
11	-2.0	-1.9	34.80	34.81	4810.3	87.9	12.1	0.0
12	-2.0	-1.9	34.76	34.77	4399.7	68.1	31.9	0.0
13	-2.0	-1.9	34.81	34.82	3951.3	87.9	12.1	0.0
14	0.3	0.4	34.70	34.71	3710.0	82.8	17.2	0.0
15	-2.0	-1.9	34.75	34.76	3280.3	68.0	32.0	0.0
16	0.8	0.9	34.70	34.71	3269.4	58.8	30.0	11.2
17	1.0	1.1	34.71	34.72	3205.6	65.2	20.9	13.8
18	0.3	0.4	34.69	34.70	2953.8	64.4	33.7	1.9
19	0.6	0.7	34.71	34.72	2873.8	48.0	26.3	25.8
20	-2.0	-1.9	34.74	34.75	2846.3	60.4	39.5	0.1
21	0.2	0.3	34.69	34.70	2833.8	92.4	7.6	0.0
22	-2.0	-1.9	34.82	34.83	2751.9	91.1	8.9	0.0
23	-2.0	-1.9	34.83	34.84	2505.6	97.8	2.2	0.0
24	0.4	0.5	34.69	34.70	2275.6	45.5	45.3	9.2
25	-2.0	-1.9	34.84	34.85	2183.8	100.0	0.0	0.0
26	-2.0	-1.9	34.73	34.74	2084.7	56.2	43.6	0.2
27	0.9	1.0	34.70	34.71	1951.9	62.1	26.5	11.4
28	-1.9	-1.8	34.72	34.73	1949.1	95.8	4.2	0.0
29	-1.9	-1.8	34.73	34.74	1933.8	96.1	3.9	0.0
30	0.5	0.6	34.69	34.70	1873.8	32.6	46.4	20.9
31	-1.9	-1.8	34.71	34.72	1784.4	91.3	8.7	0.0
32	1.0	1.1	34.70	34.71	1759.4	66.0	24.5	9.4
33	-1.9	-1.8	34.74	34.75	1755.9	95.3	4.7	0.0
34	-1.9	-1.8	34.70	34.71	1671.3	81.0	19.0	0.0
35	0.1	0.2	34.69	34.70	1670.6	100.0	0.0	0.0
36	-2.0	-1.9	34.72	34.73	1621.9	49.4	50.2	0.4
37	-1.9	-1.8	34.75	34.76	1610.6	98.5	1.5	0.0
38	1.1	1.2	34.71	34.72	1579.4	68.5	25.9	5.6

Rank	Pot. Temp (°C)		Salinity		Volume (km^3)	% of Ross Sea West	Cent	East
39	-1.9	-1.8	34.76	34.77	1421.9	98.3	1.7	0.0
40	-2.0	-1.9	34.85	34.86	1411.9	100.0	0.0	0.0
41	0.6	0.7	34.69	34.70	1408.1	38.5	37.5	23.9
42	-1.9	-1.8	34.69	34.70	1383.8	82.5	17.4	0.1
43	-2.0	-1.9	34.71	34.72	1383.1	35.7	63.9	0.5
44	0.9	1.0	34.69	34.70	1195.0	62.2	25.3	12.5
45	-1.9	-1.8	34.68	34.69	1145.3	80.2	19.5	0.2
46	-1.9	-1.8	34.77	34.78	1133.4	99.8	0.2	0.0
47	-1.9	-1.8	34.53	34.54	1132.5	0.0	12.9	87.1
48	0.8	0.9	34.69	34.70	1087.5	43.0	36.0	21.0
49	0.7	0.8	34.69	34.70	1086.3	41.9	29.0	29.1
50	-2.0	-1.9	34.70	34.71	1067.8	30.7	68.6	0.7
51	-1.9	-1.8	34.52	34.53	1034.3	0.0	4.8	95.1
52	1.0	1.1	34.69	34.70	1024.4	61.7	28.1	10.1
53	-1.9	-1.8	34.49	34.50	991.3	0.0	0.0	100.0
54	1.1	1.2	34.70	34.71	971.6	58.4	36.3	5.3
55	-1.9	-1.8	34.48	34.49	957.5	0.1	0.0	99.5
56	1.0	1.1	34.72	34.73	948.8	39.8	7.0	53.2
57	1.2	1.3	34.71	34.72	921.3	53.4	41.7	4.9
58	-2.0	-1.9	34.67	34.68	901.3	10.3	88.9	0.8
59	-1.9	-1.8	34.54	34.55	880.3	0.0	26.3	73.7
60	-1.9	-1.8	34.50	34.51	868.1	0.0	0.0	100.0
61	-1.9	-1.8	34.67	34.68	840.6	70.0	29.1	0.9
62	-1.9	-1.8	34.55	34.56	840.6	0.0	45.7	54.3
63	0.9	1.0	34.72	34.73	791.3	22.7	2.8	74.4
64	0.2	0.3	34.70	34.71	786.9	100.0	0.0	0.0
65	0.9	1.0	34.68	34.69	758.4	60.9	26.9	12.3
66	-1.8	-1.7	34.65	34.66	753.4	63.0	37.0	0.0
67	-1.9	-1.8	34.66	34.67	752.8	54.5	41.8	3.7
68	-2.0	-1.9	34.69	34.70	745.6	24.4	74.3	1.3
69	0.3	0.4	34.68	34.69	745.0	42.7	55.6	1.7
70	0.8	0.9	34.68	34.69	742.8	55.2	27.1	17.8
71	-2.0	-1.9	34.68	34.69	738.1	15.2	83.7	1.2
72	-1.9	-1.8	34.47	34.48	735.0	0.0	0.0	100.0
73	0.5	0.6	34.71	34.72	732.5	40.6	11.3	48.1
74	0.9	1.0	34.67	34.68	732.2	70.6	19.6	9.7
75	-1.9	-1.8	34.56	34.57	720.3	1.6	53.7	44.8
76	-1.9	-1.8	34.65	34.66	707.2	44.3	52.5	3.2
77	-1.9	-1.8	34.78	34.79	701.6	100.0	0.0	0.0
78	-1.8	-1.7	34.69	34.70	690.6	91.1	8.9	0.0
79	-1.8	-1.7	34.67	34.68	688.1	86.7	13.3	0.0
80	-1.8	-1.7	34.66	34.67	687.8	79.3	20.7	0.0

Rank	Pot. Temp (°C)		Salinity		Volume (km^3)	% of Ross Sea West	Cent	East
81	0.7	0.8	34.68	34.69	682.5	32.4	39.7	27.9
82	0.8	0.9	34.67	34.68	674.7	61.1	27.0	11.9
83	-1.8	-1.7	34.68	34.69	674.1	92.8	7.2	0.0
84	0.2	0.3	34.68	34.69	672.5	44.6	54.3	1.1
85	-1.9	-1.8	34.59	34.60	668.4	8.4	82.1	9.5
86	-1.8	-1.7	34.49	34.50	665.6	0.1	4.5	95.4
87	1.1	1.2	34.72	34.73	643.8	52.5	14.5	33.0
88	0.6	0.7	34.68	34.69	643.8	32.0	35.9	32.0
89	-1.9	-1.8	34.58	34.59	640.0	6.9	77.3	15.8
90	-1.8	-1.7	34.55	34.56	636.8	8.5	79.7	11.8
91	-1.9	-1.8	34.57	34.58	633.8	2.7	72.3	25.0
92	-1.9	-1.8	34.51	34.52	630.6	0.1	1.4	98.5
93	-1.9	-1.8	34.60	34.61	624.7	15.0	76.6	8.4
94	0.0	0.1	34.69	34.70	617.5	100.0	0.0	0.0
95	-1.6	-1.5	34.52	34.53	613.7	19.3	57.4	23.3
96	1.2	1.3	34.72	34.73	609.4	79.0	3.9	17.1
97	0.4	0.5	34.68	34.69	609.4	35.5	57.9	6.6
98	-1.7	-1.6	34.65	34.66	609.4	59.0	41.0	0.0
99	-1.7	-1.6	34.64	34.65	605.3	64.3	35.5	0.2
100	-1.7	-1.6	34.52	34.53	600.6	10.7	65.0	24.2

VITA

Christina Lee Stover received her Bachelor of Science degree in marine science from Coastal Carolina University in 2002. She entered the Oceanography program at Texas A&M University in 2003, and she received her Master of Science degree in May 2006.

Ms. Stover mailing address is Department of Oceanography, Texas A&M University, College Station, TX 77843-3146. Her email address is cstover@ocean.tamu.edu.